Modeling of soft robots made of anisotropic mesostructured materials

Félix Vanneste

▶ **To cite this version:**

Félix Vanneste. Modeling of soft robots made of anisotropic mesostructured materials. Modeling and Simulation. Université de Lille 1, Sciences et Technologies; CRIStAL UMR 9189, 2022. English. ⟨NNT : ⟩. ⟨tel-03788950⟩

HAL Id: tel-03788950

https://hal.science/tel-03788950v1

Submitted on 27 Sep 2022

HAL is a multi-disciplinary open access archive for the deposit and dissemination of scientific research documents, whether they are published or not. The documents may come from teaching and research institutions in France or abroad, or from public or private research centers.

L'archive ouverte pluridisciplinaire **HAL**, est destinée au dépôt et à la diffusion de documents scientifiques de niveau recherche, publiés ou non, émanant des établissements d'enseignement et de recherche français ou étrangers, des laboratoires publics ou privés.

HAL Authorization

Université de Lille

Inria

UNIVERSITÉ DE LILLE

ÉCOLE DOCTORALE MADIS

Modeling of soft robots made of anisotropic mesostructured materials

THÈSE présentée par :

Félix VANNESTE

soutenue le : 23 Juin 2022

Pour obtenir le grade de : **Docteur de l'université de Lille**

Discipline / Spécialité : simulation/modélisation

Rapporteurs:

Nancy Pollard	Professor at Carnegie Mellon University
Pierre Renaud	Professor Strasbourg University, INSA/ICube

Examinateurs:

Sylvain Lefebvre	Research Director at INRIA Nancy
Maud Marchal	Professor at Rennes University, INSA/IRISA
Stelian Coros	Associate Professor ETH Zurich

Thèse dirigée par:

Christian Duriez	Research Director at INRIA Lille
Olivier Goury	Research Scientist at INRIA Lille

Abstract

Soft robotics is a recent field of robotics. It differs from classical rigid robotics by exploiting the compliance of the robot to create motion by deformation, rather than relying on articulations. Thanks to their inherent compliant composition, soft robots are particularly adapted for motion for deploying through unknown environment, grasping fragile objects or notably for human interactions.

Soft systems are essentially fabricated with a homogeneous compliant material, like silicone. However, other, more relevant material choices could be made to design these robots. Recent works started to investigate the use of multimaterials, metamaterials or even smart materials inside soft structures to build systems with programmed compliance. In this work, we make the choice of using a stochastic foam to program soft robots structures with anisotropy using fiber direction on a given geometry.

Using this foam, we show that we can create new controllable kinematics without changing the geometry of soft robots. The anisotropic soft robots are modeled using a Finite Element Method (FEM) with homogenised mechanical properties. We present a complete workflow: from model simulation and design to fabrication and interactive control with inverse simulation. Finally, we present a new generic mechanical calibration method and use it to reduce the sim2real discrepancy.

Contents

List of Publications **1**

1 Overall introduction **3**
1.1 Soft robotics . . . 4
1.1.1 From a medical need to various industrial applications . . . 4
1.1.2 Soft robotics community history . . . 4
1.1.3 Difficulties and perspectives . . . 6
1.2 Design and fabrication . . . 8
1.2.1 Additive manufacturing . . . 8
1.2.2 Material available for soft robots AM . . . 9
1.2.3 New material designs . . . 12
1.3 Soft robot simulation . . . 13
1.3.1 Specificity of the simulation of soft robots . . . 13
1.3.2 Model classification . . . 14
1.3.3 Available implementation . . . 15
1.4 Contributions . . . 18
1.5 Organisation of the manuscript . . . 18

2 State of the art **21**
2.1 Metamaterial definition and usage . . . 23
2.1.1 Metamaterial history and global presentation . . . 23
2.1.2 Main usage for each field . . . 24
2.1.3 Flexible mechanical metamaterial . . . 26
2.1.4 Structure characterisation and generation process . . . 28
2.2 Integration in soft robotic systems . . . 31
2.2.1 Current usage in soft robotics . . . 31
2.2.2 Simulation and design of soft systems with metamaterials . . . 37
2.3 Conclusion . . . 39

3 Fabrication and numerical representation **41**
3.1 Mesostructure based on stochastic foam . . . 43
3.1.1 Stochastic foam: from generation to fabrication . . . 43
3.1.2 Interest in the context of soft robotics . . . 43
3.2 Stochastic foam modeling . . . 45
3.2.1 Material elasticity tensor . . . 45
3.2.2 Mechanical characterisation with homogenization . . . 50
3.3 Numerical implementation with FEM . . . 52
3.3.1 Soft robots Finite Element Model . . . 52
3.3.2 Geometrical non-linearities and their numerical computation . . . 54

3.3.3 Anisotropy implementation . . . 56
3.3.4 Requirements for stable simulation . . . 58
3.4 Fabrication and reality gap . . . 59
3.4.1 Foam generation with IceSL . . . 59
3.4.2 FDM technology and its inherent imperfections . . . 61
3.5 Conclusion . . . 64

4 Kinematics of anisotropic soft robots 67
4.1 Direct simulation validation with real setup . . . 69
4.1.1 Validation of the anisotropic model on a cantilever beam . . . 69
4.1.2 New kinematics on a tripod robot . . . 69
4.2 Inverse modeling presentation . . . 75
4.2.1 Robot kinematic control via external target . . . 76
4.2.2 Constraint solving . . . 76
4.3 6 DOF controllable parallel soft robot . . . 77
4.3.1 Simulation design . . . 78
4.3.2 Workspace capabilities assessment . . . 80
4.3.3 Setup presentation and results . . . 81
4.4 Conclusion and results discussion . . . 85

5 Optimisation and calibration 87
5.1 Differentiation and optimisation on multiple configurations . . . 89
5.1.1 Differentiable models . . . 89
5.1.2 Sim2real using inverse model . . . 90
5.1.3 Multi-Configuration optimisation . . . 90
5.2 Parameterisation of anisotropy . . . 92
5.2.1 Simulation - mechanical structure . . . 92
5.2.2 Fabrication - slicing configuration . . . 92
5.3 Problem conditioning . . . 93
5.3.1 Simple problem setup . . . 94
5.3.2 Influence of the configurations on the convergence . . . 94
5.3.3 Conditioning analysis on soft anisotropic beams . . . 95
5.4 Practical use: calibration of a real anisotropic parallel robot . . . 97
5.4.1 QP problem setup . . . 98
5.4.2 Results . . . 99
5.5 Conclusion . . . 101

Conclusion 103

List of Figures 107

List of Tables 113

List of Publications

Journal articles

- [1] Vanneste, F., Goury, O., Martinez, J., Lefebvre, S., Delingette, H., & Duriez, C.
Anisotropic soft robots based on 3D printed meso-structured materials: design, modeling by homogenization and simulation.
IEEE Robotics and Automation Letters (Proc. ICRA), 2020. video.

- [2] Vanneste, F., Goury, O., Duriez, C.
Calibration method for soft robots modeled with FEM: application to anisotropy.
IEEE Robotics and Automation Letters (Proc. RoboSoft, **best paper finalist**), 2022. video.

Conference papers

- [3] Vanneste, F., Goury, O., & Duriez, C.
Enabling the control of a new degree of freedom by using anisotropic material on a 6-DOF parallel soft robot.
IEEE 4th International Conference on Soft Robotics (RoboSoft), 2021. video.

Other scientific contributions

- [4] Vanneste, F., Goury, O., & Duriez, C.
Roadmap on Soft Robotics: multifunctionality, adaptability and growth without borders: Section 09–Modeling Soft
Multifunctional Materials, 2022.

Chapter 1

Overall introduction

Contents

1.1 Soft robotics **4**
1.1.1 From a medical need to various industrial applications 4
1.1.2 Soft robotics community history 4
1.1.3 Difficulties and perspectives 6
1.2 Design and fabrication **8**
1.2.1 Additive manufacturing 8
1.2.2 Material available for soft robots AM 9
1.2.3 New material designs 12
1.3 Soft robot simulation **13**
1.3.1 Specificity of the simulation of soft robots 13
1.3.2 Model classification 14
1.3.3 Available implementation 15
1.4 Contributions **18**
1.5 Organisation of the manuscript **18**

1.1 Soft robotics

1.1.1 From a medical need to various industrial applications

Soft robotics is a recent sub-field of robotics arising from numerous factors. It was first introduced in the end of the 90s by Suzummori [5] and had for primary intention to be of help in medical applications. The medical field advancing and beginning to incorporate robots during operation (minimal invasive surgery) the need for the "compliance" of robots became crucial to avoid damaging the internal organs of patients.

In a broader perspective, rigid robotics is lacking the safety for human robot interactions (HRI) in all types of environment. To bring answers to this new challenges, researchers took inspiration from highly functional and compliant existing examples present in nature. Many well known examples of soft robots are bio-inspired systems that try to emulate living animals (octopus [6],worm [7],fish [8]) or adapt part of living organism to new kind of manipulator (elephant trunk [9]).

Apart from HRI, interacting with fragile or unknown environment also has a direct application in the industry. The need for new kinds of "not so rigid" manipulators is growing. In particular to be able to handle with a same system numerous objects with different geometries and at the same time handles frail and delicate objects (for example fruits or vegetables). This is not possible without requiring quite complex systems for traditional rigid robots. Hybrid systems emerge from this reflection combining fast, efficient, and simple rigid arms with soft versatile compliant grippers (jamming robot arms [10], pneunet gripper [11]).

Since these first fields of application, researchers have since proposed many different situations in which soft robotics systems can be used. From just easing HRI we now have devices which can be directly used on humans to do for example rehabilitation or even enhance human with assisting devices [12, 13, 14]. Robots were also created to handle unknown terrain or navigate in tight spaces [15, 16].

1.1.2 Soft robotics community history

The field of soft robotics has really grown from its early start to a now multi-disciplinary one, with complex systems developed for many different situations/applications. Even if the first application was developed in the 90s, it still took 10 years to really emerge and an additional 10 years to mature (from 2010 to today) as illustrated on Fig. 1.1. Therefore, if the field is now bustling with many contributions per year, it is far from mature and most of its potential remains to be achieved.

The field of soft robotics lacks structures and a systematic design methodology resulting from its fast growth, multi-disciplinary inspiration and the diversity of its potential applications. Moreover the definition of soft robotics is still not totally stable. Majidi [18], Rus and Tolley [19] as well as McKee et al. [16] tried to define soft robots based on which material they are made of and its corresponding Young modulus. The range of Young

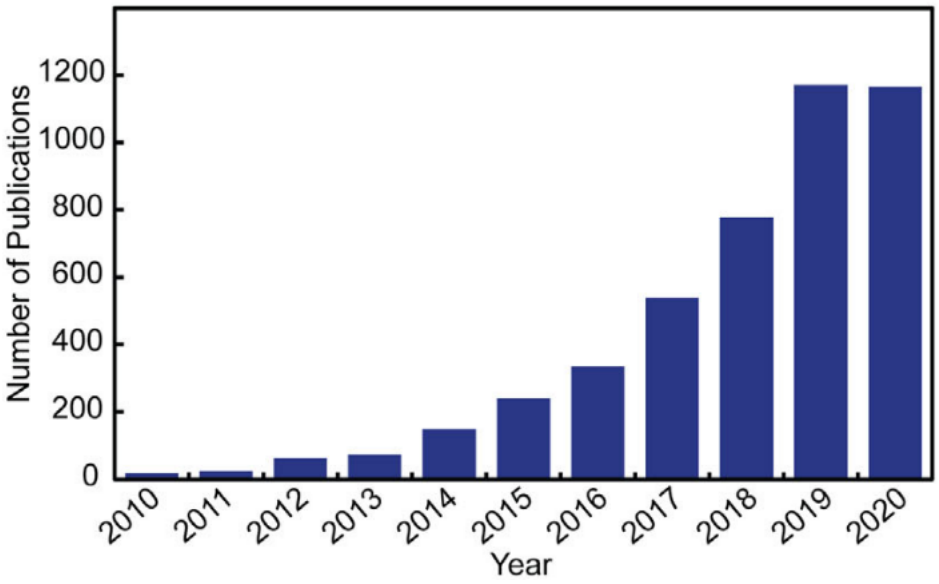

Figure 1.1: Total number of publications in soft robotics research for each year from 2010 to 2020. Figure from [17].

moduli proposed by Rus, from 10^4Pa to 10^9Pa, as we can see in Fig. 1.2, allows for a wide variety of materials. However, according to the methods of measurement, the Young modulus that we obtain differs, so even this range is not stable: being either between $10^2 - 10^6$ or $10^4 - 10^9$ Pa. Furthermore it is not because a material has a high Young modulus and is not inherently "soft" that it can not be compliant: it also depends on its layout organization and density.

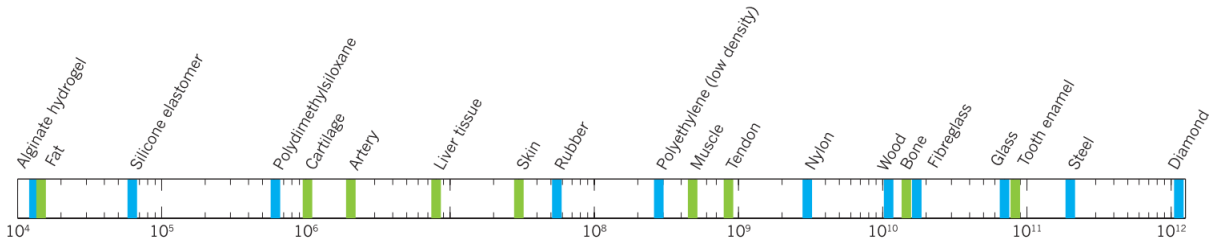

Figure 1.2: Approximate tensile modulus (Young modulus in pascal (Pa)) of selected engineering and biological materials. Figure from [19].

Apart from the choice of material, many systems are characterized as soft robots, but are not entirely soft or even have a majority of rigid structures compared to the flexible parts. Recently Chubb et al. [20] have tried to classify the different soft robots, which is better to be called soft systems. They have separated them in 4 categories which can be seen in Fig. 1.3, going from level (tier) 4 being entirely soft and totally untethered to level 1 being conventional robots adapted to achieve more compliance, i.e. like adding some soft gripper at their ends.

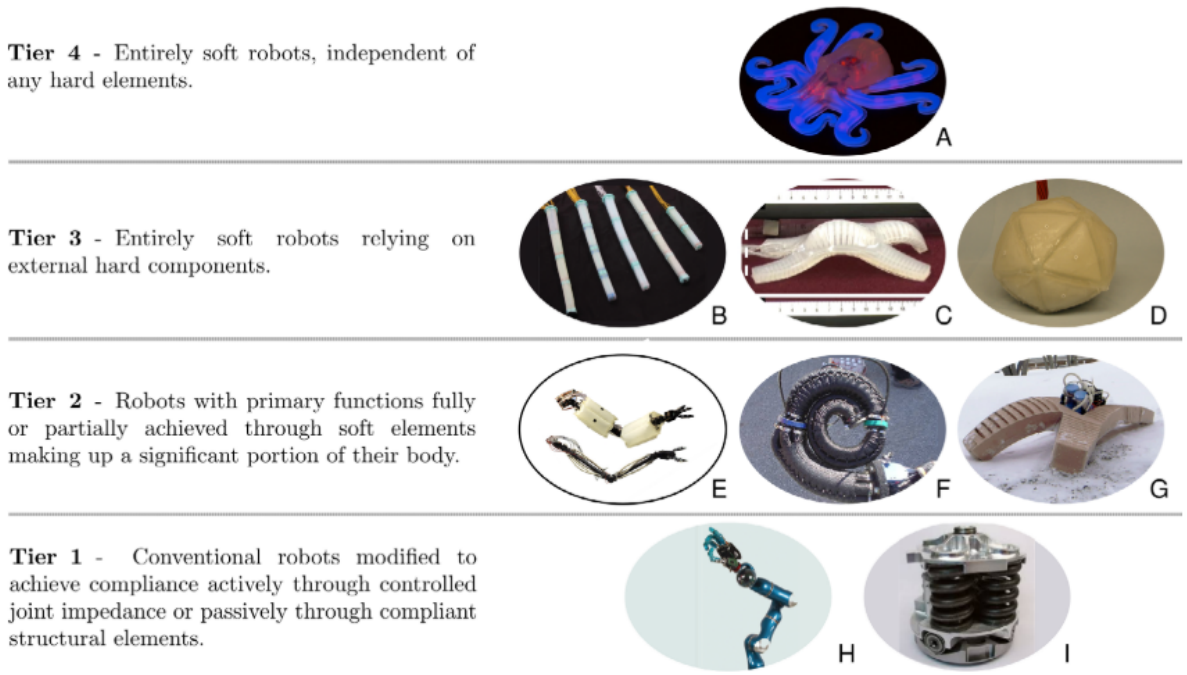

Figure 1.3: Soft systems classified according to their dependence on rigid structures. Octobot (A) is an untethered robot comprising only soft components [21]. Marchese and Rus's soft spatial manipulator (B), the multigait soft robot (C) (a precursor to (G)), and the spherical jamming mobile robot (D) comprise only soft materials but require external supplies [22, 15, 23]. The lightweight soft robotic arm (E) moves using pneumatic actuators that also provide a compliant covering [24]. OctArm (F) uses pneumatic actuators to create a continuum manipulator but requires rigid plates to separate each section of the manipulator [25]. The resilient untethered soft robot (G) moves using pneumatically powered actuators but relies on hard batteries, compressors, and micro-controllers [26]. DLR Robotics' LWR-III (H) [27] achieves softness through lightweight materials, sensor redundancy, and active compliance control. Variable impedance actuators (I) incorporate compliance into a rigid robot, creating a 'soft' robot, by exploiting passive or actively controlled elastic elements [28]. Figure from [20].

1.1.3 Difficulties and perspectives

A tier 4 system is really difficult to make and, to date, only a few examples exist [29]. This comes from the difficulties to, from one part: have efficient untethered systems, and from another part: the current lack of available "soft" actuators/power source rending their incorporation into a soft structure detrimental to its initial compliance. Moreover, to be able to add control to these complex structures, we usually need important computation power that is performed "outside" of the soft system. Recently, some works have pushed forward morphological computing [30, 31, 32, 33] in order to reduce computation demand by unloading some of it directly on the structure and alleviate the structural compliance of the systems. Additionally, one of the main approach for actuation is using fluidic pressure to inflate/deflate cavities and this needs a cumbersome external structure to

work. We can see on Fig. 1.4 a classification of the different soft systems forming a soft robot into 3 categories: physical, non-physical (but controlled externally) and completely untethered. It clearly shows what we have said earlier about the lack of compliant and efficient actuators and it is even more pronounced for sensors.

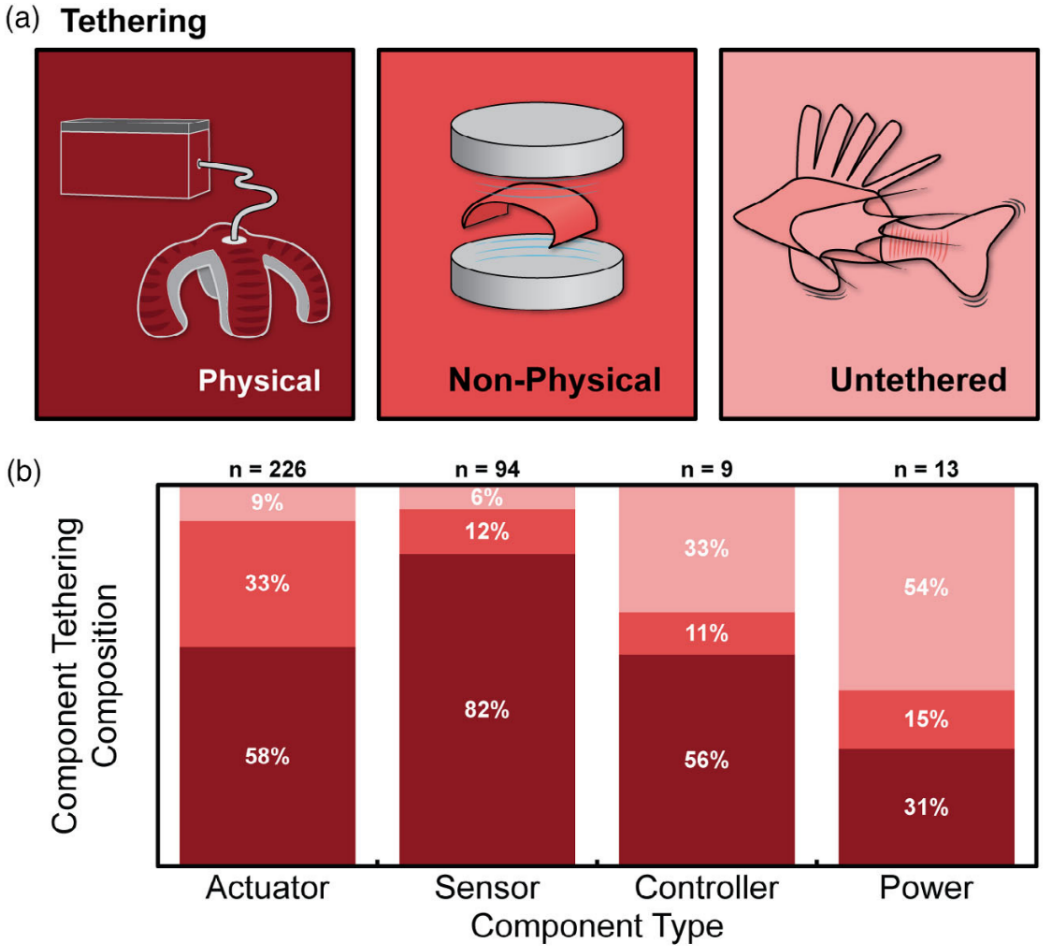

Figure 1.4: Differentiation of the soft robot components (Actuator/Sensor/Controller/Power) of the top 10% soft robotics paper in number of citation per year. They are classified based on their tether composition (Physical/Non-Physical and totally Untethered). a) Tethering category examples and legend. b) Device tethering shown relative to the number of component types a given device contained. Figure from [17].

One of the main "way to go" to reduce this physical dependency, is to develop further the potential of the soft systems structure. Indeed exploiting morphological computation can reduce computing and sensor needs. Concerning actuation with passive and/or active programmed compliance, we can control more behavior with less actuation sources. Developing material capabilities with shape memory allow (SMA) or using multimaterial structures or metamaterial can bring the soft robotic fields closer to developing monolithic systems with structures incorporating sensors, actuation, computation and power.

To do so, works on designing automatic and/or intuitive tools assisting roboticist will

be needed to structure the actual global approach that is similar to a "do it yourself" (DIY) approach. Indeed DIY is useful to develop the soft robotics horizons, but it is not adapted to the development of robust and reliable systems for specific tasks, particularly in non-academic contexts.

1.2 Design and fabrication

Soft robotics has particularly emerged with the democratisation and use of additive manufacturing (AM) which has since continued to evolve in parallel with new processes for building soft robots. We will briefly present the different AM technologies at our disposal and the available materials compatible with soft robotics. We will then present the most common design of soft robotics and how it is made. We will conclude with some perspectives on new types of materials.

1.2.1 Additive manufacturing

1.2.1.1 available technologies

Fused deposition modelling (FDM)	Direct ink writing (DIW)	Selective laser sintering (SLS)	Inkjet printing	Stereolithography (SLA)
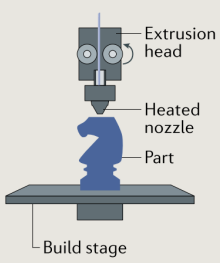	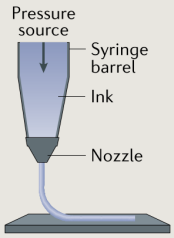	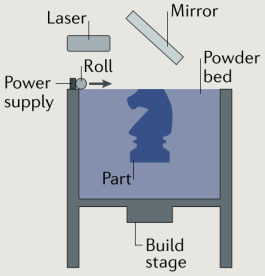	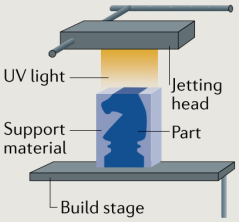	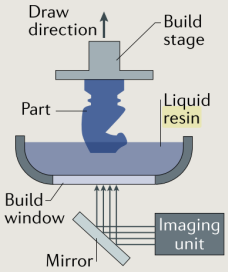
Approximate deposition rate				
10^5 mm^3 h^{-1} Inversely proportional to resolution[59]	10^5 mm^3 h^{-1} Inversely proportional to resolution[76]	10^6 mm^3 h^{-1} (REF.[103])	5×10^5 mm^3 h^{-1} (REF.[28])	10^6 mm^3 h^{-1} Slower rates for microsystems[102,103]
Approximate resolution				
100 µm (REF.[59])	1–100 µm (REF.[76])	100 µm (REF.[82])	50 µm (REF.[28])	1 µm (microsystems)[98,99] 50 µm (projection-based)[116]
Starting material requirements				
Thermoplastic (filament)	Flowable (ink) that solidifies	Thermoplastic (powder)	Low viscosity ink ν_{app} < 0.25 Pa s (REF.[28])	Low viscosity ink ν_{app} < 5 Pa s (REF.[106]) photopolymerizable

Figure 1.5: Visual representation and description of the different available technologies of additive manufacturing. Figure from [34].

AM is now really diverse in terms of available technologies, each with their advantage and drawbacks depending on the design and intended application of the 3D object to manufacture. We can see on Fig. 1.5 a representation of the most common processes:

- **Fused deposition modelling**: A solid thermoplastic filament is extruded through

a heated nozzle to melt, deposit and fuse the material.

- **Direct ink writing**: A liquid ink flows through a nozzle. Upon deposition, the ink solidifies into a solid object.
- **Selective laser sintering**: A bed of solid, thermoplastic powder is selectively heated by a scanning laser. This irradiation causes localized melting and fusion of the material. Powder is then cast to recoat the bed, and the process is repeated. This technique is also called 'selective laser melting' when thermoplastic polymers are printed.
- **Inkjet printing**: Small droplets of liquid ink are simultaneously ejected from print heads. These droplets then solidify on the surface, often in response to light or heat. The injection and solidification are repeated iteratively until the entire object is built.
- **Stereolithography**: A bath of liquid photopolymer is selectively exposed to light (through either a scanning laser or a projected photopattern). The liquid resin polymerizes into a solid layer in response to photoirradiation. The object is then translated, liquid recoats the interface and the next layer is similarly exposed.

From these technologies, FDM is the most used AM due to its convenience, reducing the cost to have such systems. Moreover having an important community of "maker" behind able to rely on/help in case of issues is really convenient. Additionally it has a wide variety of commercially available "filament". Considering these advantages, we will use this technology for the experiments of this thesis.

1.2.2 Material available for soft robots AM

As described by Wallin et al. in [34], Young modulus (E) is not enough to characterise a material "softness" and its applicability to soft robotics application. Three additional parameters are important: γ_{ult}, Γ and U_r, γ_{ult} being the ultimate elongation before failure, Γ the toughness, meaning the total mechanical energy absorbed by material before rupture and finally U_r the modulus of resilience, i.e. the maximum energy that can be entirely elastically recovered during a loading cycle to return the robot to its original, undeformed state, i.e. without plasticity effect or failure.

As a consequence for any soft application the material should have a specific E (generally low) for the targeted application and a maximum or at least sufficient γ_{ult},Γ and U_r to enable large, recoverable local strain differentials and to impart resistance to failure and fatigue. This greatly reduces the number of materials available for 3D printing soft robots.

Polymers have a very wide range of physical properties from 1 kPa to 100 MPa for the Young modulus and are the most commonly used in soft robotics, particularly the elastomers as can be seen in Fig. 1.9 which are polymers having viscoelasticity. One of the most common in soft robotics is polydimethylsiloxanes (PDMSs) which is a kind

of silicone. It is generally not 3D printed but "casted" into rigid mold (which are typically 3D printed). Silicone materials possess excellent elasticity and resilience (elastic regimes up to $\gamma_{ult} \approx 700\%$ strain), chemical inertness, thermal resistance, biocompatibility, dielectric strength, low permeability and thermal conductivity compared with other polymer systems, making them the first and most used materials for soft robotics. The other widely used polymers which can be 3D printed are polyurethanes. They can be used as foam, casted like silicone [35], or as 3D printing filament with the thermoplastic elastomer (TPE) or the thermoplastic polyurethanes (TPU). Beside these two, there are also hydrogels but they are generally difficult to print in 3D structure. Additionally there are three others categories which are composites and/or complex material engineered to create smart material: shape memory alloy (SMA), Shape Memory Polymer (SMP) and smart composite (SP). They are generally difficult to incorporate into systems and costly. We won't go into details about them. A summary of the different material can be seen in Fig. 1.6 with some examples of commercially available product.

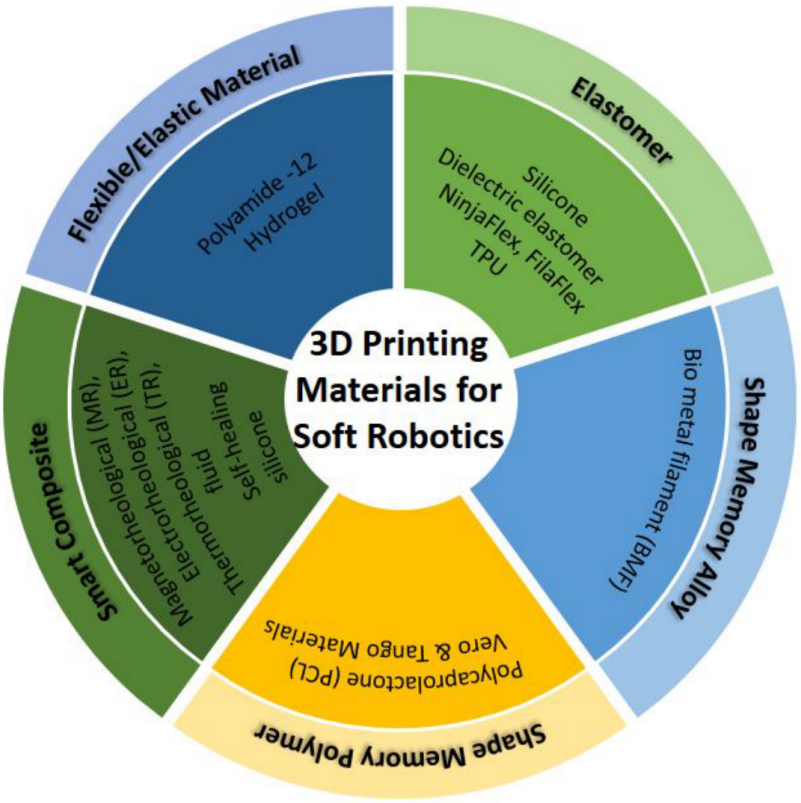

Figure 1.6: The Five categories of 3D printing materials for soft robotics with commercially available examples. Figure from [36].

Range of hardness/softness at disposal

To have a better idea of the different softness of these materials, particularly silicone and polyurethanes, we can look at Fig. 1.7 which give their different shore hardness range. Shore hardness is particularly relevant when we speak about filament; it classifies

a filament given the depth of an indentation in the material created by a given force using a durometer (i.e. hard to soft scale : D to 00). The flexibility of the filament can be determined from this data.

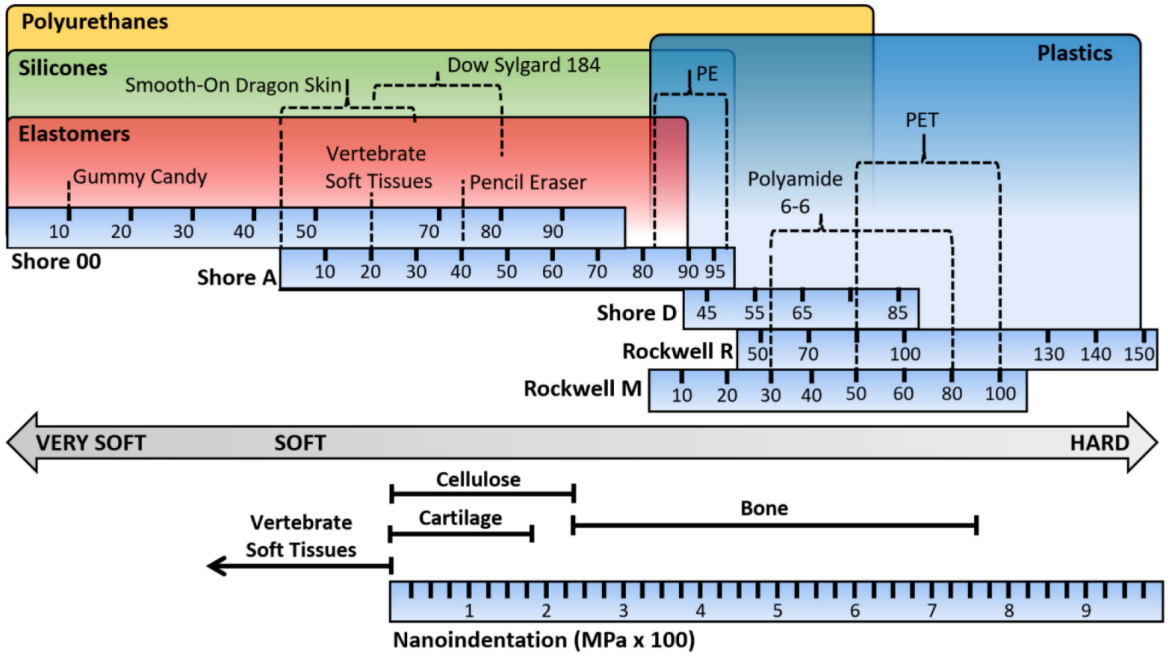

Figure 1.7: Comparison of hardness, or softness, of materials suitable for use in soft robots. Some common materials have known hardness values and are shown in the figure. Figure from [14].

Typical soft robots composition

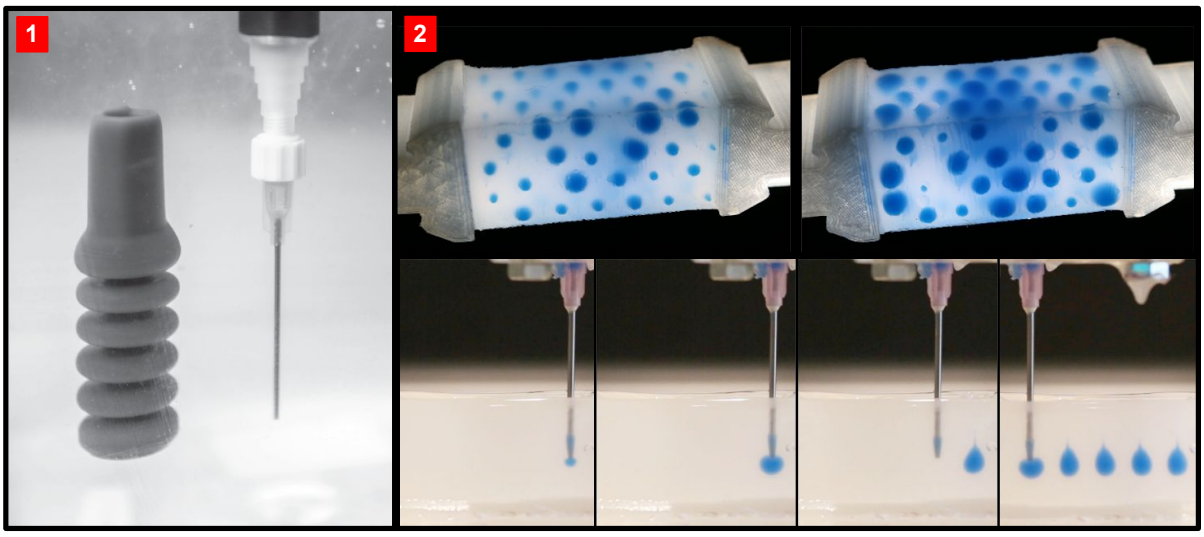

Figure 1.8: (**1**) 3D printed silicone from [37]. (**2**) graded properties of silicone with bubbles of liquids from [38].

Even if the 3D printing techniques have evolved, the majority of soft systems are silicone-based and are actuated by either pulling cables or pressurising cavities to create deformation, i.e. silicone being casted into a certain geometry, it implies sealing. Silicone had a primary downside, which is the inability to be 3D-printed, but it is now outdated, to some extent, due to recent works of Sparrman et al. [37] which can be seen in Fig. 1.8 left. In a general way we can refer to Fig. 1.9 to have a global overview of the soft systems composition.

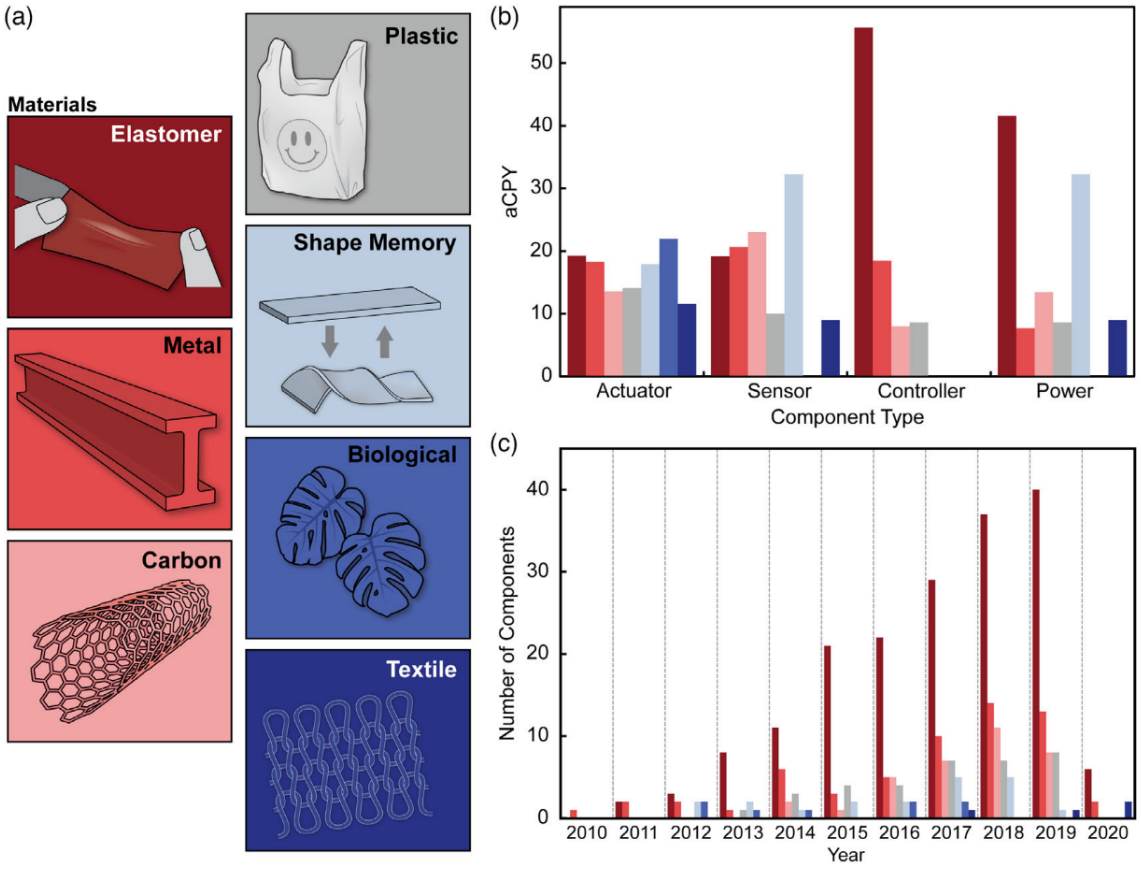

Figure 1.9: Overview of soft systems material composition of top 10% of publications by average citations per year (aCPY). a) Material category examples and legend. b) Number of robotic components using a given material in each year. c) aCPY based on the material used for a given robotic component. Figure from [17].

1.2.3 New material designs

Despite all its advantages, silicone is lacking one important and useful characteristic on which soft systems particularly rely on: its mechanical grading. Mechanical gradation means the ability to program heterogeneous properties into a structure allowing different compliances at different locations in the material. Even if some work has been done in this direction [38] (see in Fig. 1.8 right), it is still in its infancy and difficult to implement.

On another side, 3D printing, and particularly FDM, has improved and provides relatively accurate manufacturing possibilities at small cost. Silicone pieces are completely filled unlike FDM ones which are generally mainly hollow in order to save matter. This allows to easily manage a piece density, as well as its filling pattern. It is hence possible to vary its flexibility by creating repeating pattern and create what is called a metamaterial (precise definition in the next chapter). Moreover multimaterial printers already exist which can fuse different materials on a same piece, which again is complicated and not precise for silicone. It involves using glue to fix different parts together which is not satisfying.

In conclusion, graded flexibility is not yet properly achievable with silicone. On the other hand FDM techniques with compliant material seems ideal for conceiving complex structure allowing mechanical gradation and, in doing so, for programming the heterogeneities of a structure.

1.3 Soft robot simulation

One of the main challenge of soft robotics is the ability to create an accurate simulation of their structures, describing how it behave when actuated as well as when experiencing diverse interaction with known or unknown environment. We will see in this section the different theoretical models used for soft robotics. We will develop further the one we will used in this thesis and present the framework implementing it.

1.3.1 Specificity of the simulation of soft robots

Simulation in general allows to predict a system capabilities and can allows, when made before hand, to be used as an assisting tool for design purposes, i.e. by varying its actuators placement, its global geometry, its material properties or evaluating the performances. Once the system is built, it can also be used for control by predicting the best actuation pattern to achieve certain goals. Using inverse kinematics (IK) and sensor feedback for example, allows to control efficiently a real setup by its end-effector position, adjust the simulated system with reality and have closed loop control. Simulation is then crucial to master the complexity of soft robotics systems. If we want to go further than the DIY approach and have task optimized systems and efficient control, a precise and generic simulation is needed.

Any simulation is based on a model representation of a system. Traditionally for rigid structure we have analytical models which are fast and efficient. This comes from their structural assumption that remains true during their actuation pattern. Concerning soft systems we have the opposite: it is hard to get an analytical model that describes the mechanical behavior with accuracy due to the theoretically infinite passive degrees of freedom (DoF).

Moreover this large amount of DoFs can lead to multiple solutions for a same position of an end-effector, leading to non-unique solution of the IK problem. As an additional

challenge, many of these DoFs are not directly controllable. Moreover their kinematics do not only depend on their geometry, but also on their material properties. Indeed, their material properties have an important and direct influence on their configuration as illustrated in Fig. 1.10.

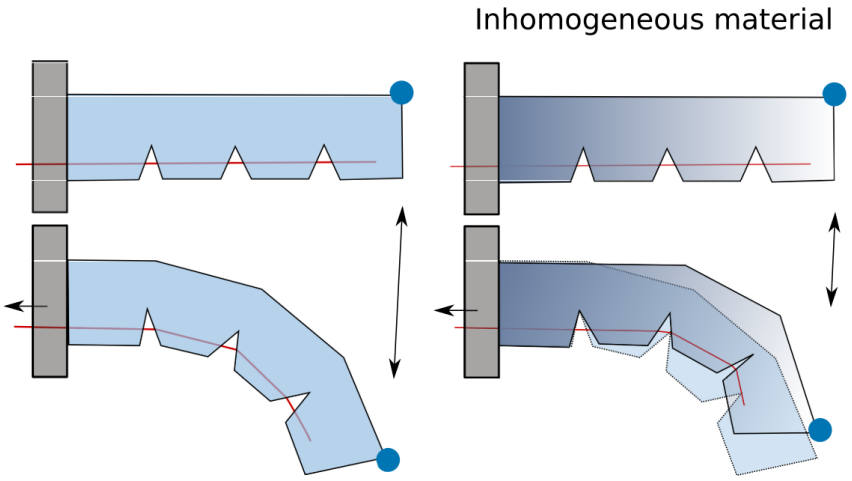

Figure 1.10: In this example a tendon is pulled to create the motion of an elastic soft robot. Starting with the same geometry, the material stiffness has an influence on the kinematics (output vs input displacements). Figure from [39]

Numerical models can be used to tackles these issues. They discretize the geometry and use a numerical solver, which makes approximations to solve its deformation.

As always for soft robotics, because of the diversity of a robot structure, geometry, behavior and its purpose, the modeling of it is not unique and the most efficient methods can vary from one system to another. We will present next different theoretical models and some of their use case.

1.3.2 Model classification

The modeling of a mechanical system is the mathematical representation of the considered physical problem. It can be classified in 4 main categories [40, 41] for soft robotics, which can sometimes overlap:

- **Continuum Mechanics models**: They are characterized by a continuous configuration space of the system which takes into considerations the physical aspect of the soft bodies deformations. To solve continuum problems, the most well-known and widely-spread numerical technique is the Finite Element Method (FEM) which finds approximate solutions to Partial Differential Equations (PDE).
- **Geometrical models**: they are based on some sort of geometrical assumptions on the deformed shape undertaken by the soft body when specific loads are applied. The most popular approach falling in this category is the so called Piece-wise Constant Curvature (PCC) model, which discretizes a soft body in a finite number of sections

having a circular arc shape.

- **Discrete material models**: these models are based on a discretization of the continuous body in a finite number of discrete material components. Some models are based on traditional approaches employed for the modeling of rigid link robots, like pseudo-rigid models [42]. Other models, on the other hand, are based on the discretization of the soft body in a finite number of discrete elastic rods, like the lumped-mass models [43].
- **Surrogate models**: also referred to as "data-driven", they do not require a physical model, on the other end they rely on large amounts of representative data, that are sometimes difficult to collect. Most of data-driven approaches presented for soft robotics modeling are based on machine learning algorithms, mostly involving neural networks models.

Due to its first sources of bio-inspiration being octopus or elephant trunks, a large portion of the soft robots produced to date are trunks actuated by cables. As a consequence the most commonly used model representation of it is PCC. This model, while being efficient, really reduces the design space to slender simple robot.

In this thesis we focus on the usage of complex structures having graded properties. This requires a continuous description. That is why we will use FEM, which has no geometries restrictions thanks to the use of meshes composed of multiple elements. It is thus possible to vary the mechanical properties of a geometry in a gradual manner by defining properties for each element. One drawback may be its computation cost, but several strategies have been proposed in the literature to alleviate these costs through hardware (cluster, GPUs [44]) or reduction methods (Model Order Reduction [45]).

1.3.3 Available implementation

The most well known available implementation of FEM are commercial softwares such as Abaqus, ANSYS or Comsol. They are powerful general tools that can be applied to a wide spectrum of physical problems ranging from structural dynamics, fluid-structure interactions, contact and thermodynamics. They provide a ready made and user-friendly framework that can be easily used for specific studies on multiphysics systems. They have been widely used to model soft robots, for example in [46], [47] and [48]. At the same time, their generality intrinsically entail an increased computational cost and the simulations, especially when dynamics are involved, can take a lot of time to converge.

There are also software alternative which are "academic friendly" compared with the commercial software, which are more suited for engineering purpose than theoretical model testing and implementation. For example [35] to design and simulate tendon driven soft robot, or the FEniCSx computing platform [49] that allows user to program efficient FEM through high-level python interface. In addition to these, exist the open source software SOFA for Simulation Open Framework Architecture, which provide a wide variety of tools to simulate deformable structures and is used for medical application as well as soft

robotics. We will use this framework in this thesis.

1.3.3.1 SOFA

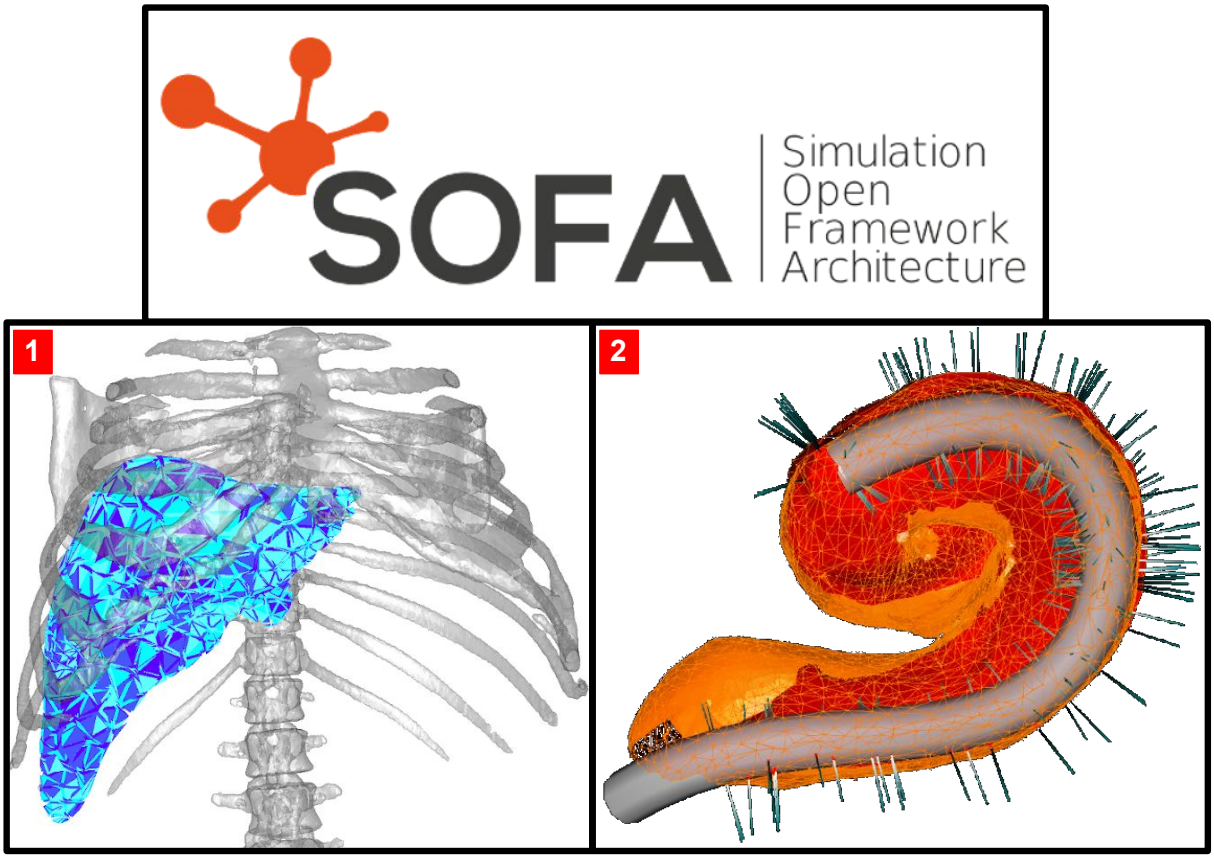

Figure 1.11: SOFA logo with two example of medical application. (**1**) Representation of organs in order to assist or train surgeon [50] for example with cochlea operation (**2**) [51].

In 2007 [52], a group of researchers from different institutes released SOFA as an open-source C++ library (github sources) which was originally presented as a computational environment for medical simulations [53]. In the following years, SOFA became a comprehensive high-performance library (implemented for multi-core, multi-GPU [54, 44]) that have been widely implemented for different application fields. It handles collisions and contacts precisely [55], as well as multi-physics behaviors [56, 57]. It is also capable of interacting with sensing hardware (Kinect, OptiTrack, LeapMotion) that are commonly used in robotics, as well as with haptic devices [58].

On top of this already quite versatility software, SOFA can have "add-on" plugins which are developed for specific usage like the simulation of discrete Cosserat representation in combination with FEM (Cosserat plugin,github), the reduction of models (MOR) and in our case a plugin developed specifically for soft robotics: SoftRobot.

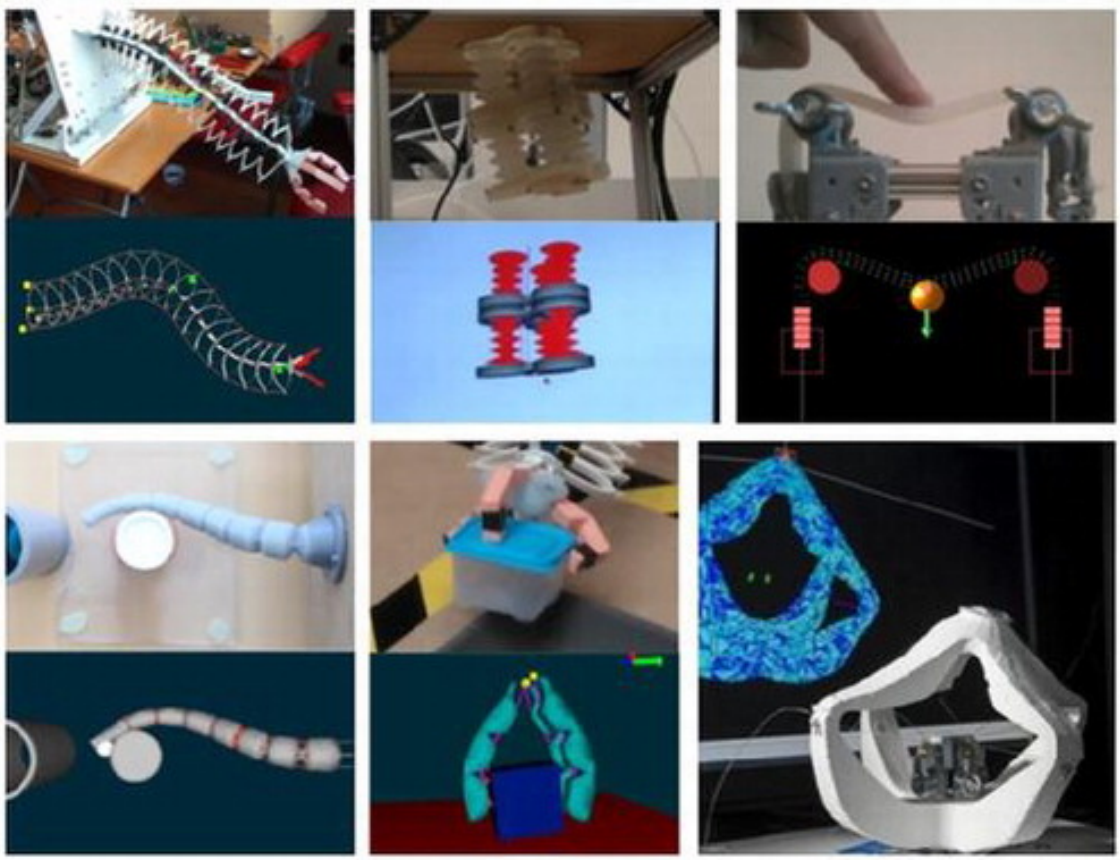

Figure 1.12: From left to right and top to bottom : control of a deformable manipulator robot based on a compliant spine [59], control from inverse simulation of pneumatic manipulator [60], Stiffness rendering [61], Optimization-based inverse model of soft robots with contact handling [62], Coupling numerical deformable models in global and reduced coordinates [63], Visual servoing control of soft robots [64].

1.3.3.2 SoftRobot plugin

The SoftRobot plugin is available in open access at: github). This plugin allows to represent different types of actuators (cable,pressure), design [65] them into complex soft systems, and control these systems via inverse simulation modeling in real time [66]. These simulations may include interaction with the environment and even self-collision scenarios [67]. We can also reduce these complex models [45] to have really fast simulations allowing dynamic control of real soft robots [68].

1.4 Contributions

As mentioned in this introduction, soft robotic is still a young field and soft robots have been first and foremost designed with homogeneous silicone. Interestingly, AM has improved dramatically since its beginning, allowing to print various flexible materials and create compliant structures with them. In these regards the contributions of this thesis are the following:

- **Design of soft robots with metamaterial**: we propose a new way of designing soft robots using a programmed metamaterial made of stochastic foam. We provide an adapted homogenisation technique that results in an anisotropic constitutive law. We demonstrate that this metamaterial can radically change the kinematic of a soft robot without changing its external shape. The results have been published in [1]. Their theoretical part is presented in chapter 3 and their validation in chapter 4.
- **Inverse simulation of anisotropic metamaterial**: we implement the material anisotropic behavior into a simulation software. It allows a user to parameterize any mesh and grade its mechanical properties. We can tune these parameters inside the simulation in a design approach and then, thanks to an inverse implementation, we are able to do initial workspace assessment. We show with the simulation and with a real setup that we are able to control a new degree of freedom not previously available with standard homogeneous silicone. The results have been published in [3]. Their theoretical part is presented in chapter 3 and their validation in chapter 4.
- **Calibration based on multi-configuration optimization**: when we compare a simulated setup and its physical counter part we have differences appearing in part from modeling approximations (in our case homogenization) of reality. We developed a new calibration approach in order to reduce these differences between simulation/reality, called sim2real gap. We used this methods in the specific case of anisotropic soft robot calibration. Finally we show the genericity of this approach and its potential for design purposes. The results have been published in [2] and are presented in chapter 5.

1.5 Organisation of the manuscript

From this point, the rest of the manuscript will be organized as follows:

In the chapter 2 we will explore more thoroughly what are metamaterials to better understand their possible application for soft robotics. We will review the current literature about its current usage in soft robotics systems, how they are incorporated into the design process and how they are simulated.

Then in the chapter 3 we will expose the solution we use in term of metamaterial, review its advantages/disavantages, present its mathematical representation and finally its numerical implementation into SOFA.

The chapter 4 will then be a general presentation of the simulation results compared to real setups. We will explain briefly the inverse model and its implementation and use it to clearly show the interest of our approach by creating a new controllable DoF.

We will finish the scientific results with chapter 5 in which we will present the new calibration approach we have developed, its theoretical explanation and its application in the use case of reducing the sim2real gap of an anisotropic soft system.

We conclude this manuscript in the chapter 6 going back about the new global approach presented during the three previous chapters, its current results, their future improvements and then the potential perspectives of these works, and its inclusion in the development of soft robotics on a global scale.

Chapter 2

State of the art

Contents

2.1 Metamaterial definition and usage **23**
2.1.1 Metamaterial history and global presentation 23
2.1.2 Main usage for each field 24
2.1.3 Flexible mechanical metamaterial 26
2.1.4 Structure characterisation and generation process 28
2.2 Integration in soft robotic systems **31**
2.2.1 Current usage in soft robotics 31
2.2.2 Simulation and design of soft systems with metamaterials . . 37
2.3 Conclusion **39**

CONTENT

In this chapter we will a do a state of the art of the metamaterial field and of its current use in soft robotics.

In section 1 we will define what are metamaterials precisely and present a global overview of their different properties depending on their fields of application: electromagnetic and optical or acoustic and mechanical.
We will then focus on a particular recent category of mechanical metamaterials which is flexible mechanical metamaterial. We will present and define its sub-categories and show for each an available existing example from the literature. We will emphasize on linear mechanical metamaterials by presenting their advantages for efficient programming of structural compliance. We will finish this section by presenting the different approaches to design and characterise this types of metamaterials.

In section 2, we will do a literature review of soft systems using metamaterials to create programmed behavior. We will classify them into the previously presented categories linear mechanical / instability-based / mechanism-based metamaterials and present for each systems the main design approach and intended application. Finally we will summarise the different approach of simulation and design of soft systems made with metamaterial and describe a task-specific generic design optimization process including, as design variable, metamaterial.

2.1 Metamaterial definition and usage

2.1.1 Metamaterial history and global presentation

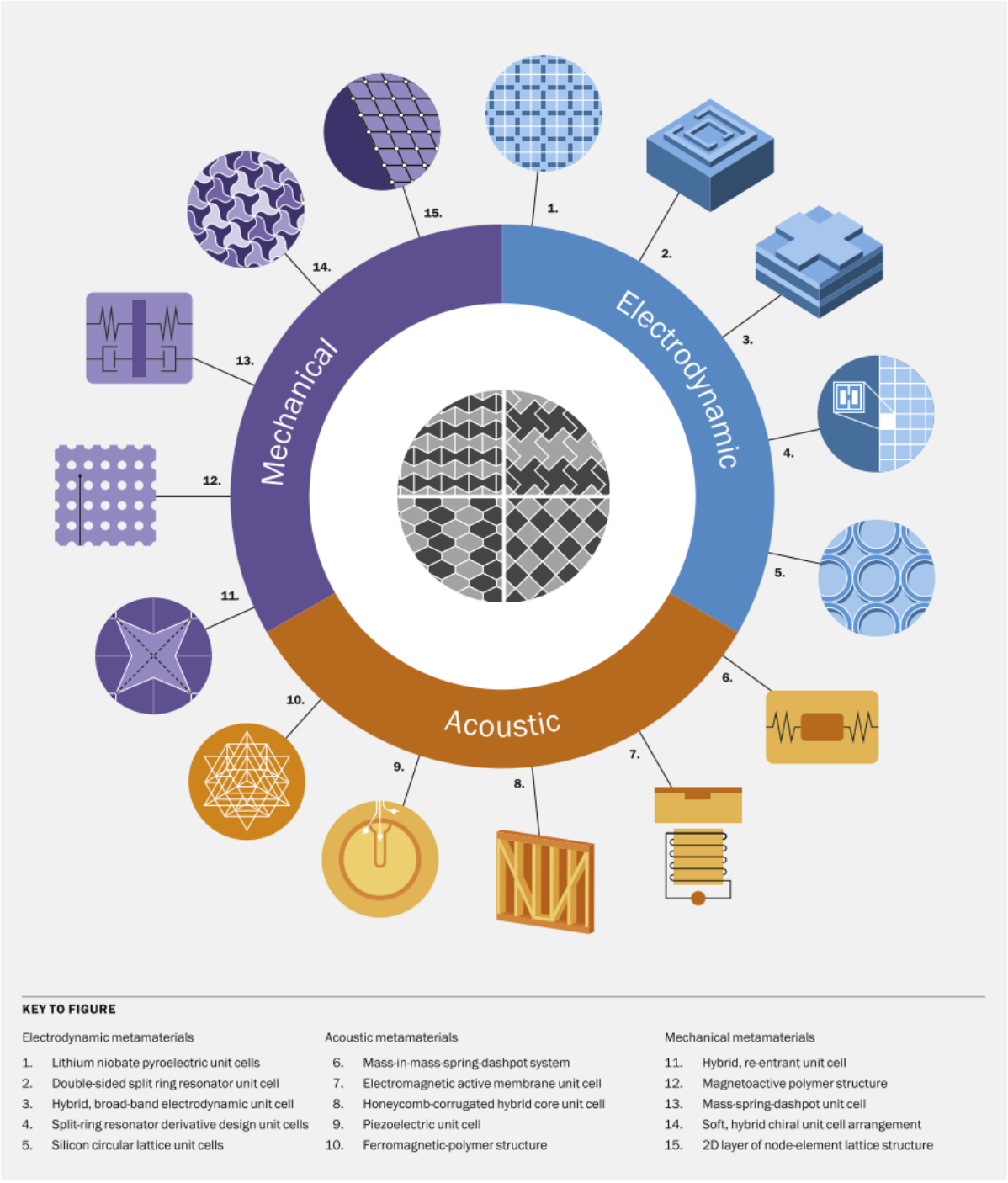

Figure 2.1: Multifunctional metamaterial composites considered under acoustic, electrodynamic and mechanical realms with a artist representation of a typical structure for each. Figure from [69].

The best way to understand the concept of metamaterial is to study its etymology: "Meta" which comes from greek means "beyond" and the Latin word materia, meaning "matter" or "material". By deduction these kind of material are artificial and mimic and/or surpass "natural" materials. More specifically, they are man-made and usually designed in order to obtain unusual effective properties which are attained by their inherent structure rather than chemistry.

This word is quite recent. It was first pinpointed 20 years ago by Rodger Walser [70] but before that, some works had already been done about their design. For example in 1920, Lindman [71] investigated arrangements of metal helices that lead to a giant effective chiral response; some say that, stained glass windows are also some kind of metamaterial due to their refraction capacity. For its part, the art of origami/kirigami allows to organize matter in repetitive patterns and can be used in order to shape matter or obtain specific behavior and mechanical properties. These properties explain why they are particularly studied and used for the design of metamaterials [72, 73].

Walser really democratised metamaterial in the electromagnetic discipline and its corresponding applications. Even nowadays, now that metamaterials have a full application spectrum ranging from mechanical, acoustic and electrodynamic (see Fig. 2.1), the default fields is electrodynamic due to its anteriority and the resulting bulk of the scientific results and the importance of its scientific community.

The rise of these metamaterials and particularly in this field follow the rise of nanotechnology which has enabled the manufacture of metamaterials composed of unit cells with sub-wavelength feature sizes, allowing by carefully designed structures to "control" some part of the spectrum. Since, electromagnetic applications and new fields have emerged: thermodynamic, optical, elastodynamic (mechanical) and acoustic [74, 75].

Mechanical metamaterials appeared more recently with the development of additive manufacturing but in itself, mechanical metamaterial were conceived well before. It is hard to say when the first was made, but the first with really unusual behavior comes from Lakes in 1987 [76] with materials that expand laterally upon stretching due to their negative Poisson's ratio. This particular property is called **auxetic**.

2.1.2 Main usage for each field

2.1.2.1 Electromagnetic and optical

With their sub-wavelength design, these metamaterials are particularly suited for **antennas** application. For example, it is now possible to create negative-index material (NIM) which is a material whose refractive index for an electromagnetic wave has a negative value over some frequency range [77, 79]. We can see on Fig. 2.2 top a conceptual representation of this phenomenon. With this property we can create **perfect lenses** which are lenses capable of going beyond the diffraction limit. We can see on Fig. 2.2 bottom an electromagnetic (2) and an optical (3) metamaterial with negative refractive indices.

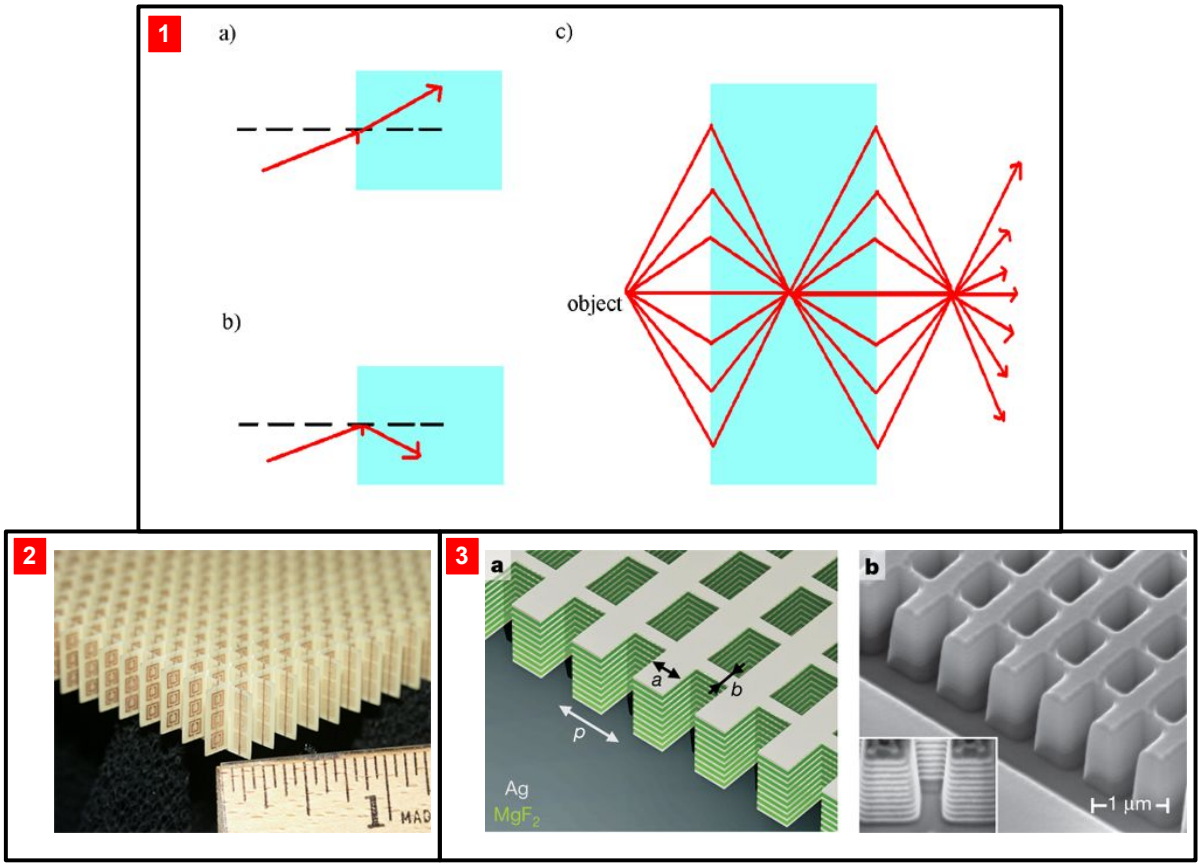

Figure 2.2: (**1**) a) When a wave strikes a positive refraction index material from a vacuum. b) When a wave strikes a negative-refraction-index material from a vacuum. c) When an object is placed in front of an object with n=−1, light from it is refracted so it focuses once inside the lens and once outside. This allows subwavelength imaging. (**2**) A split-ring resonator array arranged to produce a negative index of refraction, constructed of copper split-ring resonators and wires mounted on interlocking sheets of fiberglass circuit board [77]. (**3**) Three-dimensional optical metamaterial with a negative refractive index [78].

These materials can also have **absorbing** capabilities with impedance matching using balanced electric and magnetic responses and create perfect absorbers [80], which are materials that neither reflect nor transmit any light. Going further we can even create **cloaking devices** that direct and control the propagation and transmission of specified band of the spectrum and demonstrate the potential to render an object seemingly invisible in these frequencies [78].

2.1.2.2 Acoustic and mechanical

Acoustic metamaterial are engineered to either transmit, or trap and amplify sound waves at certain frequencies. It has similar applications as electromagnetic/optical: resonators/cloaking... For example with [81] creating a material slowing down sound propagation that we can see in Fig. 2.3.

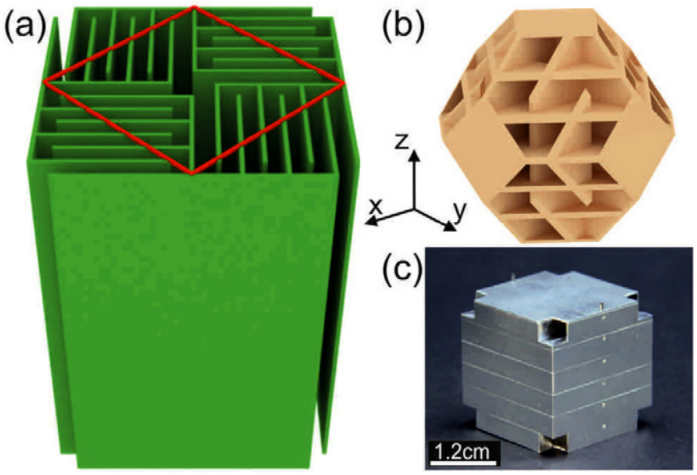

Figure 2.3: 3D labyrinthine channel system that leads to slowing down of sound propagation. Figure from [81].

For mechanical metamaterials, although they borrow design ideas from wave-based metamaterials [82, 83, 84, 85]. They also provide new challenges and opportunities. In the context of mechanical metamaterials, several recent designs have also harnessed:

- **shape morphing** [86, 87].
- **topological protection** [88, 89, 90].
- **instabilities and nonlinear responses** [91, 92].

With these material, we do not focus only on wave propagation but also on the ability to control the material deformation. It has even been theoretically demonstrated that carefully designed architectures can be used to achieve any combination of linear elastic coefficients that is not forbidden by thermodynamics [93].

In this work we will focus particularly on this aspect more than any wave propagation/resonance. More particularly what interests us in soft robotics is the ability soft robots have to deform. Hence we will focus on **flexible mechanical metamaterial** [94].

2.1.3 Flexible mechanical metamaterial

This sub-categories of metamaterials is really recent and arise from additive manufacturing (particularly 3D printing) which ease the manufacturing process and in doing so, the prototyping process. These materials are either mainly rigid with hinges (like paper) or made from flexible material and organized in lattice. The material and fabrication process lead to working with "mesostructures" (between macro and micro). Focusing in deformation rather than wave manipulation also lead to above-wavelength structural pattern.

In the review made by Bertoldi et al. [94], this new field was decomposed in 4 main categories depending on the metamaterial main composition and behavior principle. We

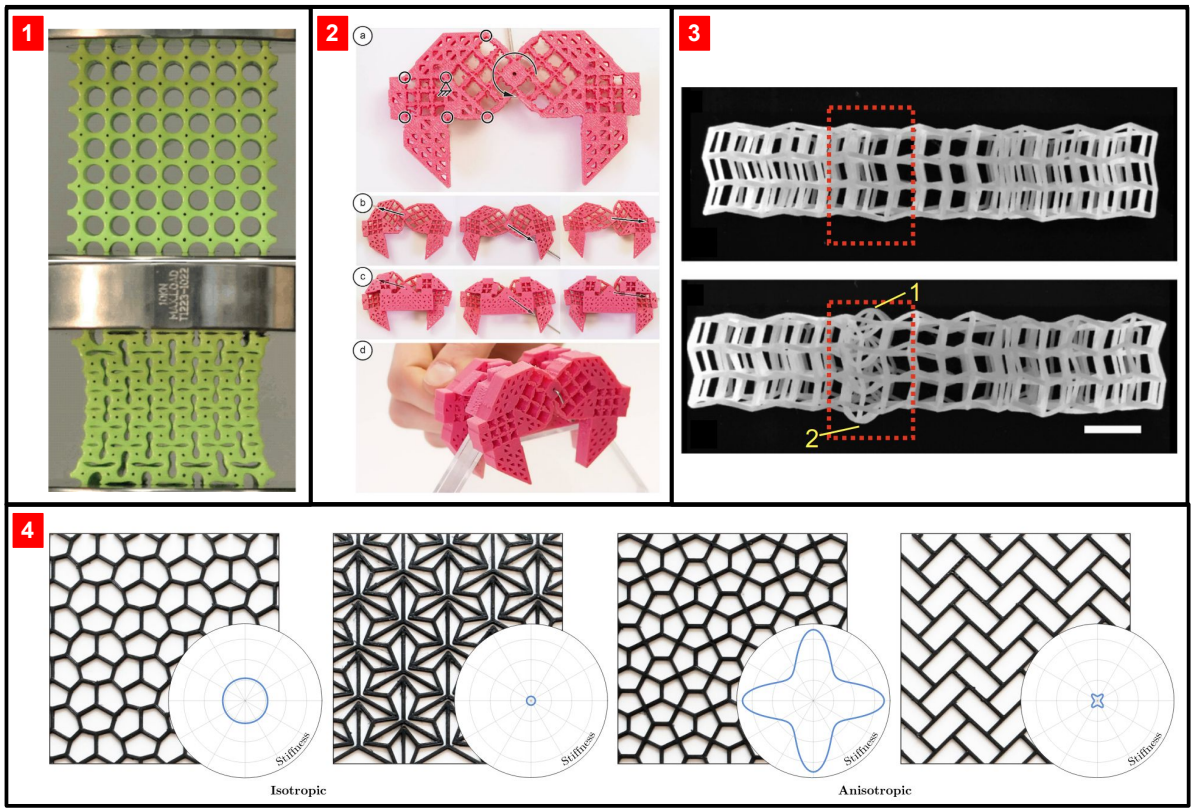

Figure 2.4: Example of one flexible metamaterial of each categories. (**1**) **Instability-based** : A rubber slab patterned with circular holes undergoes a reversible pattern transformation when compressed as a result of a collective buckling-like instability [95]. (**2**) **Mechanism-based** : Jansen walker build with metamaterial (a) leg of the Jansen walker has 6 hinges (b) As the center is actuated by a crank, the legs deform in a walking motion. (c) two hinges are constrained to rotate, but not translate, using a layer of hinges. (d) The complete walker [96]. (**3**) **Topological** metamaterials : sculpted localized buckling regions in the interior of periodic cellular metamaterials. They are robust against structural perturbations [90]. (**4**) **Linear mechanical** metamaterials : Tilings geometry with complex mechanical behavior characterized by anisotropy, nonlinearity, and large variations in stiffness among different patterns [97].

can find in Fig. 2.4 a structural example for each of these categories that will be defined below:

- **Instability-based**: Material harnessing elastic instabilities and large deformations, enabling the achievement of strongly nonlinear relations between macroscopic stresses and strains. The metamaterial building blocks can undergo buckling instabilities that result in strong but reversible non-linearities under precisely designable loading conditions. Creating mechanical metamaterials by assembling these nonlinear and multistable building blocks leads to a range of completely new functionalities. See figure example (**1**).
- **Mechanism-based**: Collections of rigid elements linked by flexible hinges, with

a geometric design that allows for a zero-energy, free motion. They generally are origami or kirigami-based, but rigid beam with soft links or organised lattice can also produce mechanisms like the one proposed by [96] that can be seen in the middle of Fig. 2.4. See figure example (**2**).

- **Topological**: Material displaying properties that are topologically protected. The properties of non-topological metamaterials are sensitive to both random and systematic changes in their micro structure. By contrast, topologically protected properties are not affected by smooth deformations of the underlying geometry or by the presence of disorder. See figure example (**3**).
- **Linear mechanical metamaterials**: Material where most of the deformations are localized at the hinges, such that the global response of the material is entirely different from the local behaviour of its constituents. Such qualitative differences between the constituents and the collective are crucial for a wide variety of heterogeneous, structured media, such as foams, granular media, and fibrous materials. This dependence of the bulk elastic properties on the geometry of the network enables the design of geometries that result in specific elastic properties. See figure example (**4**).

In this thesis we will focus on the use of this last type, linear mechanical metamaterial (LMM), which is particularly well suited for soft robotics applications. With soft robots, we usually want to control the whole deformation of our soft structure and its compliance. With LMM, we can do so in a graded fashion by controlling the heterogeneities of the structure.

Furthermore these materials are generally organized in lattices and can be assimilated as linear elastic materials. This simplifies their simulation and design process by removing instabilities and considering the metamaterial as a continuum.

Lastly these materials are manufactured in a "on-go" process (3D printing), allowing to simplify the prototyping and building phase while simplifying the global soft robot structure.

2.1.4 Structure characterisation and generation process

How does this metamaterial comes to be created is really important, because if we want to grade the flexibility of a structure this step is essential. As said previously, LMM are mostly organised in lattice but it can also be foam-like materials. In a broader description, LMM can be assimilated as cellular solids [98] for which we have the following classification on Fig. 2.5.

Lattice structure is an architecture formed by an array of spatial periodic unit cells with edges and faces. There are two- and three-dimensional lattice structures. They have good connectivity and hence a great resistance. We can see in Fig. 2.6 a collection of different programmable lattice structures coming from the literature.

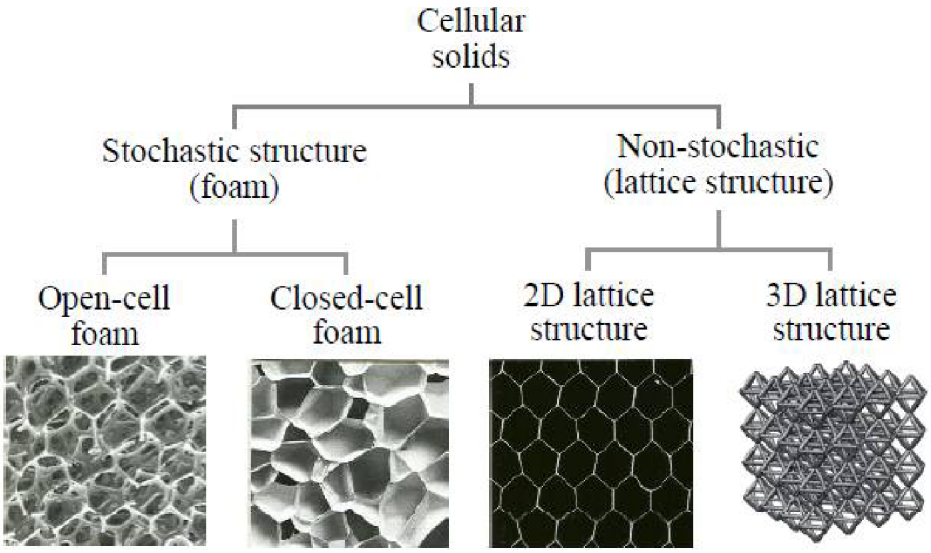

Figure 2.5: Categories of cellular solids from [98]

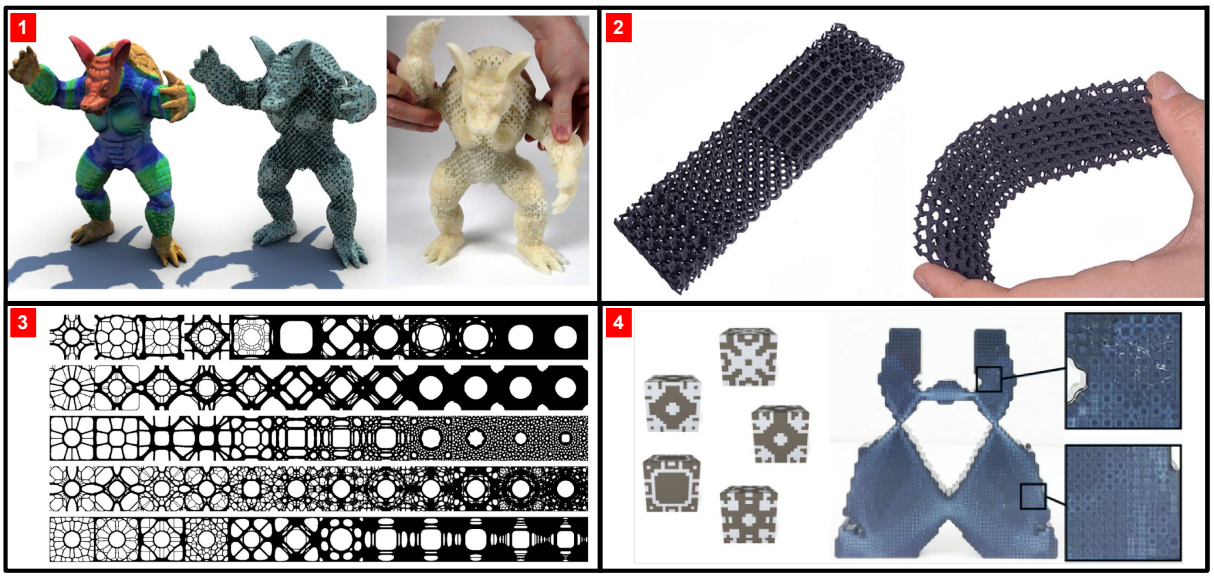

Figure 2.6: Example of different lattice structures. (**1**) Given a virtual object with specified elasticity material parameters (blue=soft, red=stiff), the method computes an assemblage of small-scale structures that approximates the desired elastic behavior [99]. (**2**) 3D Periodic Cellular Materials with Tailored Symmetry and Implicit Grading [100]. (**3**) 2D functionally graded materials optimized for maximum bulk modulus under linearly-varying volume [101]. (**4**) Two-scale topology optimization framework allowing to optimize continuous material properties mapping to printable microstructures [102].

Stochastic structures are radically different. They have a more chaotic organisation due to being generated in a stochastic way. In natural material they are akin to foam, which can be closed-cell or open-cell. They often have lower nodal connectivity as compared to lattice, and thus, their failure mechanism is dominated by bending of members. Low

nodal connectivity and the resulting failure mechanism ultimately lead to their lower mechanical strength and stiffness compared with lattices structure (like honeycombs and truss for example). But the structures are by nature simpler to conform to the gradients of a field as they do not require specific spatial alignments, allowing to conform to target elasticity fields in space without introducing artificial boundaries. We can see in Fig. 2.7 a collection of different stochastic structures coming from the literature.

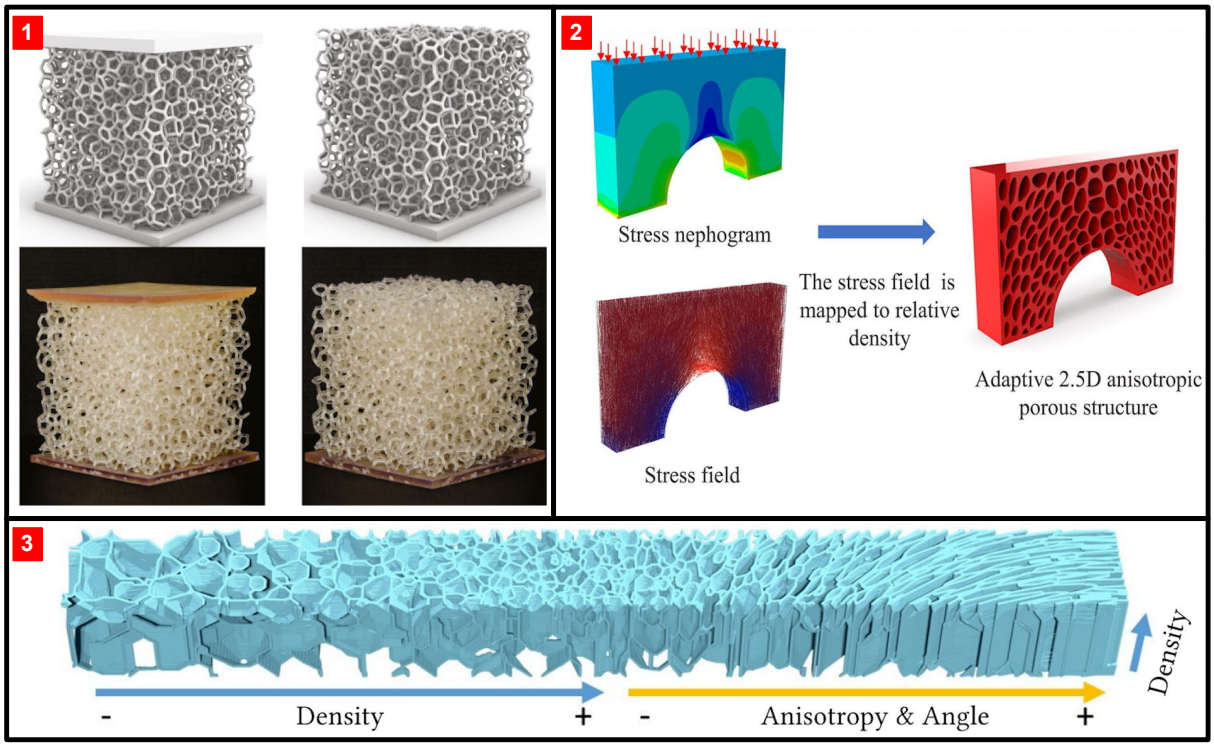

Figure 2.7: Example of different stochastic structures. (**1**) Additive manufacturing and characterisation of brittle foams [103]. (**2**) Adaptive anisotropic porous structure design and modeling for 2.5D mechanical parts [104]. (**3**) Microstructures well suited for FDM fabrication which afford a wide range of elastic behaviors, from isotropic to orthotropic [105].

Designing the fine and detailed geometry of a metamaterial while attempting to achieve specific properties is difficult. In addition, the structures are intended to fill comparatively large volumes, which quickly leads to large data structures and intractable simulation costs. Thus, most metamaterials are defined as periodic structures repeated in regular lattices. The periodicity simplifies modeling, simulation, and reduces memory costs – however it limits the possibility to smoothly grade properties along free directions.

Most approaches cast the problem as a two-scale optimisation [102]. A parametric metamaterial is defined either as a set of (parametric) periodic microstructures [106, 99] or as a random process producing geometry [107, 105]. The link between microstructure parameters and their average elastic behavior is analyzed, defining a material space. Each entry of the material space relates a choice of structure parameters to an elasticity tensor.

Linear mechanical		**nbr ref**
auxetic	[110, 111, 112, 113, 114, 115, 116, 117, 118]	9
lattice	[119, 120, 121], knitted: [122, 123]	5
Instability-based		
Buckling-based	[124, 125, 126, 127]	4
Snapping-based	[128]	1
Mechanism-based		
origami/kirigami	[129, 130, 131, 132, 133, 134, 73] [135, 136, 137, 138, 139, 140]	13
mechanism	[96]	1

Table 2.1: Current literature on integration of metamaterials into soft robots/systems and their classification.

A user or an algorithm can directly work at a coarser scale and specify the desired elastic behavior in different regions of space. For example [108] design materials with prescribed deformation from a set of predefined base materials. Most results in this area produce microstructures that can be made only with SLS/SLA.

2.2 Integration in soft robotic systems

As seen in the previous section, metamaterials offer new techniques to program into matter specific behavior. In addition, mechanical metamaterials are of particular interest for soft robotics due to their particular unusual deformation behaviors (auxetic/bistability/...) and the ability for the designer to code into matter elastic behavior of a wide range of possible linear elastic coefficients.

Taking a metamaterial approach for the design of soft machines substantially increases the number of degrees of freedom in deformation and the available geometrical parameters. Although this makes design more challenging, it also offers exciting opportunities to enrich robots with sensing, actuating, and interactive functionalities that are not accessible using conventional approaches.

Metamaterials, and particularly mechanical metamaterials, have only just begun to be integrated into soft robotic systems. In 2019 Rafsanjani et al. [109] have done a review on their current usage and has classified the different type of mechanical metamaterials used into 3 categories : Beam based, folding and cutting systems and reinforced systems.

In the following, we will study the current literature on the integration of metamaterials into soft robotics system and classify them following the flexible metamaterial categories coming from the works of [94] explained in the previous section.

2.2.1 Current usage in soft robotics

We can see in Tab. 2.1 existing works classified by their main and sub-categories. We separated linear mechanical metamaterial in two. We wanted to put forward lattices

made essentially for auxetic purpose with respect to lattices varying the general elasticity properties (including Young modulus variation). This table is probably non-exhaustive but we can extract interesting trends from it.

We can observe from this table that metamaterial-based soft robots are mostly split between Mechanism-based and linear mechanical metamaterial, more specifically between systems either harnessing auxetic behavior or systems based on origami/kirigami.

Apart from that, we have not put the topological categories because we have not found any current examples of use in soft robotics so far. This may come from the difficulty of design and the novelty of the metamaterial.

We will dive deeper into this literature and extract for each categories which approach is used to design the soft systems, with which methods the systems were simulated if it is, and for which potential application.

2.2.1.1 Soft Robots with linear mechanical metamaterials

Auxetic

Auxetic structure examples are numerous and some of them can be seen in Fig. 2.8. They have already been used for applications ranging from sensory devices [116], to actuation [115, 114, 110, 118] as well as locomotion [113, 112, 111].

These structures are essentially in 2D and based on a well known pattern which allows to variate easily the Poisson ratio from negative to positive, see Fig. 2.9 for a schematic representation of it. Concerning their simulation, a FEM of the structure, or part of it, is usually done before hand to estimate its mechanical response.

Lattice

Lattices can be composed of interconnected beams forming 3D truss, allowing to create for example locomotion in a tensegrity robot [119] but also control the global deformation of a structure with varying stiffness [121]. These lattices are formed from unit cells that are assembled depending on user specifications. Each unit cell behavior is assessed using common finite element software, like ABAQUS. To our knowledge, there is no work extrapolating this local behavior to obtain a global model of the robot. Concerning knitted lattices, depending on the woven pattern, we can also control deformation allowing for special filaments to be used as actuators [122]. In this case, only tensile response were studied.

2.2.1.2 Instability-based metamaterials

Buckling-based

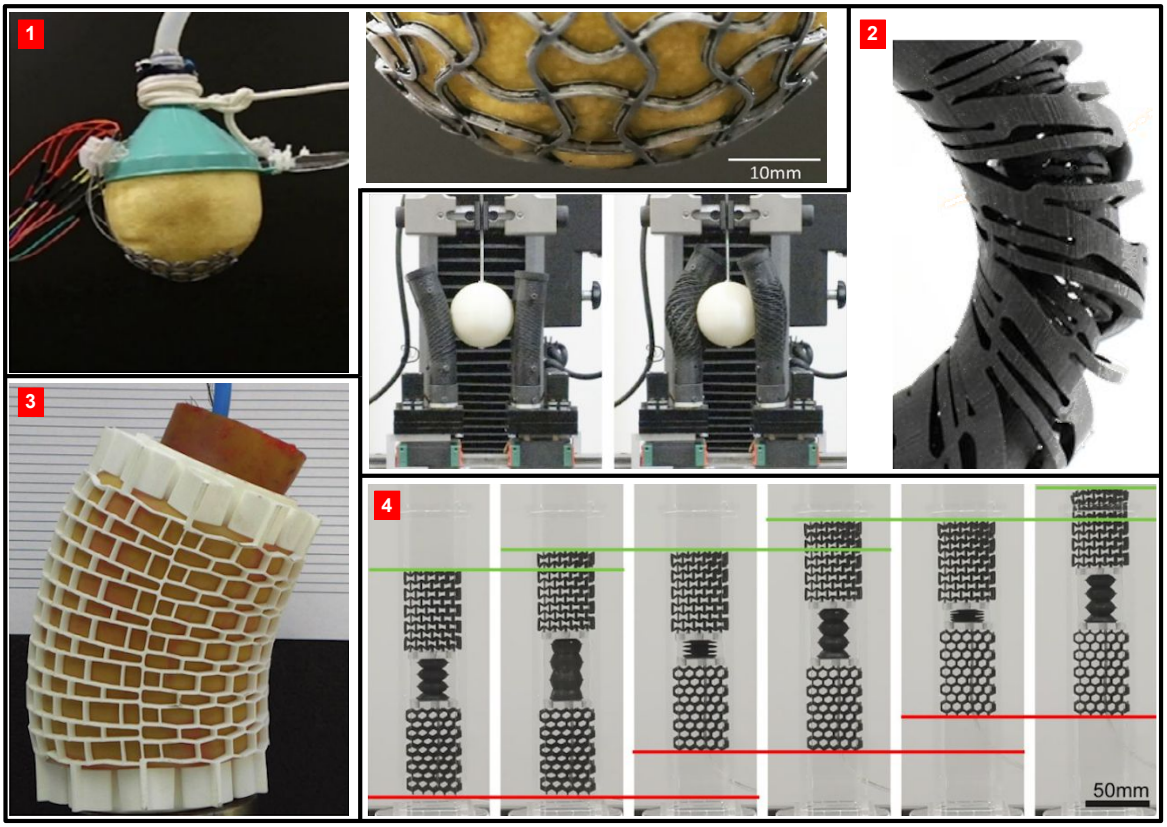

Figure 2.8: Example of different soft robotics systems using auxetic behavior has main principle. (**1**) Application of 6×6 soft capacitive auxetic sensor array to soft universal jamming gripper [116]. (**2**) Soft Robotic Grippers with 3D Printed handed shearing auxetics material [115]. (**3**) Poisson Induced Bending Actuator for Soft Robotic Systems [114]. (**4**) Locomotion of a soft metamaterial robot based on complementary auxetic materials acting as passive clutches [111].

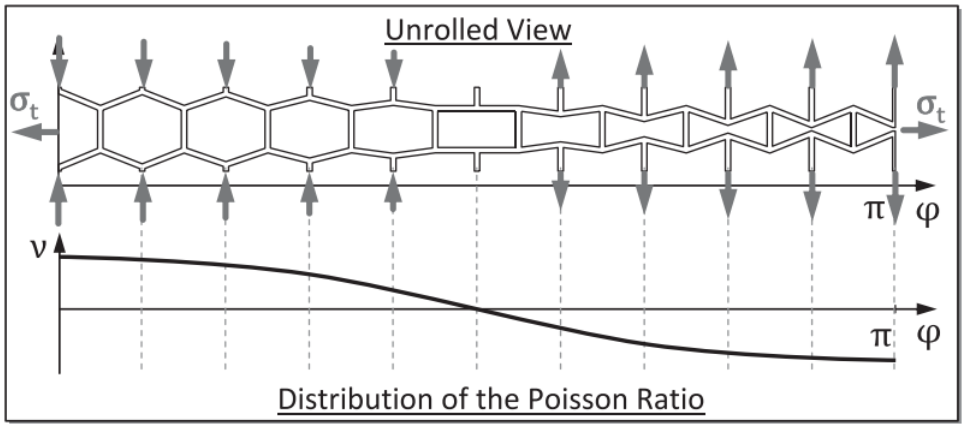

Figure 2.9: Distribution of the Poisson ratio depending on the structure geometry. Figure from [114].

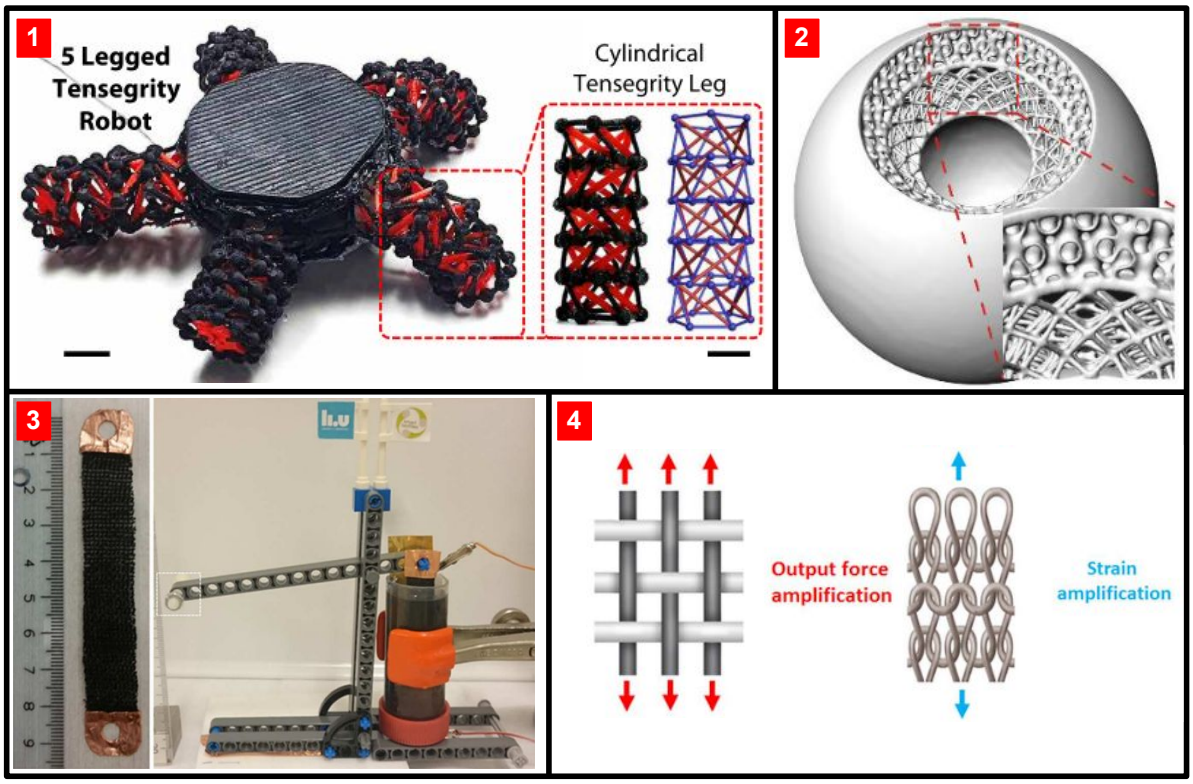

Figure 2.10: Example of different soft robotics systems using lattice structure. (**1**) Multi-directional locomotion of starfish robot with legs composed of cylindrical tensegrity beam [119]. (**2**) Hybrid lattice structure configurations allowing stiffness modulation for soft robot joint [121]. (**3**) Textile actuators (textuators) used as an artificial muscles and (**4**) schematic of its concept [122].

These systems re-use well defined buckling patterns, like the one presented in the meta-material section [95], and close them in order to create cavities that can buckle under vacuum actuation. As a result, circular movements are generated as shown in Fig. 2.12.

This circular movement can then be used in grasping systems [124] or put in lattices to compress the whole structure and produce muscle-like actuator [125]. Furthermore, by putting different air pressure actuators, we can even create rippling effects allowing locomotion [127]. These lattices can be designed by assembling different buckling cell or cells to create intended behavior. The cell geometry can even be optimized using FEM and gradient-based optimizer [126].

Snapping-based

In [128], shape memory polymer (SMP) are used to actuate a bi-stable snapping element which propels an underwater soft system. Designs were investigated in an iterative fashion to determine the influence of geometrical parameters on the mechanism. FEM was used to guess the activation energy needed by the SMP to trigger the snapping effect.

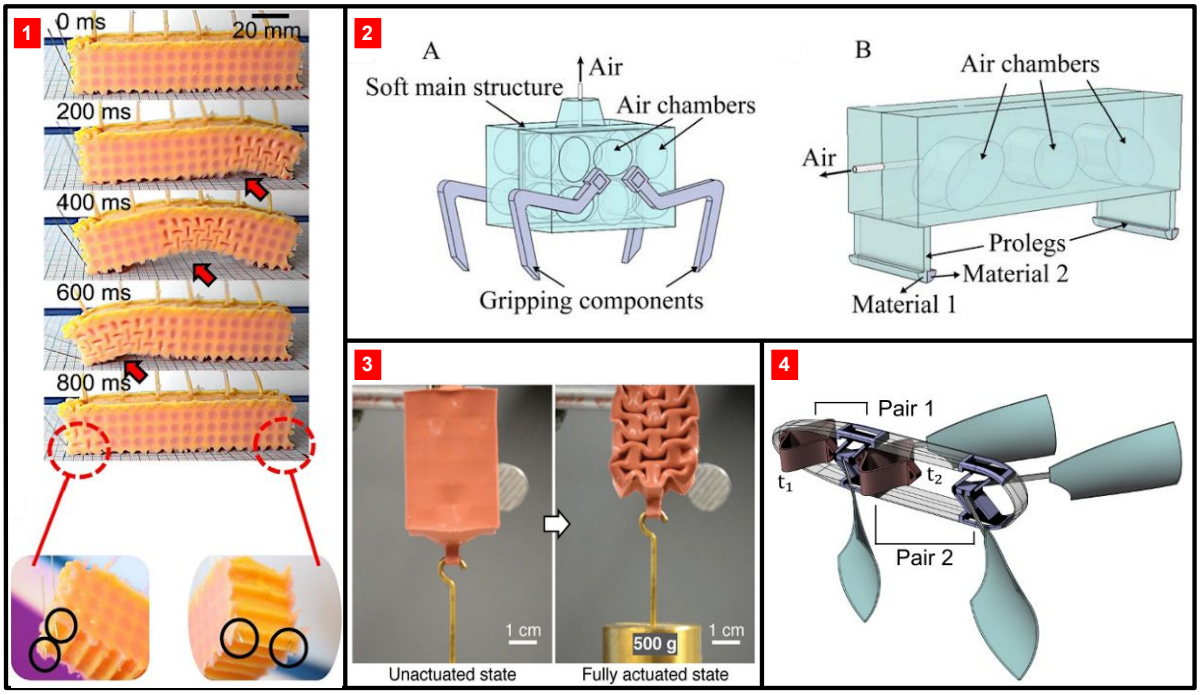

Figure 2.11: Example of different soft robotics systems using instability-based metamaterials. (**1**) Bio-inspired soft robot (Metarpillar) based on buckling actuator metamaterial units [127]. (**2**) 3D sketch of two soft pneumatic robots using buckling for (A) a soft gripper and (B) locomotion [126]. (**3**) A VAMP (vacuum-actuated muscle- inspired pneumatic structures) lifting 500g [125]. (**4**) Schematic of a robot actuated with two bistable element–muscle pairs [128].

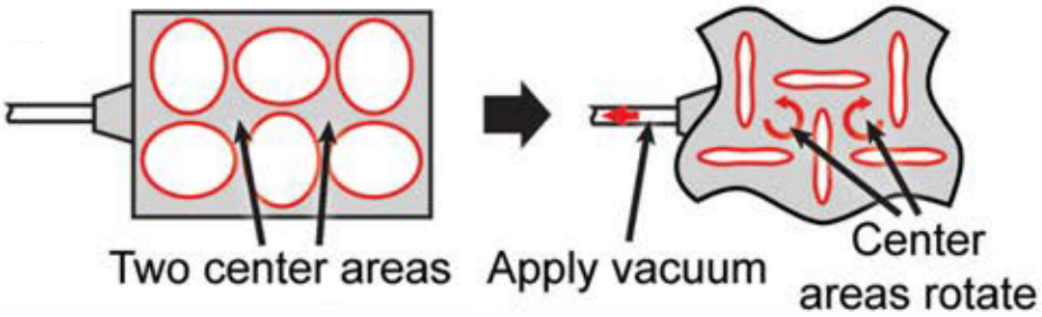

Figure 2.12: Schematics of a buckling actuator with two actuation units inducing a rotary actuation mechanism. Figure from [124].

2.2.1.3 Mechanism-based metamaterials

Origami/Kirigami

It is the most active and developed fields using the metamaterial principle. This is due to the heritage of Japanese folding/cutting art and its application in many different

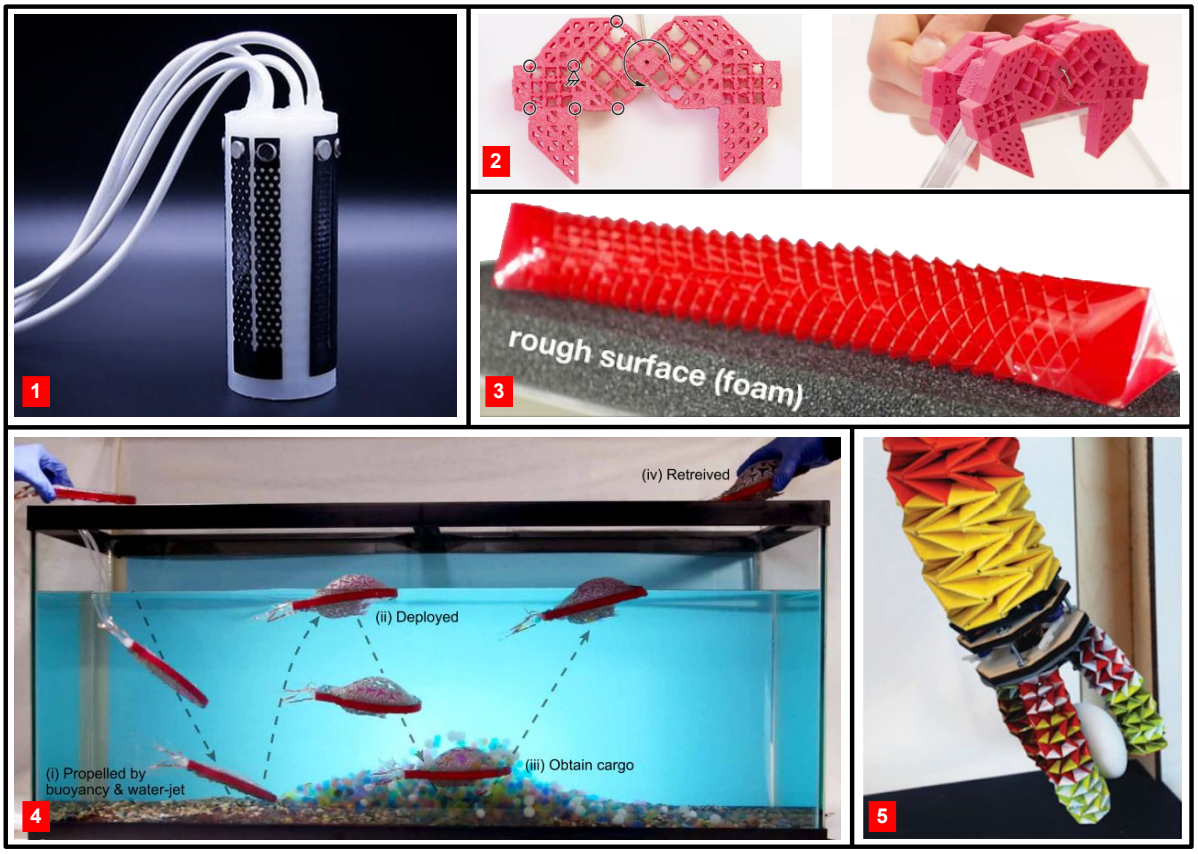

Figure 2.13: Example of different soft robotics systems using mechanism-based metamaterials. (**1**) Sensorized, soft robotic arm segment using kirigami conductive sensors [135]. (**2**) Jansen walker build with metamaterial using hinges [96]. (**3**) Kirigami-skinned soft crawlers using controllable buckling anchors [133]. (**4**) Morphing and deployable underwater machine using a multimaterial kirigami composite allowing shape and rigidity morphing [139]. (**5**) OrigamiBot-II: Three-finger origami manipulator using the origami twisted tower concept [130].

fields, which has pushed their studies and understanding further. According to the current literature, the community is capable of designing soft robots based on origami/kirigami principles for a wide range of application : from grasping [130], to locomotion [133, 139] as well as sensing [135].

Due to the maturity of the fields, lots of tools exist for design (the first protocols for design in 1996 [141]): for example, with commercial software such as the Origamizer[1] or popupcad[2] to do CAD-like design. Concerning simulation, there are also softwares available, like Merlin[3] for example [142, 143].

[1] https://origami.c.u-tokyo.ac.jp/~tachi/software/
[2] http://www.popupcad.org/
[3] https://paulino.ce.gatech.edu/software.html

Mechanism

The work of [96] provides a complete workflow from design to simulation and finally to creation of mechanism-based metamaterials thanks to a 3D editor[4] which can be used for, among others, soft robotics. It allows the creation of truss cells pattern determined by their stiffness. Their patterns are then organized around hinges and, depending on their interconnections, constrain more or less the movement around hinges.

2.2.2 Simulation and design of soft systems with metamaterials

Due to the wide range of available designs of mechanical metamaterial and their recent use in soft robotics, there is no common way to simulate and design soft systems with metamaterials. We can at least distinguish 2 main processes from this literature. One is the usage of configurable ordered lattices based on a main cell design which can morph geometrically, allowing to grad flexibility of the structure. The other corresponds to origami/kirigami metamaterial which has a great library of already existing patterns, creating mechanisms that you can choose from and organise depending on the system purpose.

The fields of soft robotics build with structures based on metamaterials lacks global cohesion on a approach or methodology. In fact it cannot have a unique process due to the diversity of the possible approaches. New examples of application will arise with type or sub-type of metamaterial, organising the usage of certain type around one efficient method like for the case of origamis or auxetic metamaterials.

At any rate, The design of soft robots is being increasingly investigated and we have to find ways to incorporate metamaterials in the process. In a review about design optimization, Chen et al. [144] address the general way of designing soft robots and incorporating metamaterials as a **design variable** in the general optimisation process, which is represented in Fig. 2.14. This variable can be iterated upon by first defining the desired properties of a given structure and then searching for a mesostructure exhibiting them. This process is called inverse design and allows to obtain a desired mechanical behavior.

To conclude, the possibility given by metamaterials to soft robots to program the mechanical properties and desired responses to external stimuli unlocks new functionalities in the paradigm of so-called morphological computation and embodied intelligence [145, 146]. The increased complexities of soft robotics systems, which may come from their geometry, material, actuation, and their intricate coupling, are making conventional theories of robot design poorly applicable. The difficulties come not only from the lack of simulation and analysis tools to effectively and efficiently predict complex mechanical behaviors of soft robots but also from the lack of powerful optimization algorithms to automate the design process. One must often rely on intuitions, experiences, or bio-inspiration for soft robot design, which can provide only limited scope.

[4] https://jfrohnhofen.github.io/metamaterial-mechanisms/

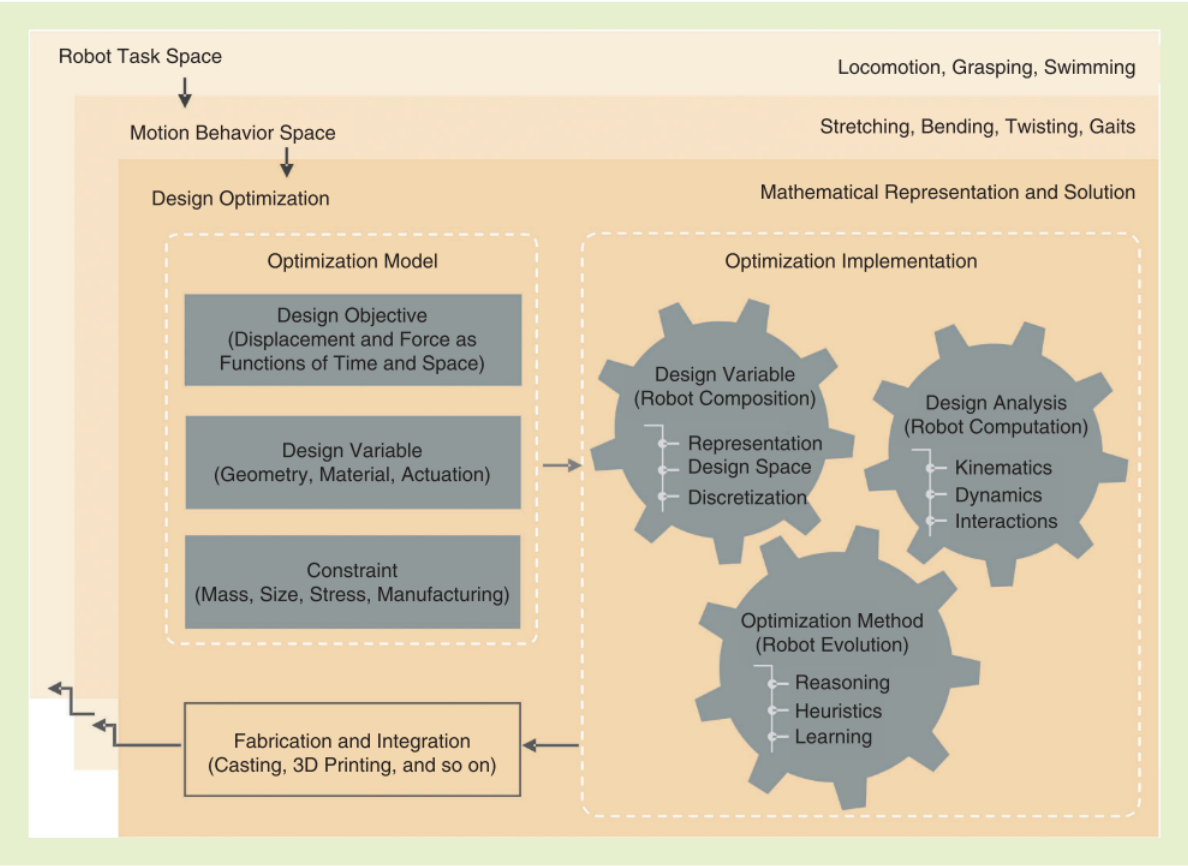

Figure 2.14: Generic architecture for design optimization of soft robots. Figure from [144].

2.3 Conclusion

In this state of the art we have first presented metamaterials throughout their development to better understand the current context of the field. In particular, we showed why it is dominated by electromagnetic applications and how the new fields of mechanical metamaterials take inspiration from it but also distinguish itself with its new applications. They are more based on deformation of mesostructure than wave propagation/refraction in microstructured material.

We then presented in more details the mechanical metamaterials. We show their interest for the creation of unusual mechanical behaviors and their transferability to soft robotics, by describing the different subcategories and illustrating them with existing examples. In particular, we focused on linear mechanical metamaterials, about the main ways to create and design them, to best justify our choice of metamaterial in the next chapter.

Finally we have done a global survey about mechanical metamaterials usage in the recent soft robot literature. We have observed that two main categories were particularly investigated: linear mechanical, for its auxetic behavior, and mechanical-based metamaterials through its wide variety of origami/kirigami application. We concluded on the difficulty of having a common design and simulation method for flexible metamaterial-based systems. This comes from the new challenges arising from their usage and their really recent incorporation into the field. Nonetheless we underline a global design process of soft robots including metamaterials by using inverse design.

To conclude, metamaterial as a reseach field is still under heavy development which offers many configurable possibilities for soft robotics, and it is hard to focus on one in particular. Their diversity is a strength but also a weakness when it comes to ease the design processes as well as having common simulation tools due to their wide range of behavior (mechanism,instability,linear) but also their different scale (macro/meso/micro). Nevertheless design and simulation complexity is inherent to soft robotic systems and the field has already come forward with diverse solutions to handle this complexity.

In this thesis we won't be presumptuous as to present a unique way of doing for design, simulation and integration of metamaterials into soft systems. We will study a specific type of metamaterial and how we can use it to design soft robots. We believe that this work is part of a larger vision and contributes to show the interest of soft robots made of metamaterials.

Chapter 3

Fabrication and numerical representation

Contents

3.1 Mesostructure based on stochastic foam **43**
3.1.1 Stochastic foam: from generation to fabrication 43
3.1.2 Interest in the context of soft robotics 43
3.2 Stochastic foam modeling **45**
3.2.1 Material elasticity tensor 45
3.2.2 Mechanical characterisation with homogenization 50
3.3 Numerical implementation with FEM **52**
3.3.1 Soft robots Finite Element Model 52
3.3.2 Geometrical non-linearities and their numerical computation . 54
3.3.3 Anisotropy implementation 56
3.3.4 Requirements for stable simulation 58
3.4 Fabrication and reality gap **59**
3.4.1 Foam generation with IceSL 59
3.4.2 FDM technology and its inherent imperfections 61
3.5 Conclusion **64**

CONTENTS

In this chapter we present the metamaterial that we use in this thesis. We explain how we model it and how this model is integrated numerically into our simulation software. Finally, we present its fabrication process with additive manufacturing.

In section 1 of this chapter we present the metamaterial we use which is a stochastic foam with gradable mechanical properties. We discuss this foam advantages/disavantages which makes it appropriate for soft robotics applications.

In section 2 we explain how we model this stochastic foam by first presenting the material elasticity tensor, how the stress and strain are linked together with the linear relation of Hooke's law. We then explain how material symmetries can reduce the number of mechanical constant needed to describe the elasticity tensor. We study in particular orthotropic tensors with which we latter approximate the foam and present the different mechanical constants needed to define it. To finish this section, we present how and with which assumptions we have homogenized the foam to obtain the mechanical constants described previously.

In section 3 we present the finite element modeling of soft robots from Newton's second law and then present the co-rotational methods allowing to simulate geometrical non-linearities. From this base we will develop the anisotropy implementation and which requirements are needed to keep a stable simulation.

Finally, in section 4 we describe in details fused deposition modeling technology, how we generate the file to print the foam with IceSL, and we can tune the parameters to achieve a desired structure flexibility. Then we show the defects induced by FDM in the final material structure.

3.1 Mesostructure based on stochastic foam

In chapter 2, we have presented an overview of the different available mechanical metamaterials and classified them in 4 main categories. We have seen by an analysis of the current literature that the usage of metamaterials in soft systems are mainly split into two of them : Mechanism-based and Linear. In the following, we present the solution used in this work and justify this choice by underlining its current advantages and drawbacks.

3.1.1 Stochastic foam: from generation to fabrication

During the state of the art we have underlined that linear mechanical metamaterial were suited for soft robotics to program the compliance of a soft structure. We had presented a general classification of their structure between lattices and stochastic structures. For this thesis, we choose to use the latter by using the structure proposed by Martinez et al., which was first introduced in [147].

They take inspiration from procedural noises in computer graphics, where an infinite amount of content is produced at low, constant memory cost while precisely controlling the statistical properties of the produced noises [148]. With these hints, they created a microstructure which is **procedurally** generated, **stochastic**, **aperiodic** in nature and directly exhibits the desired elastic behavior, without further optimization.

- **Procedural** structures allow to only model their mesostructure's geometry when needed for fabrication, removing heavy fine mesh description which are costly to handle.
- **Stochasticity** allows to grade the properties without introducing discontinuities along pre-defined boundaries.
- **Aperiodicity** removes the need for a global optimization when conforming the structures to a surface.

This foam was at first essentially isotropic and open-cell in order to be printable with SLS/SLA printing techniques, which involve laborious process of curing. In [149], Martinez et al. improved the stochastic foam from open cell to closed-cell, allowing to 3D print with traditional FDM printer and extend the material space available for design.

More precisely this new foam now allows to have graded isotropy (by varying the density) but also graded anisotropy that can be freely oriented in the plane orthogonal to the fabrication direction. We can see this foam in Fig. 3.1 and its continuous transition from isotropic to anisotropic.

3.1.2 Interest in the context of soft robotics

Advantages

This linear mechanical metamaterial is, compared to the ones already in use in soft systems, particularly focused on programming a global compliance of a given geometry in

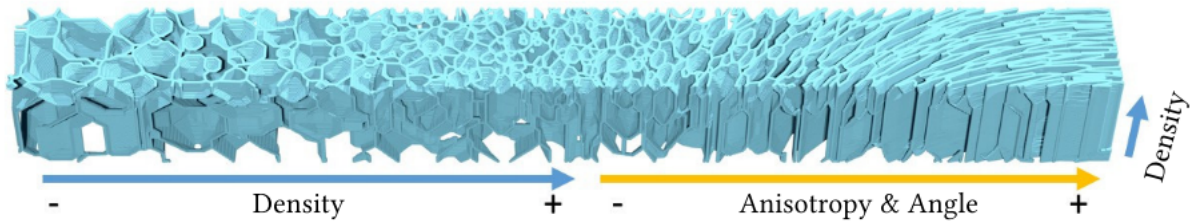

Figure 3.1: Foam elastic behaviors variation from isotropic to orthotropic by a continuous variation of its density and its material orientation. From [149]

order to have varying rigidity/softness rather than searching to exploit unusual mechanical behavior like auxetic or instabilities. This allows a wider and more continuous range of mechanical properties available to soft robot designer.

The stochastic nature of the structure and its aperiodicity allows to have smooth and graded properties distribution without any sharp jumps in mechanical properties. This will permit to have homogeneous deformation along the structure. Moreover lattice structures limit the precision to its constitutive parts which is not the case for the foam. Furthermore it is printable with FDM technology and the continuity of its structure even ease the process.

Finally a particularly important point is how to design such a foam. Fortunately, this has been made relatively easy thanks to a dedicated slicer called IceSL[1] (presented in 3.4.1) which allows to intuitively grade a geometrical shape mechanical properties, generate and fill "on the fly" the internal structure of a given shape.

Disadvantages

Concerning the modeling of the foam, a dense representation of it would be very complex due to its really intricate and stochastic pattern. Obtaining a simulation at the scale of the mesostructure details would lead to a heavy mesh in term of number of elements. It would probably be difficult to handle. Additionally, even if we simulate all the complexity of the foam, another challenge would be to take into account the self-contacts and buckling behaviors that occur in the mesostructure and that have a dominant impact on the mesoscale behavior. Due to the probably prohibitive computational time and high numerical complexity, this avenue seems difficult to explore.

Concerning its design, the choice of the printing technique limits the variation of properties in a 2D plan which is orthogonal to the printing direction as we can see on the figure showing the foam variation (Fig. 3.1). 3D printing sometimes requires the creation of material support, especially with bottom-up FDM techniques. For complex geometries such as stochastic foams, some material supports will be printed in an entangled way with

[1]IceSL: https://icesl.loria.fr

the foam, not leading always to good results. The type of filament used can also cause difficulties. This will be described later in section 4 with its consequences on the quality of the printing. Moreover, the continuity of the structure, while being in some cases an advantage, can be a disadvantage when considering multi-material manufacturing.

Finally the foam, by its definition, is porous, which can be an inconvenience because soft robots are often actuated by pressurized cavities, as explained in chapter 2.

We will see in the next section how we handle the modeling difficulty by using homogenisation. Then, in section 4 we display some of the manufacturing issues which still remain. In the future, advances in manufacturing process in addition with evolution of the presented foam conception could solve this problem.

3.2 Stochastic foam modeling

In this section we will explain the anisotropic model formulation of the foam that we will use in order to implement and simulate it in the framework SOFA. We will begin in 3.3.1 by presenting how the anisotropic mechanical behavior is represented mathematically. Then in 3.3.2 we will present how we homogenized the foam with a representative volume element (RVE) allowing to get an approximation of its mechanical parameters.

3.2.1 Material elasticity tensor

Material elasticity is defined by its deformation (ϵ) under a stress (σ), which is applied at a given time at a given location. These two notions (stress/strain) are closely related and can not be separated: any displacement of a particle will generate forces, which themselves will constrain the displacement. This relationship essentially depends on the properties of the material in question.

Hooke's law

The simplest of relations linking the constraint stress to deformation strain, or force to deformation is given by Hooke's law. It is a law of linear elasticity, which proposes to consider that the elongation is directly proportional to the force. It is assumed then that there is a linear relation between these two notions, which is a good approximation for small deformations :

$$\boldsymbol{\sigma} = \mathbb{C} \cdot (\boldsymbol{\varepsilon} - \boldsymbol{\alpha}\Delta T) \tag{3.1}$$

Here, $\mathbb{C}$ is a fourth order tensor, known as the elastic stiffness tensor which contains all the mechanical constants of the material, $\boldsymbol{\alpha}$ is the thermal expansion coefficient tensor and ΔT is the increase in temperature of the solid. In this work we choose to ignore the temperature variation and consider that we are always working under constant temperature.

We can inverse the relation defined in Eq.(3.1) as follow:

$$\boldsymbol{\varepsilon} = \mathbb{S} \cdot \boldsymbol{\sigma} \tag{3.2}$$

where $\mathbb{S}$ is known as the elastic compliance tensor. With this relation we underline that, under elastic assumption, a definition of the mechanical compliance can be found at the level of the constitutive law of the materials. This relationship also highlights an assumption of linearity between stress and strain.

However, another source of non-linearity appears in the strain, in its link to displacement field. At first, the most restrictive hypothesis is using the small displacements. This hypothesis, leads to linear equations. But this hypothesis is not very realistic, and we will see in section 3.3, how the co-rotational model allows us to extend the linear formulation to large displacements, thanks to changes of reference frame.

We characterize deformation using the infinitesimal strain tensor. We can write it as follows using Green-Lagrange form when working only on a linear regime:

$$\boldsymbol{\varepsilon} = 1/2 \, (\nabla \boldsymbol{u} + (\nabla \boldsymbol{u})^T) \tag{3.3}$$

Where $\mathbf{u}$ is the displacement vector of a particle between the initial configuration of the body and its new deformed configuration. Concerning the stress measures, in the particular case of small strain, the Piola Kirshoff tensor (in the initial configuration) or the Cauchy tensor (in the deformed configuration) are the same. As a consequence we choose to use the Cauchy stress as the stress measure.

Elastic stiffness tensor symmetries

$\mathbb{C}$ is a fourth order tensor (ie: $\mathbb{C} = C_{jikl}$) and by construction must have the following symmetries :

$$C_{ijkl} = C_{klij} = C_{jikl} = C_{ijlk} \tag{3.4}$$

Which comes from :

- The stress tensor is symmetric, which is only possible if $C_{ijkl} = C_{jikl}$.
- If a strain energy density exists for the material, the elastic stiffness tensor must satisfy $C_{ijkl} = C_{klij}$.
- The previous two symmetries imply $C_{jikl} = C_{ijlk}$, since $C_{ijkl} = C_{jikl} = C_{klij}$ and $C_{ijkl} = C_{ijlk}$.

It results that the elastic stiffness tensor only has 21 constants. With these symmetries we can now write in Voigt notation the stress-strain relations of Eq.(3.1) as follow :

$$\overline{\boldsymbol{\sigma}} = \begin{bmatrix} \sigma_{11} \\ \sigma_{22} \\ \sigma_{33} \\ \sigma_{23} \\ \sigma_{13} \\ \sigma_{12} \end{bmatrix} \boldsymbol{C} = \begin{bmatrix} C11 & \dots & C16 \\ \vdots & \ddots & \\ C16 & \dots & C_{66} \end{bmatrix} \overline{\boldsymbol{\varepsilon}} = \begin{bmatrix} \varepsilon_{11} \\ \varepsilon_{22} \\ \varepsilon_{33} \\ 2\varepsilon_{23} \\ 2\varepsilon_{13} \\ 2\varepsilon_{12} \end{bmatrix} \tag{3.5}$$

Moreover if a material has a symmetry plane, then applying stress normal or parallel to this plane induces only extension in directions normal and parallel to the plane, reducing further the number of constants. For the following symmetries we will use a three-dimensional Cartesian coordinate system, with $\boldsymbol{e_1}$, $\boldsymbol{e_2}$, and $\boldsymbol{e_3}$ as axes defined by unit vectors:

$$\boldsymbol{e_1} = \begin{bmatrix} 1 \\ 0 \\ 0 \end{bmatrix} , \boldsymbol{e_2} = \begin{bmatrix} 0 \\ 1 \\ 0 \end{bmatrix} \textit{ and } \boldsymbol{e_3} = \begin{bmatrix} 0 \\ 0 \\ 1 \end{bmatrix} \tag{3.6}$$

With this coordinate system we can see on Fig. 3.2 different classical symmetries and their plane of symmetry. We will study next some of these symmetries that we will use later on to represent the foam.

Orthotropy

We have presented the general case for the elastic stiffness tensor which has many mechanical constants (21). To simplify simulation for design purpose, we will reduce this number by considering materials with specific symmetries. A material with three mutually perpendicular symmetry planes is called orthotropic. It allows, as explained previously, to reduce the independent material constants. In this case, it brings the number down to only 9 constants to describe the material. A schematic representation of these symmetries can be seen on Fig. 3.2. The orthotropic tensor is as follows :

$$\begin{bmatrix} C11 & C12 & C13 & 0 & 0 & 0 \\ & C22 & C23 & 0 & 0 & 0 \\ & & C33 & 0 & 0 & 0 \\ & \text{sym} & & C44 & 0 & 0 \\ & & & & C55 & 0 \\ & & & & & C66 \end{bmatrix} \tag{3.7}$$

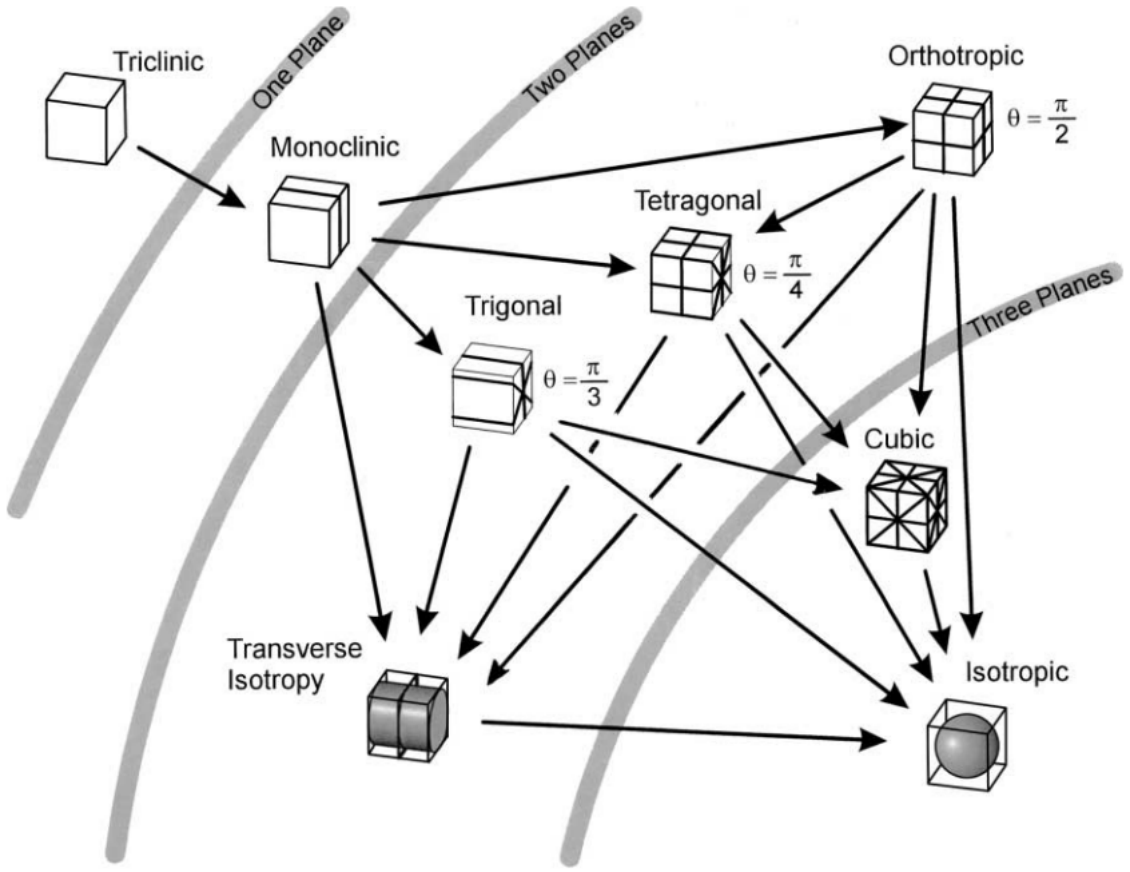

Figure 3.2: Generation of the eight types of linear elastic symmetry by the successive introduction of planes of symmetry. Figure from [150]

To simulate, and later do optimization, we can further lower the number of mechanical constants by doing another symmetry assumption, leading to a special case of an orthotropic material: transverse isotropic material. This material contains a plane of isotropy, i.e. this implies that the solid can be rotated with respect to the loading direction about one axis without measurable effect on the solid's response. We can visualise this configuration with Fig. 3.2. This reduce the number of mechanical constants down to 5. We will explain in 3.3.2 how we can parameterise the foam to be able to describe it as a transverse isotropic material. Choosing $\boldsymbol{e_3}$ perpendicular to this symmetry plane $(\boldsymbol{e_1}, \boldsymbol{e_2})$, we now have a tensor as follows :

$$\begin{bmatrix} C_{11} & C_{12} & C_{13} & 0 & 0 & 0 \\ & C_{11} & C_{13} & 0 & 0 & 0 \\ & & C_{33} & 0 & 0 & 0 \\ & \text{sym} & & C_{44} & 0 & 0 \\ & & & & C_{44} & 0 \\ & & & & & (C_{11} - C_{12})/2 \end{bmatrix} \tag{3.8}$$

Mechanical constants

To characterize elastic solids we mainly use one Young modulus (E), one Poisson's ratio (ν) and one shear (μ) modulus and that is generally enough for soft robotics. Indeed, due to the homogeneous constitution of the material we also have an homogeneous response of the material under a stimuli whatever its orientation. We can define the whole elasticity tensor of an isotropic material with 2 constants determined experimentally: E and ν (with $\mu = E/(2(1+\nu))$). Using the compliance tensor to ease the writing, we have:

$$\boldsymbol{S} = 1/E \begin{bmatrix} 1 & -\nu & -\nu & 0 & 0 & 0 \\ & 1 & -\nu & 0 & 0 & 0 \\ & & 1 & 0 & 0 & 0 \\ & \text{sym} & & 2(1+\nu) & 0 & 0 \\ & & & & 2(1+\nu) & 0 \\ & & & & & 2(1+\nu) \end{bmatrix} \tag{3.9}$$

In the context of an anisotropic, material we have different behaviors depending on which direction we apply a certain force, resulting in multiple Young, shear moduli and Poisson ratio independent from each other.

In the case of transverse isotropic material, the tensor of Eq.(3.8) can be defined only using 5 mechanical constants :

- A transversal ($E_1 = E_2 = E_t$) and longitudinal ($E_3 = E_l$) Young modulus describing the 2 different stiffness of the metamaterial.
- A transversal poisson ratio ($\nu_{12} = \nu_{21} = \nu_t$), a transversal longitudinal poisson ratio ($\nu_{13} = \nu_{23} = \nu_{tl}$) and with it we can determine the longitudinal transverse poisson ratio ($\nu_{31} = \nu_{32} = \nu_{lt} = \nu_{tl}E_l/E_t$). Poisson's ratio ν_{ij} gives the contraction in direction j when the extension is applied in direction i.
- $\mu_l = \mu_{23} = \mu_{13}$ which is the longitudinal shear modulus.

Taking the compliance tensor of Eq.(3.8) which provides the strain response when multiplied by a given stress, and including the mechanical constants defined above, we have:

$$\boldsymbol{S} = \begin{bmatrix} 1/E_t & -\nu_t/E_t & -\nu_{lt}/E_l & 0 & 0 & 0 \\ & 1/E_t & -\nu_{lt}/E_l & 0 & 0 & 0 \\ & & 1/E_l & 0 & 0 & 0 \\ & \text{sym} & & 1/\mu_l & 0 & 0 \\ & & & & 1/\mu_l & 0 \\ & & & & & 1/\mu_t \end{bmatrix} \tag{3.10}$$

.

Additionally to these mechanical constants, one last parameter is the fiber direction. It represent the direction in which the material has another property in comparison to the

simulation origin axis. Indeed, it is generally the case that the material basis is oriented differently from the simulation origin basis $\{\boldsymbol{e_1}, \boldsymbol{e_2}, \boldsymbol{e_3}\}$. In our case, the material does not have a constant fiber direction, it will vary along the material shape. This means that each element will not have an elasticity tensor based on the same basis. Due to the printing technique presented below, we work in a 2D plane so this additional parameter (fiber direction) will be a vector contained in a 2D plane. We will use a unit vector called $\vec{\boldsymbol{u}}$ for representing that direction and to construct an orthogonal basis.

We have described the relation between stress and strain and their linear link trough the elasticity tensor $\mathbb{C}$. We have shown that $\mathbb{C}$ can be simplified for certain type of materials having multiple symmetries. We have chosen to work only with transverse isotropic materials that exhibit anisotropic behavior, i.e. they have a different compliance direction while still being described by only 5 mechanical constants. This choice is limiting our use of the metamaterial foam presented but it will be justified later, when in chapter 5, we do optimization. Furthermore in a more practical approach, it eases the parameterization and design of the simulation. We explain next how we can approximate the foam presented in section 1 as a transverse material.

3.2.2 Mechanical characterisation with homogenization

As mentioned above, the complex geometry of the 3D-printed foam makes it intractable to simulate using standard numerical methods based on a mesh discretisation of the structure geometry, such as FEM. Indeed, it would require a very dense mesh. Instead, we propose to consider the foam structure as a continuum that can be assimilated to a linear elastic material described by the Hooke's law. This implies the following assumptions:

For almost any material, if we conduct a uniaxial tensile test while keeping the stress sufficiently low:

- The specimen deforms reversibly: if you remove the loads, the solid returns to its original shape, i.e. we won't study plasticity in this work.
- The strain in the specimen depends only on the stress applied to it. It doesn't depend on the rate of loading, or the history of loading. We won't study mechanical fatigue in this work, i.e. we assume the material to have an elastic behavior.
- For most materials, the stress is a linear function of strain if the strain is sufficiently small. As we wish to remain in the elastic regime, we will not apply large strains, i.e. simulation will give good approximation for only small strain. Note that the formulation will be extended to large displacement and rotations thanks to co-rotational formulation presented in the next section.

The anisotropic elastic constitutive law is based on homogenized mechanical parameters. This is a well-known method in the computational mechanics community (see for example [151, 152, 153]), which is used to model materials that are heterogeneous at a

small scale. An average macroscopic response is computed from a representative volume element (RVE), and this information allows to find the homogenized constitutive law of the macroscopic material.

To obtain the numerical homogenization of the parameterized foam, similarly to [149], we used the open source software CrAFT[2]. Given a RVE sample like in Fig. 3.3, this software uses Fast Fourier Transform (FFT) to compute the homogenized mechanical parameters.

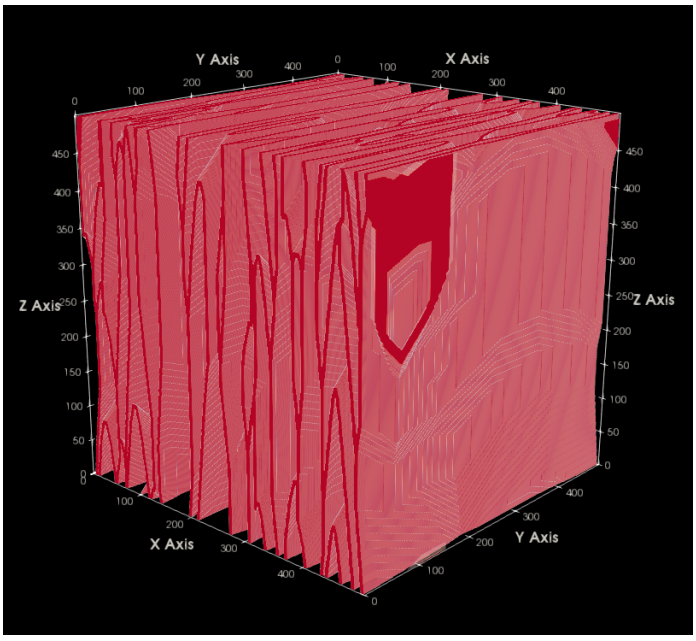

Figure 3.3: Example of a foam representative volume (RVE) used to find the homogenised properties. Here the foam shows a strong transverse isotropy.

We are making 2 additional important assumptions:

- **First**, we assume that the overall behavior of the aperiodic foam is similar to the periodic behavior of a sufficiently large base volume.
- **Second** we consider them as orthotropic material and fit the results of the homogenization $\boldsymbol{C}_{homo}$ to an ideal orthotropic tensor $\boldsymbol{C}_{ortho}$. In [149], Martinez et al. has shown that a good correspondence existed between the homogenized elasticity and a detailed simulation. We therefore assume that the mechanical constants produced with this methods are a good approximation for the foam.

In total, because the foam is considered orthotropic, the homogenization give us 3 Young moduli (E_1, E_2, E_3) in each directions of our basis $(\boldsymbol{e_1}, \boldsymbol{e_2}, \boldsymbol{e_3})$, 3 Poisson ratios $(\nu_{12}, \nu_{13}, \nu_{23})$ and finally 3 shear moduli $(\mu_{12}, \mu_{13}, \mu_{23})$.

As explained previously, we choose (for design reasons) to focus on transversely isotropic

[2]http://craft.lma.cnrs-mrs.fr

material which is a special case of orthotropy and the foam parameterization (explain later in 3.4.1) allows us to grade the flexibility from isotropic to transverse.

In the end we use only foams that are as close as possible to transversely isotropic materials (like the RVE of the foam on Fig. 3.3) or totally isotropic. We can see given different densities of the foam in Fig. 3.4 A and B that we can do this approximation because we find back $E_2 \approx E_3$.

For the homogenized samples that are nearly transverse, we take the mean of Young's moduli y and z. For the isotropic case, we do the mean of Young's moduli x,y and z.

3.3 Numerical implementation with FEM

In this section, we will first present briefly the FEM we use to simulate soft robots 3.3.1 then the co-rotational model which will allows to simulate large displacements and rotations in 3.3.2. In 3.3.3 we will present how the anisotropic constitutive law was integrated in the framework SOFA and finally, in 3.3.4, we will conclude with some stabilities requirement that we have to respect in order to avoid simulation crash.

3.3.1 Soft robots Finite Element Model

For the FEM, we rely on the framework SOFA. We assume the robot's geometry is discretised by a mesh. For the modeling of the deformations we use Newton's second law:

$$\mathbf{M}(\mathbf{x})\dot{\mathbf{v}} = \mathbf{f}_{\text{ext}} - \mathbf{f}(\mathbf{x}, \mathbf{v}) + \mathbf{H}_a^T \lambda_a \tag{3.11}$$

where $\mathbf{x}$ is the vector of position of the FEM nodes, $\mathbf{v}$ is the vector of velocity, $\mathbf{M}(\mathbf{x})$ is the mass matrix, $\mathbf{f}(\mathbf{x})$ is the vector of the non-linear internal forces of the deformable structure (depending on the material the soft robots is made of) computed by FEM, and $\mathbf{f}_{\text{ext}}$ is the vector of the external forces f_{ext}, such as gravity forces. We use a Lagrangian formulation to model the loads exerted by the actuators, assimilated as constraint forces, $\mathbf{H}_a^T \boldsymbol{\lambda}_a$ [154], with $\mathbf{H}_a^T$ the Jacobian matrix of the actuation and $\boldsymbol{\lambda}_a$ the vector of the Lagrange multipliers (one for each actuator).

In this thesis we consider the static equilibrium of the soft robot in its current configuration. This is true if the robot has a fixed part, and its motion is performed at low velocity, we can ignore the dynamics and use a quasi-static approach. The configuration of the robot at a given time is then obtained by solving the static equilibrium between the internal forces of the deformable structure and the external loads, yielding to, on any equilibrium configuration:

$$\mathbf{f}_{\text{ext}} - \mathbf{f}(\mathbf{x}) + \mathbf{H}_a^T \boldsymbol{\lambda}_a = 0 \tag{3.12}$$

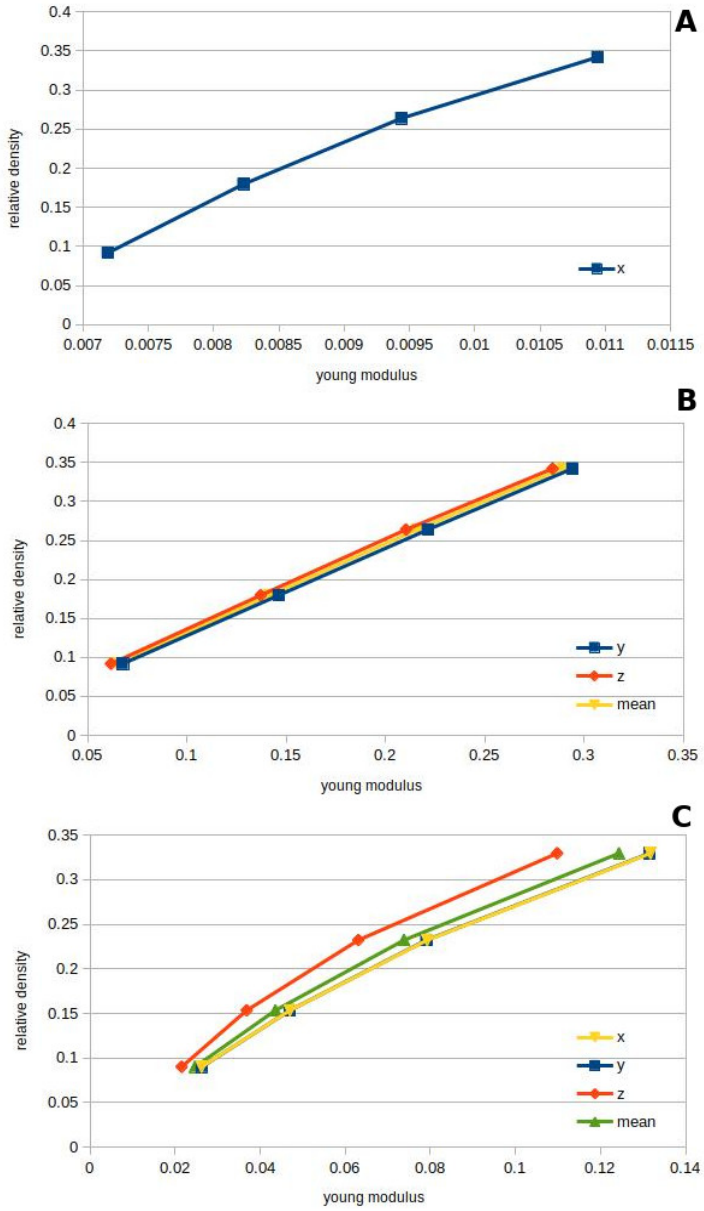

Figure 3.4: Data from homogenization of 4 samples with a relative density varying between 9 to 34%. A and B are for the transverse isotropic case and C correspond to the isotropic case. The Young's modulus shown here are normalized to a base isotropic material having a Young's modulus E = 1 and Poisson's ratio v = 0.3

When the static equilibrium is perturbed (by a change in the loads exerted by the actuators), we will classically try to find a new equilibrium position. To perform this non-linear computation, a limited series expansion of the forces around the current con-

figuration allows to bring back the problem to a (changing) linear formulation:

$$\mathbf{f}(\mathbf{x} + d\mathbf{x}) \approx \mathbf{f}(\mathbf{x}) + \underbrace{\frac{\partial \mathbf{f}}{\partial \mathbf{x}}}_{\mathbf{K}(\mathbf{x})} d\mathbf{x} \tag{3.13}$$

Where $\mathbf{K}(\mathbf{x})$ is the tangent stiffness matrix, that depends on the current position of the FE nodes. In an iterative approach to find the static equilibrium, $d\mathbf{x}$ corresponds to the displacement between two successive positions $d\mathbf{x} = \mathbf{x}_i - \mathbf{x}_{i-1}$. So at each iteration, we find $d\mathbf{x}$ and $\boldsymbol{\lambda}_a$ by solving this system:

$$\mathbf{K}(\mathbf{x}_{i-1})d\mathbf{x} = \mathbf{f}_{\text{ext}} - \mathbf{f}(\mathbf{x}_{i-1}) + \mathbf{H}_a^T \boldsymbol{\lambda}_a \tag{3.14}$$

Depending on the case, the way of obtaining $\boldsymbol{\lambda}_a$ varies. If we impose the actuator forces $\boldsymbol{\lambda}_a$, the problem is straightforward. If the actuators positions are imposed, additional equations corresponding to the actuators motion are set and $\boldsymbol{\lambda}_a$ plays the role of Lagrange multipliers for these new equations.

To model metamaterials we particularly need to focus on the internal forces $\mathbf{f}(\mathbf{x})$ and the resulting stiffness matrix. It is in $\mathbf{K}$ that the material properties are taken into account and it is here that we will adapt the constitutive elements (here tetrahedra) properties depending on its position in the mesh.

The constitutive law allows to compute the internal force vector $\mathbf{f}$ through the integration of partial differential equations coming from continuum mechanics. We have presented the Hooke's law linking stress-strain for linear elasticity and we will now see how we can represent it numerically in order to compute geometrical non-linearities to reach better accuracy in the simulation.

3.3.2 Geometrical non-linearities and their numerical computation

The linear elastic model of $\mathbf{f}$ is based on Hooke's law and the linear part of Green Lagrange tensor. It gives us the local internal force for element (e) of the mesh defined by its displacement $\boldsymbol{u}_e$ between current and initial configuration:

$$\boldsymbol{f_e} = \boldsymbol{K}_e \boldsymbol{u}_e \tag{3.15}$$

With this model, the stiffness matrix remains constant which is problematic when a given element is subjected to large displacement including rotation. The stiffness matrix basis being fixed, this leads to unrealistic deformation, notably a ballooning effect. We

have to take into account this geometrical non-linearities in a way allowing to still have relatively fast simulation.

Co-rotational model

The co-rotational model for 3D deformable object provides a relatively simple way to handle this issue while offering a good compromise between computational efficiency and accuracy.

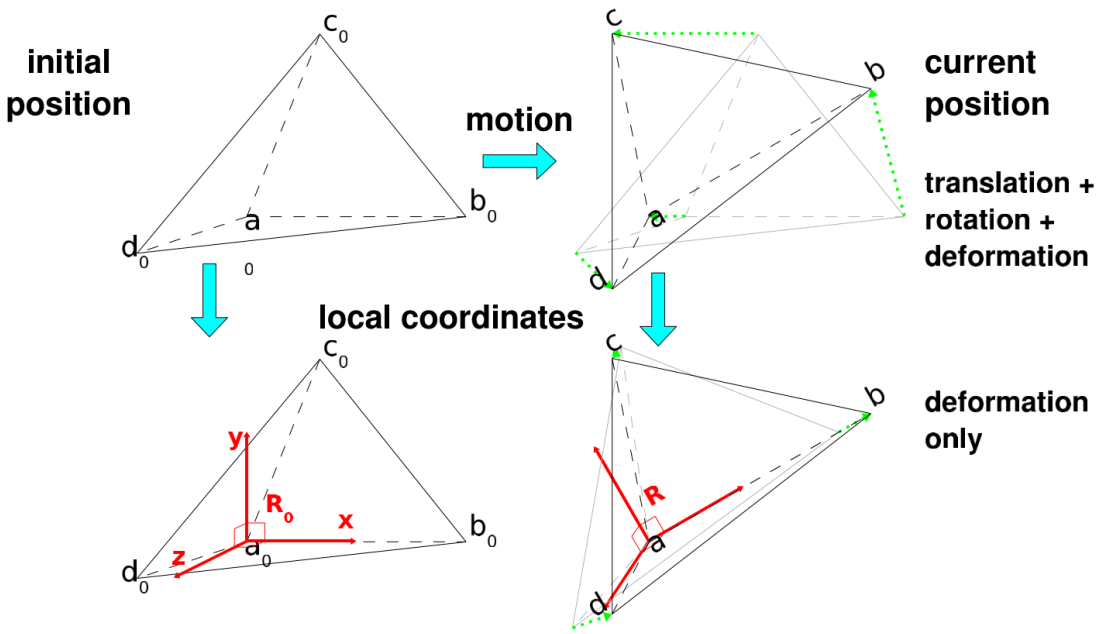

Figure 3.5: Co-rotational FEM : a local frame is computed on each element to handle large rotations. Figure from [44].

The method involves the calculation of the rotational component $\boldsymbol{R}_e$ of the element, determined via polar decomposition of the deformation gradient. For each element, the local frame is represented by the matrix $\boldsymbol{R}_e$, and $\boldsymbol{R}_e^T$ is used to put back the element into the original global frame. The displacement and forces are computed in the rotated coordinate, then transformed again into the object coordinate, we can see in Fig. 3.5 a schematic representation of this method.

This implies that the measure of strain defined in Eq.(3.3) is changed as:

$$\boldsymbol{\varepsilon} \;=\; 1/2\;(\nabla(\mathcal{R}(\boldsymbol{u}))\;+\;(\nabla\mathcal{R}(\boldsymbol{u}))^T), \tag{3.16}$$

where $\mathcal{R}$ is the rotation operator that applies a local rotation $\boldsymbol{R}_e$ back to initial state for each element of the FE mesh.

With this formulation, the force f_e at the level of the element is then equal to:

$$\mathbf{f}_e = \mathbf{R}_e\mathbf{K}_e(\mathbf{R}_e^T\mathbf{x}_e - \mathbf{x}_0) \tag{3.17}$$

where $\mathbf{x}_e$ provides the current local position in the global frame, whereas $\mathbf{x}_0$ is the rest position of the nodes, in the local frame of the element. $\mathbf{K}_e$ is the elementary stiffness matrix which remains constant in the element's reference frame. The final stiffness matrix of the element ($\mathbf{K}$) is then built from the product of the matrices $\mathbf{R}_e\mathbf{K}_e\mathbf{R}_e^T$. From a computational point of view, with respect to a purely linear model, co-rotational model adds the cost of a polar decomposition, and a need to solve an additional system at each time step to compute $\mathbf{K}$. However, for most of our soft robots, using this model provides a good approximation of their global behavior at high rates, although the non-linear elastic behaviors are neglected (hypothesis of large displacement but small strain). Co-rotational formulation have been shown to give goods results to represent material like silicone ([155, 156, 157]) as long as the deformations are mostly large rotations [45].

In the case studied for this thesis, the hypothesis of large displacements and small deformations is adapted: The large displacements on the robots will be realized by deformation, but the stochastic foam must not be locally deformed too much, especially in compression, in order not to undergo self-collisions (and radically change its behavior) and not to break (3D printed material are often fragile).

3.3.3 Anisotropy implementation

We will now explain how $\mathbf{K}_e$ is built using the previously defined elastic stiffness tensor. We decompose the tensor thanks to its eigenvalues and project them using Kelvin modes as described in the work of [158, 159].

This allows to define the fourth-order elasticity tensor by its material parameters and common projection tensors. This is called a spectral representation of C_{ijkl} and has the form :

$$\boldsymbol{C} = \sum_{k=1}^{n_{mode}} \bar{\lambda}_k \mathbf{P}_k \tag{3.18}$$

where λ_k are the distinct eigenvalues of $\boldsymbol{C}$, $n_{mode} \in \{1...6\}$ represents the number of distinct eigenvalues, or, the number of modes and $\mathbf{P}_k$ a 6×6 projection tensors that depend on the eigentensors ($\mathbf{A}_k$) also called the Kelvin modes ($\mathbf{P}_k = \mathbf{A}_k \otimes \mathbf{A}_k$). We won't go into details about the Kelvin modes here, please refer to Sandrine Germain work for an in-depth presentation [159].

For transverse isotropy the number of Kelvin modes is four. Two eigenvalues have multiplicity two and two eigenvalues have multiplicity one. The four eigenvalues for the

tensor previously defined in the e_3 direction (see orthotropy) are thus defined by:

$$\begin{aligned}\lambda_1(M_1=1) &= C_{33}+\sqrt{2}C_{13}(tan\ \alpha + sec\ \alpha)\\ \lambda_2(M_2=2) &= C_{11}-C_{12}\\ \lambda_3(M_3=1) &= C_{33}+\sqrt{2}C_{13}(tan\ \alpha - sec\ \alpha)\\ \lambda_4(M_4=2) &= 2C_{55}\end{aligned} \tag{3.19}$$

with

$$tan\ \alpha = \frac{\sqrt{2}}{4C_{13}} * (C_{11}+C_{12}-C_{33}) \tag{3.20}$$

with the four projection tensors $\boldsymbol{P}_i$ we then have :

$$\boldsymbol{C} = \lambda_1\mathbf{P}_1 + \lambda_2\mathbf{P}_2 + \lambda_3\mathbf{P}_3 + \lambda_4\mathbf{P}_4 \tag{3.21}$$

With Eq.(3.18) we have a more concise way to write $\overline{\boldsymbol{\sigma}} = \boldsymbol{C}\ \cdot\ \overline{\boldsymbol{\varepsilon}}$ (in Voigt notation as in Eq.(3.5)) but to implement it and to avoid ambiguity between notation its better to work directly with the stress and strain 3×3 tensor form $(\boldsymbol{\sigma}, \boldsymbol{\varepsilon})$. We can re-write it as follow :

$$\boldsymbol{\sigma} = \sum_{k=1}^{r_d} \lambda_k \mathbf{A}_k(\mathbf{A}_k : \boldsymbol{\varepsilon}) \tag{3.22}$$

The gradient of the displacement when descretized for FEM can be describe as the sum of tensor products between shape vectors and nodal displacements. Thus the Green-Lagrange representation Eq.(3.3) is written:

$$\boldsymbol{\varepsilon} = \sum_{\bar{p}} \frac{1}{2}(\mathbf{u}_p\mathbf{D}_p^T + \mathbf{D}_p\mathbf{u}_p^T) \tag{3.23}$$

with $\mathbf{D}$ being the shape vector. We can replace Eq.(3.23) in $\mathbf{A}_k : \boldsymbol{\varepsilon}$ and using the equivalence $\mathbf{A} : \mathbf{B} = Tr(\mathbf{A}^T\mathbf{B})$, we have Eq.(3.22) becoming:

$$\boldsymbol{\sigma} = \sum_{k=1}^{r_d} \lambda_k \sum_{|p|} \mathbf{u}_p^T\mathbf{A}_k\mathbf{D}_p\mathbf{A}_k \tag{3.24}$$

Using the weak form :

$$1/2 \int_\Omega \boldsymbol{\sigma} : (\nabla\mathbf{v} + \nabla\mathbf{v}^T)\, dx \tag{3.25}$$

Where $\mathbf{v}$ are test functions and Ω represent the geometry on which we work. When we develop it we have:

$$\boldsymbol{\sigma} : (\nabla \mathbf{v}) + (\nabla \mathbf{v})^T) = \sum_{k=1}^{r_d} 2\lambda_k \sum_{|p|=n} ((\mathbf{u}_p^T \mathbf{A}_k \mathbf{D}_p)(\mathbf{D}_q^T \mathbf{A}_k \mathbf{v}_q)) = 2 \sum_{|p|=n} \mathbf{u}_p^T \mathbf{K}_{pq} \mathbf{v}_q \tag{3.26}$$

With this we can now build our local stiffness matrix ($\boldsymbol{K}_e$):

$$\mathbf{K}_e = V(\sum_{k=1}^{n_{mode}} \lambda_k \mathbf{P}_k \mathbf{D} * \mathbf{D}^T) \tag{3.27}$$

with V the volume of the tetrahedron.

3.3.4 Requirements for stable simulation

Independently from the values found for a given homogenized RVE, if we experiment manually different mechanical properties, we have to respect certain relationships between parameters in order to guarantee the stability of our simulation. First to ensures that the stiffness matrix $\boldsymbol{C}$ is symmetric, we must follow:

$$\mu_t = \frac{E_t}{2(1+\nu_t)} \tag{3.28}$$

$$\frac{\nu_{lt}}{E_l} = \frac{\nu_{tl}}{E_t} \tag{3.29}$$

Also in order for the elastic strain energy to be a positive-definite function of ϵ, the elasticity tensor must be positive-definite. Material is unstable if $\boldsymbol{C}$ is not positive-definite because then, there exists a strain direction that causes a negative stress, i.e., the deformation is further amplified and the material permanently collapses into a "black hole".

To avoid that and guarantee stability Li et al. [160] propose to follow guidelines that ease the parameters settings for the Poisson's ratio longitudinal (ν_l) and for the shear modulus longitudinal (μ_l) while insuring simulation stability:

$$\nu_l = \nu_t \sqrt{\frac{E_t}{E_l}} \tag{3.30}$$

$$\mu_l = \frac{\sqrt{E_t E_l}}{2(1+\sqrt{\nu_l \nu_t})} \tag{3.31}$$

By following Eq.(3.30) and Eq.(3.31) we can now characterize our transverse isotropic material with only three mechanical parameters E_t, E_l, ν_t. This will be useful when doing material space exploration particularly for optimization. chapter 5 will present this kind of approach.

3.4 Fabrication and reality gap

We have presented the material, its properties and how we represent it numerically. The numerical model has been integrated into our software to simulate it in real time. We now present how we transfer our simulated design into a real sample with the slicer IceSL then we investigate how the printing technique induces defects and the potential consequences on the gap between modeling and reality.

3.4.1 Foam generation with IceSL

General principle of Fused Deposition Modeling

To 3D print any part, a 3D geometrical representation is used and imported in a slicer. The slicer is a software that take as input the 3D representation of a piece and then given some settings (depending on which 3D printer we will use, with which filament ect...) output a new file containing **gcode**, also called machine codes. It is basically a step by step spatial instructions that tell how the printer has to print. We call this tool a slicer because concretely it cut the piece into many slices and the printer will process them each one at a time hence the name additive manufacturing because it will superimposed each slice together reconstructing the numerical model in real 3D model.

In the work presented in this thesis we are using FDM printing technique which is one of the most affordable and easy way to 3D print. More specifically we use the printer **prusa i3 MKS** which is well known in the maker world. On Fig. 3.6 we can see the printer and in more details how the "hot end" is made. the filament which can be of varying material (the most common are PLA,PETG,ABS) will be inserted from the bowden into the heatsink and then will pass through the heater block that, depending on the material, will melt the filament at a certain temperature.

Generally a 3D printed piece is mainly empty and what interest the user is the external part of the piece and how precise this surface is. The user choose some internal density and a filling pattern which will achieve this density. We can see on Fig. 3.7 a result produced by a commonly used slicer (Cura) with the visualisation of the internal filling pattern.

On the contrary, in this work, we do not care about the fineness and precision of the surface: we focus mainly on filling the 3D volume of the part in order to have a certain behavior in case of deformation.

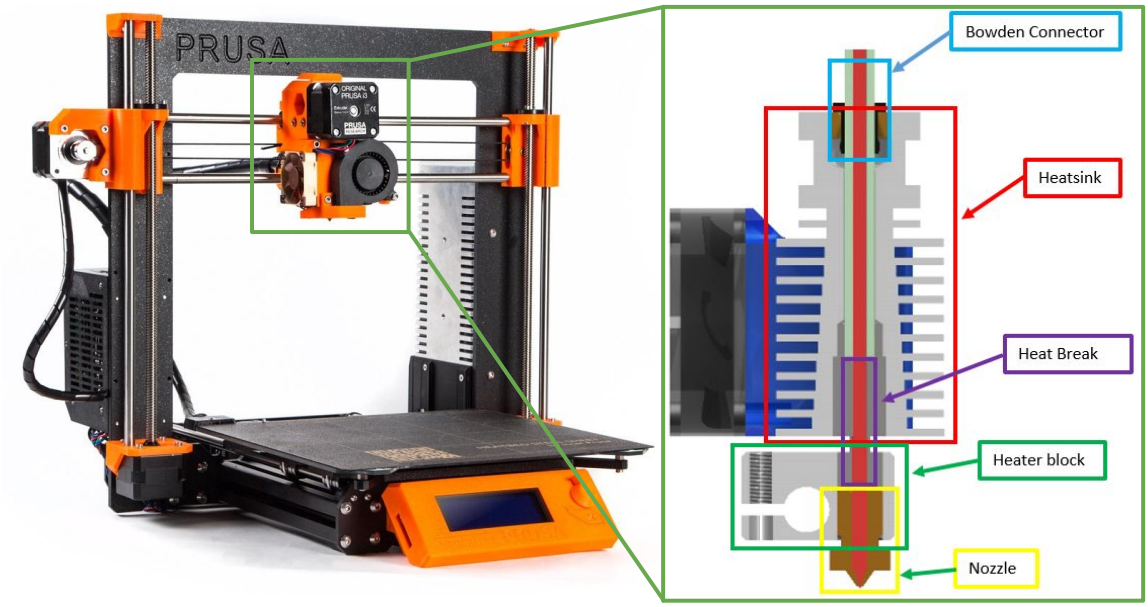

Figure 3.6: Image of a Prusa 3D printer with an additionnal schematic showing the different parts composing the "hot end" and their emplacements.

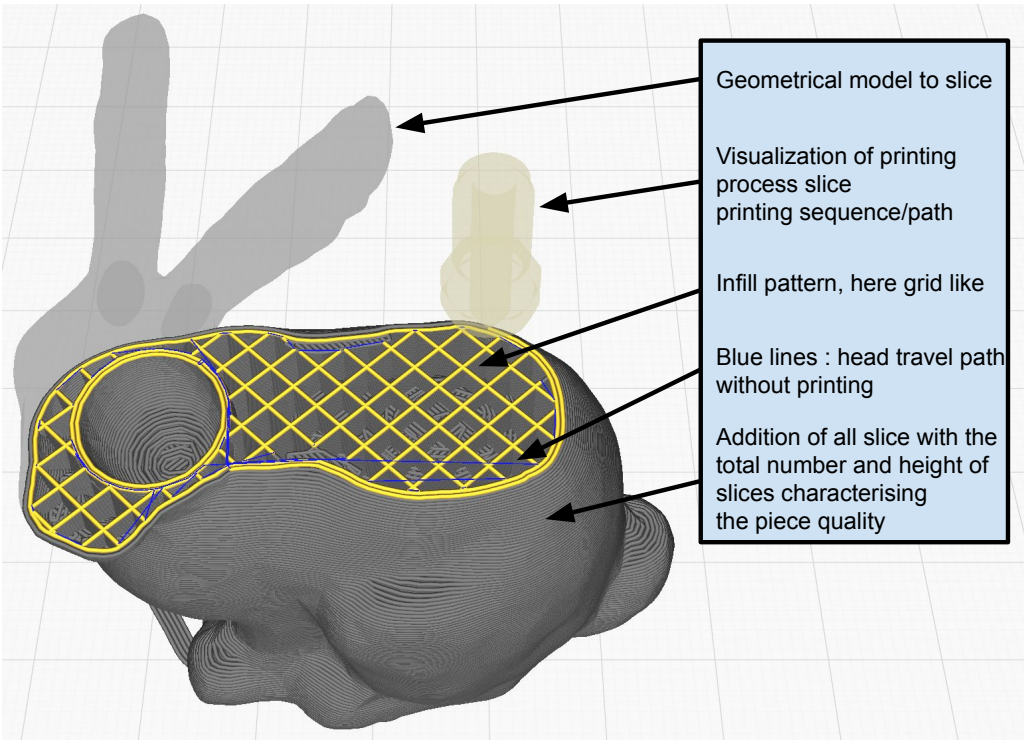

Figure 3.7: 3D visualisation of a slicing of a 3D bunny made in the Cura slicer.

IceSL Slicer

To slice our parts we use IceSL which is a slicer including the work of Jonàs et al. allowing us to print the metamaterial presented in 3.2.1.

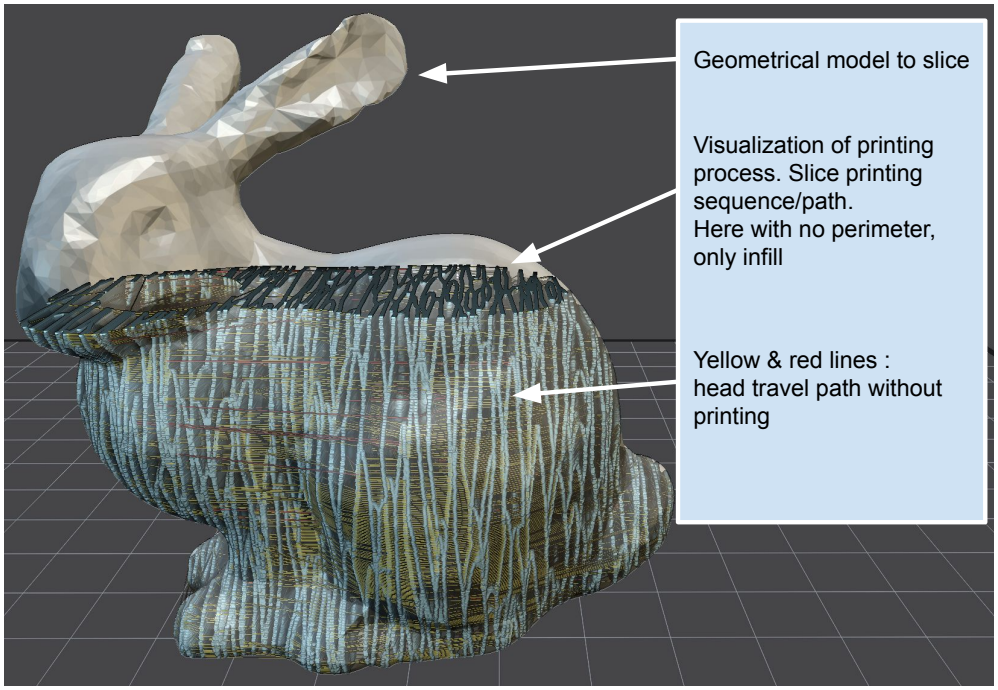

Figure 3.8: 3D visualisation of a slicing of a 3D bunny made in the IceSL slicer.

This slicer has many interesting options including the ability to "paint" on a given shape a desired flexibility and the directions in which the densities are increased or reduced, Fig. 3.9 show an example of a part sliced with the different field we can aply to it and the resulting 3D printed piece.

In this work, we will use the foam with two different "degrees" of anisotropy. As defined in [149], the scalar parameter $\gamma \in [0, 1]$, called degree of anisotropy, is one of the parameters defining a convex distance function that is used in turn to define the Voronoi diagram (used later to generate the foam geometry) of a set of points in $\mathbb{R}^3$.

In terms of linear elastic behavior, decreasing γ decreases the E_1 and increases E_2, E_3, since the Voronoi faces become comparatively more elongated in the direction 2 and 3 compared to the 1 direction.

In this work we will focus on the two extremes values of γ : either giving a near transverse isotropic foam with 0.1 or isotropic with 1. We can see in Fig. 3.3 and 3.8 examples of a meso-structure with a γ of 0.1.

3.4.2 FDM technology and its inherent imperfections

On top of the approximation done in 3.3.2 we also have to be aware of the imperfection of the printing technique. In practice, FDM induces, due to the juxtaposition of multiple slices in a vertical way, a natural orthotropy along the printing direction, which is not taken into account during the homogenization.

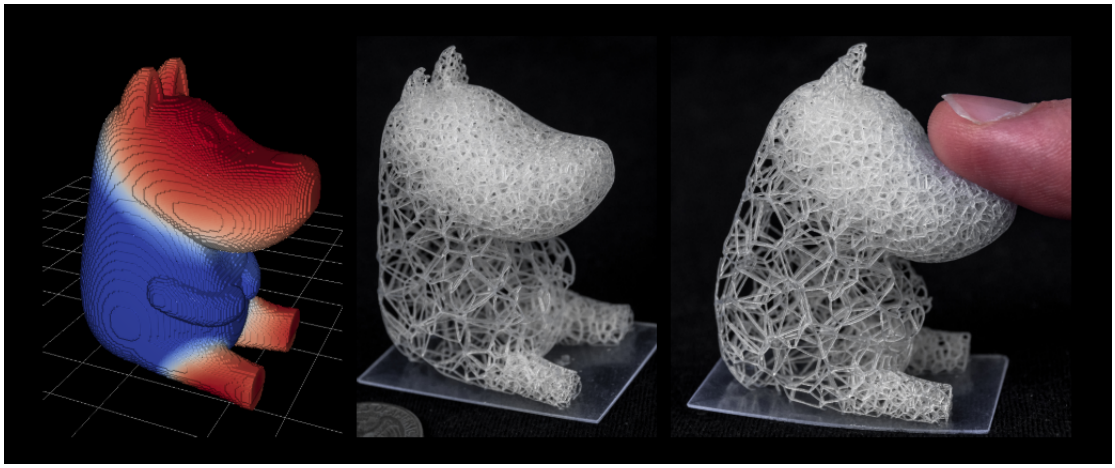

Figure 3.9: Visualisation in IceSL of a the gradation of the density applied with a "brush" (less to more density: blue to red) on a bear geometry (left). Results of the 3D printing geometry (middle) with its different compliance (right).

We also have to take into account that the printer does not always do perfect copy and give slightly different results even with a same model. This comes from the printer period of use, quality and maintenance of its part, particularly the nozzle which can be for example internaly clogged and influence the flow of matter coming out of it. Furthemore the initial calibration are different and little adjustment made during its use can influence the print quality.

Additionally the material itself used for the print can play some influence upon the final results. In this work in practice, the soft structures used are 3D printed with a thermoplastic polyurethane (TPU) called NinjaFlex (Shore Hardness: 85A and a tensile modulus of 12MPa : data from the constructor) with 1.75 mm of diameter. We print with a layer thickness of 0.3 mm and a print speed of 25 mm/sec.

The use of a flexible filament adds new problems that can be observed in Fig. 3.10. One of the main issue is oozing: it adds extra matter and render the sides a little bit stiffer. Also because the flexible filament sticks really well to the building plate the first layer of every pieces is a bit stiffer, this with the oozing creates pieces which are stratified. Depending of the size and configuration of the part, it can influence the final behavior greatly. For example if we design a beam with a fiber direction perpendicular to its length, like the one of 3.10, we have an unwanted rigidification of its longest sides changing significantly the beam behavior along them. We must therefore be careful about the piece geometry relative to the fiber direction we want to apply to it in order to reduce as much as possible these rigidified areas.

In any case we choose to use TPU because it is inherently compliant and, printed as a stochastic foam, we obtain great deformations without having to put to much load.

In practice, we observed that errors in the homogenization data of stochastic foams remain acceptable, this will be shown in the next chapter. Furthermore we will also

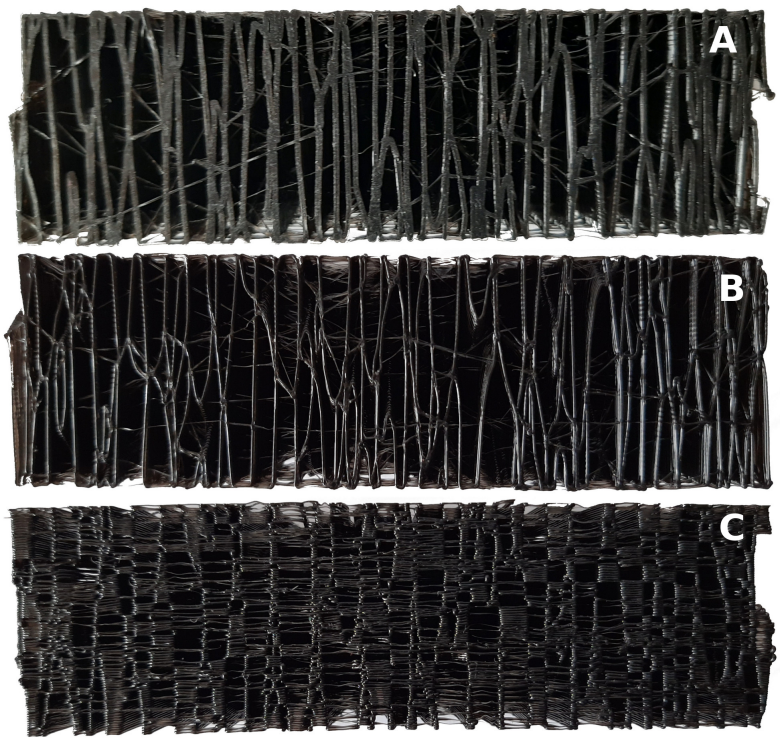

Figure 3.10: Different faces of a same beam showing the differences added due to the printing technique. The beam was printed vertically from A being the first layer to B the last. —A We can see that the filament deposit is broader. —B We clearly see the difference with the first layer —C Due to oozing the sides are rigidified.

develop in chapter 5 a way to correct among others things, setup and structural defects of a soft robots structure allowing to adjust the idealize model with the real built one.

3.5 Conclusion

In this chapter we justified our choice of metamaterial and we expose the model we use to represent it and finally how it was integrated inside the simulation framework SOFA.

With this laid out we now have a complete process beginning from the possibility to design a soft structure with anisotropic behavior which we can parameterise allowing the user to test different configurations and then print with a simple 3D printer the final design while assuring its mechanical parameters. We can see on 3.11 a schematic summary of this process.

Along this process we have made several approximation concerning our model, the main ones being :

- We describe the foam as an orthotropic continuum and we choose to restrain our anisotropy to only transverse isotropic material.
- We find the mechanical parameters by doing an homogenisation of the generated structure
- We place ourselves in the case of linear elastic material and consider with its co-rotational implementation we simulate with good accuracy large displacement and rotation but an overall small deformation.

We also pointed out that in addition to these approximations we do not take into account the manufacturing defaults particularly the one coming from the printing technique.

In the following chapters we will first present in chapter chapter 4 the results we have with the presented model on different soft robots and then in chapter chapter 5 we will present a method allowing to minimize the approximations impacts on the simulation precision.

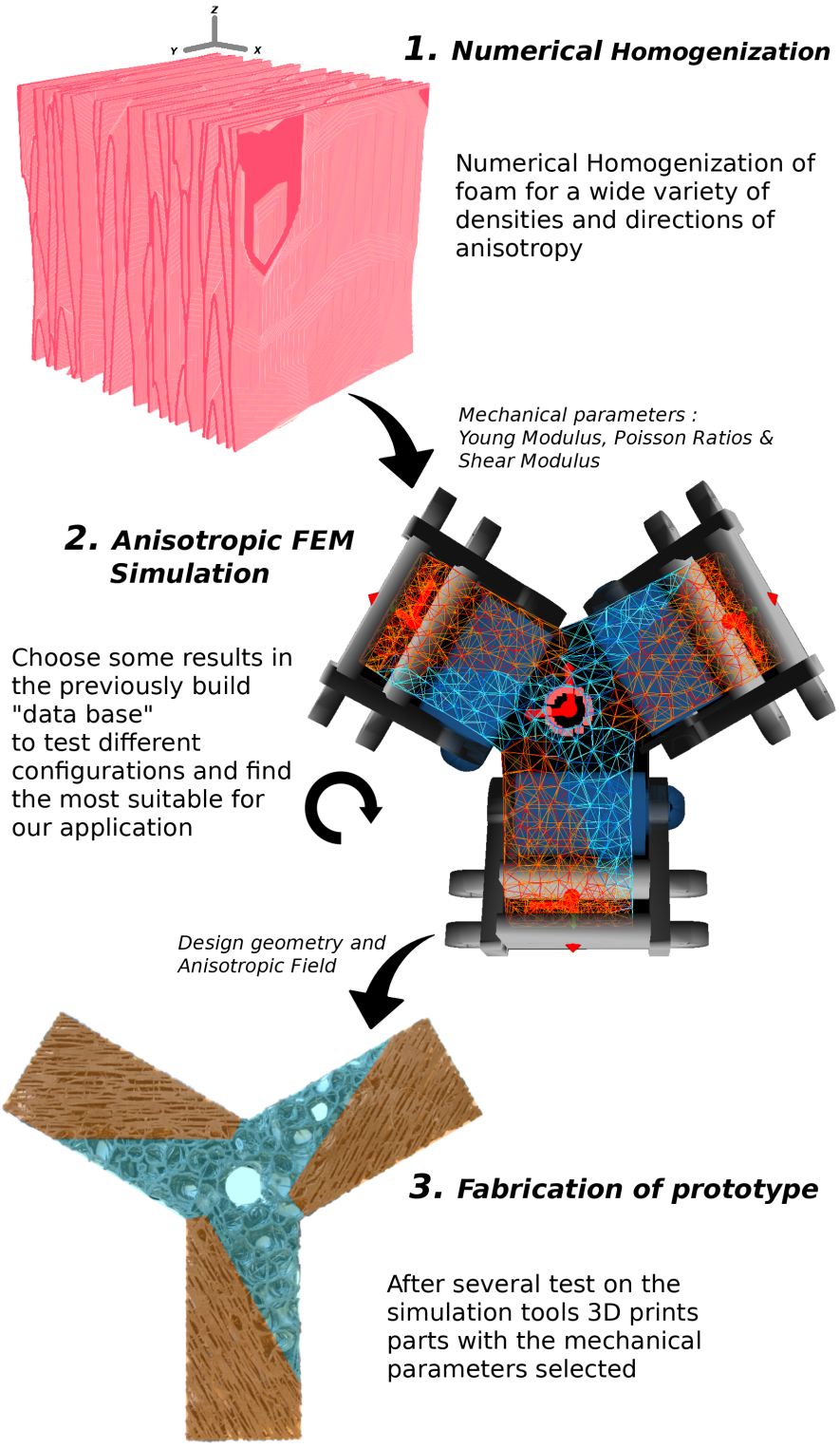

Figure 3.11: Workflow proposed: from the homogenization of the mechanical properties of the meso-structure, through the design of a robot on simulation, to the fabrication of the robot with a 3D-printer.

Chapter 4

Kinematics of anisotropic soft robots

Contents

4.1 Direct simulation validation with real setup **69**
4.1.1 Validation of the anisotropic model on a cantilever beam . . . 69
4.1.2 New kinematics on a tripod robot 69
4.2 Inverse modeling presentation **75**
4.2.1 Robot kinematic control via external target 76
4.2.2 Constraint solving 76
4.3 6 DOF controllable parallel soft robot **77**
4.3.1 Simulation design 78
4.3.2 Workspace capabilities assessment 80
4.3.3 Setup presentation and results 81
4.4 Conclusion and results discussion **85**

CONTENT

In this chapter, we test the validity of the simulation pipeline to predict the behaviour of bodies made of 3D-printed stochastic foam. We demonstrate the ability to program new kinematics using anisotropy. In particular, we actuate an additional DoF without adding new actuation source.

In section 1 a cantilever validation is done to verify if the simulation provides good results compared to the 3D-printed beams made of foam. Then we investigate the influence on kinematics of the anisotropic foam by replacing a tripod robot silicone sheet with the mesostructured foam having programmed anisotropic compliance. We test different configurations on real setup which create a new torsional movement. We parameterise the simulation for these different cases and assess the similarity between real/simulated behavior.

Section 2 presents how we can control the robot kinematics by solving an inverse problem. We explain the two steps of the method: first, a free motion resolution and second a projection of the problem into the effector/actuator space to be able to efficiently optimize it.

In section 3 we design a new simulation setup that take the previously presented tripod and use it in a more complex configuration allowing to create an additional DoF. With the inverse simulation, we are able to do an initial workspace assessment. We do multiple experiment evaluating the consequences on the workspace results of changes of actuators boundaries. We also show the anisotropy influence on the maximum range of the new DoF. Finally we present the real setup and validate the additional controllable new DoF by positioning a maze on the end effector and controlling its angles of inclination to roll a ball inside.

4.1 Direct simulation validation with real setup

4.1.1 Validation of the anisotropic model on a cantilever beam

To do a first simple validation of the model presented in the previous chapter we choose to print 2 beams. One with a γ of 1 (isotropic) and another with γ of 0.1 (transverse), both with a density of 18%. These beams are 25cm long and of 1.5cm of width/height. In this test we do not apply any force to the beams, they are only subjected to the gravity. We can see in Fig. 4.1 a comparison of these two simulated beams to there real counter part.

We find a good match between the simulated beams and the deformations observed in reality. The rigidification due to oozing does not influence enough the real beam to have great difference with the simulation because it mainly occurs at the two tip for the transverse beam and we place the beam in order to have their printing direction perpendicular to the gravity direction except for (D) where we see a lower stiffness as expected.

4.1.2 New kinematics on a tripod robot

The previous behavior validation was done without any interaction other than gravity. We will study here a more complex case with actuation and show that we still have the expected behavior.

Robot presentation

For this experiment we use a tripod robot controlled by 3 servomotors (Fig. 4.2). The 3 motors have the action of bending a soft sheet made of silicone. These motors are simple mini servomotors (Makeblock SG90) which can be controlled thanks to an electrical board (MegaPi) in degrees from 0 to 180°. In this configuration we constrain them to a maximum actuation capacity of 90°. Lower bound : the motor is vertical (0°) and upper bound: horizontal (90°). The silicone sheet is attached to the motors by pressing it with 2 plexiglas plates in addition the silicone sheet has an hole to fix device to it.

The eletrical board is programmed with arduino which is a standard framework used by the general public to program micro-controller and their input/output. Here the board receives by USB as a command, a list of angles (output of the simulation) and translate it as a PWM electrical signal to the different motors.

This robot was primarily designed in an educational purpose to help people to familiarize with the plugin SoftRobot and its simulation and control capabilities. A website was made explaining how to build and use this device Hands on Soft Robotics.

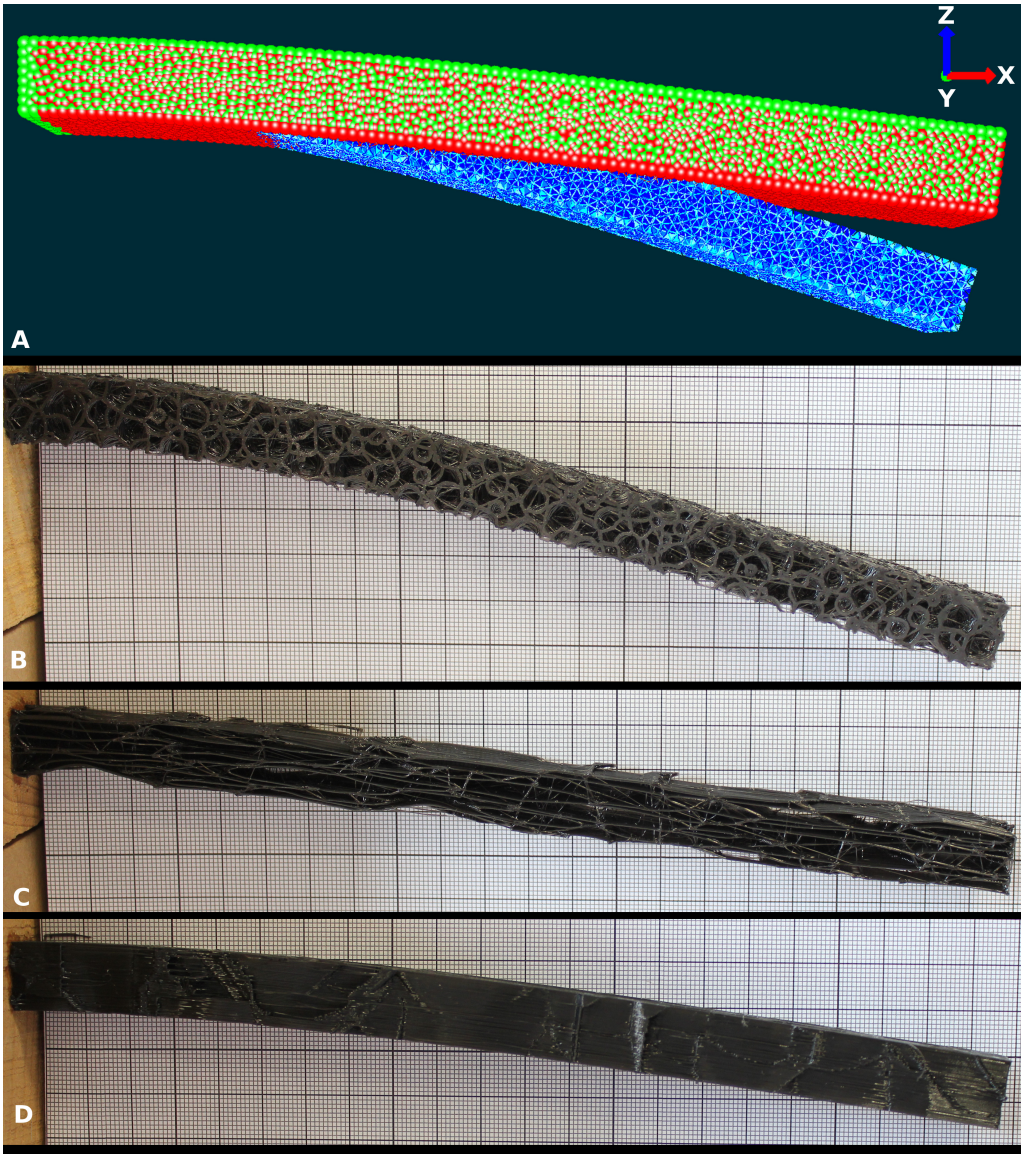

Figure 4.1: Comparison between simulated beams ($\approx 20k$ tetrahedra) and their real counter part in bending under gravity. —A. Simulation regrouping the isotropic case with the transverse isotropic in Z and Y direction with the colors blue, red and green respectively —B. correspond to the blue beam ; real bending: -48mm, simu: -47.2mm —C. correspond to the red beam; real: -24mm, simu : -22.2mm —D. correspond to the green; real: -23mm, simu: -19.1mm

Mesostructure influence on kinematics

We will show how new kinematics can be created when making the sheet in a 3D-printed mesostructure rather than in silicone.

The new movement we wanted to create and study here is torsion. We have tested two configurations in order to achieve this as shown in Fig. 4.3. The first one (A) is a combination of stiff transverse isotropic with a direction of 0,120 and 240° respectively for

Figure 4.2: The Tripod Robot is composed of a soft silicone piece actuated by three servomotors, the robot can achieve a nearly infinite number of shape configurations.

each arm with 30% of density and a softer isotropic foam of 15% of density. The second case (B) is completely transverse with a density of 15% but with a direction varying in a way to create a spiral with its fibers.

We can see in Fig. 4.4 a comparison of both mesostructured sheets with the silicone as a reference with a total angle of actuation of $+/-49°$. For both cases, a torsion is created with a reasonable total angle of rotation. We can certainly achieve, with optimization, even more torsion.

This example show clearly that by just changing from an homogeneous filling (silicone) to an heterogeneous filling using mesostructure and more particularly here an anisotropic foam we can create new behavior adding new possibility to a robot.

Simulation parameters

To simulate this setup we first have to be able to parameterize precisely the varying properties of the foam. The foam will be described by a tetrahedral mesh of 2684 elements. We study the two cases that are illustrated in Fig. 4.3 and they will be characterize as

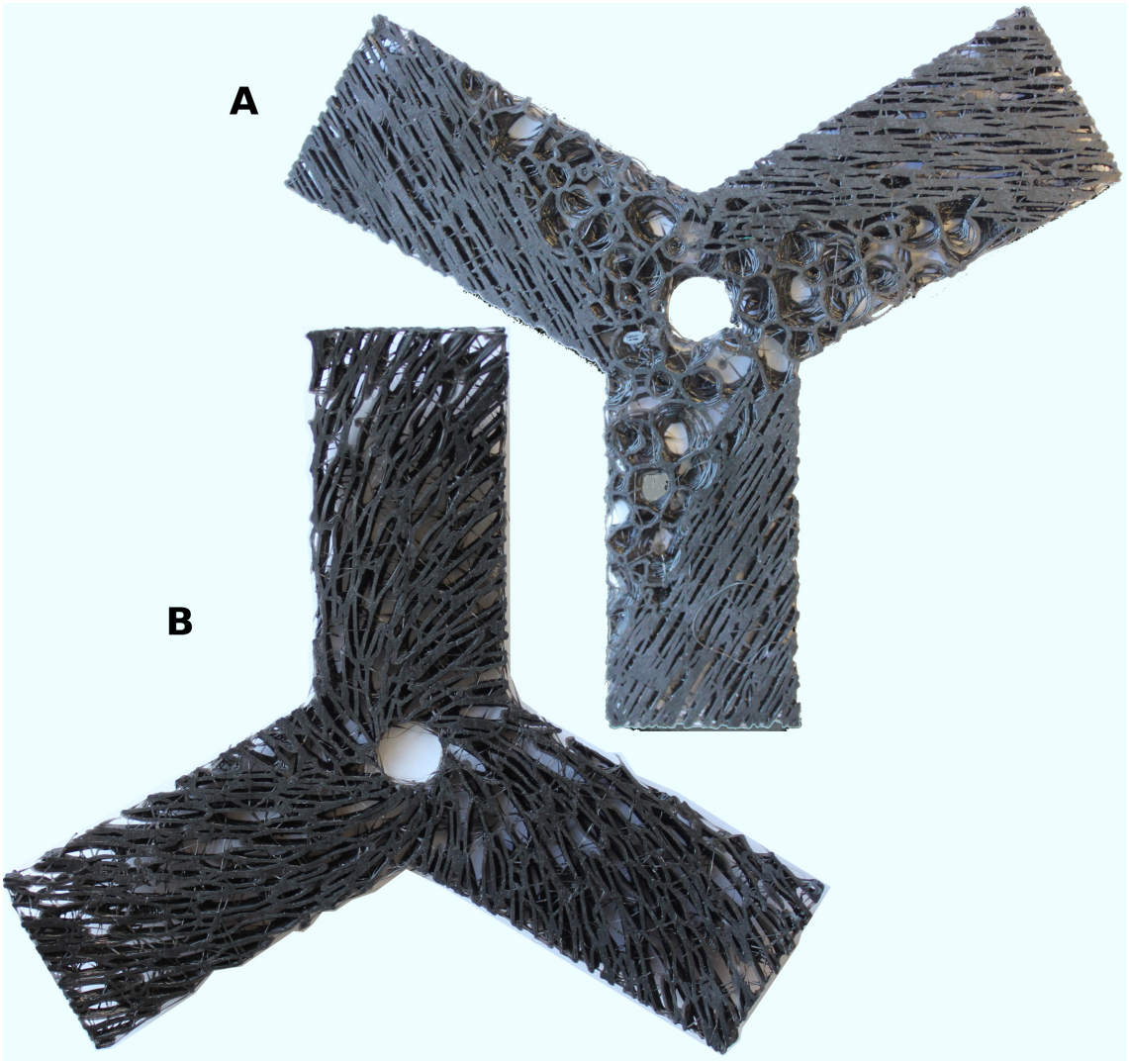

Figure 4.3: 3D-printed flexible sheets made with IceSL.

follow:

- **For A**: we have mixed isotropic and anisotropic regions. We thus select groups of tetrahedra and put to them either the homogenized mechanical parameters of the isotropic case corresponding for this density, or the transverse for which we also add the directions previously presented.
- **For B**: all the elements of the model are in transverse case and only the direction of the fiber change in order to replicate the spiral pattern. Fig. 4.5 shows that we are able to match precisely the fiber orientation of our simulated part (**B**) with the 3D printed foam (**A**).

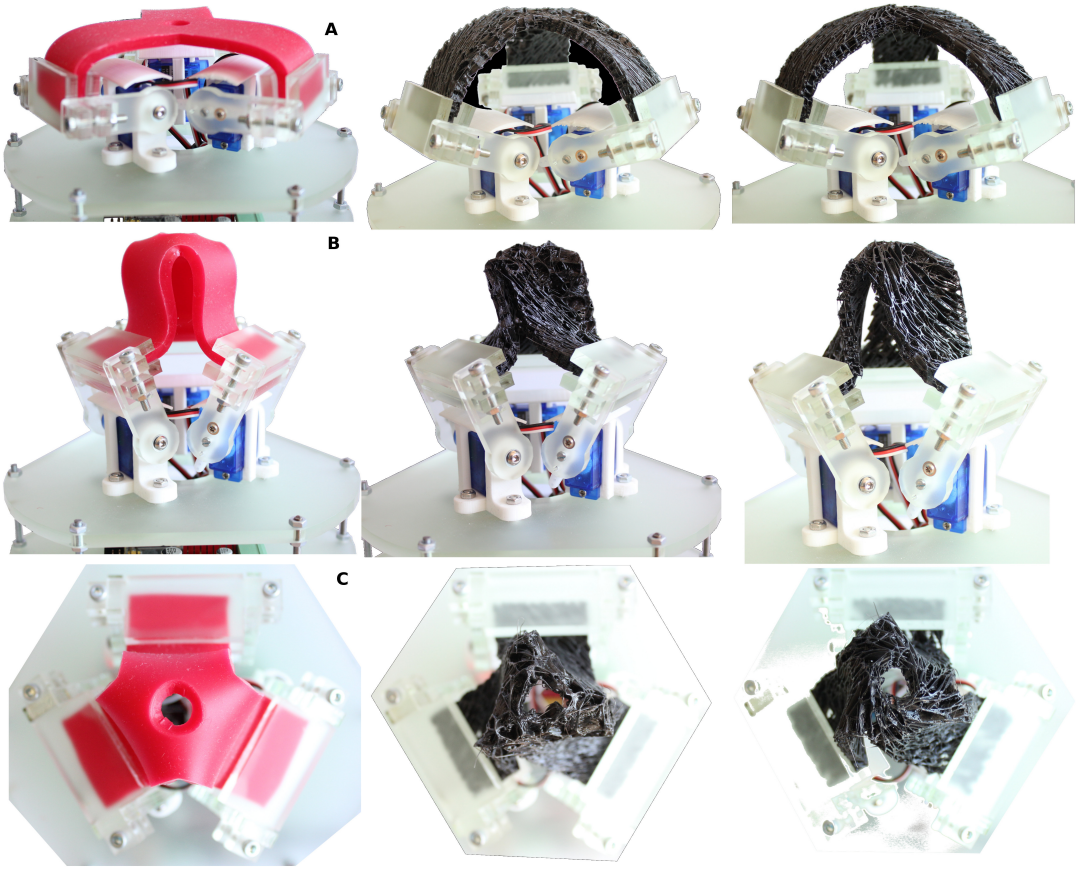

Figure 4.4: Comparison of 3 tripods : one made of silicone and totally isotropic (left) and 2 others corresponding respectively to the case A (middle) and B (right) already presented.

Sim2real results

We can see on Fig. 4.6 the 2 simulations at rest state that were made with the settings presented previously. In Table 4.1 are presented the results of these simulations when compared to their real counter part for the actuation presented in Fig. 4.4. More precisely we saved the data for 3 positions: *rest* where the robot actuation begin, *middle* is rest position plus 19° of actuation for each motors, and finally *top* position where we actuate again all motors of 19°, resulting in a total actuation range of 38°. The measure is performed by an Optitrack system with a tracker placed on the central hole of the flexible sheet. We can then compare both real and simulated movement. Here we only track the center of the soft sheet to measure its height and torsion angle.

Overall the results presented in Table 4.1 demonstrate that the global behavior of the robot can be captured by the modeling process. The direction of motions are correct and the kinematics is reproduced. In the displacements both in rotation and translation, the order of magnitudes are coherent. However, the errors in Height are between 2.5mm to 4.2 mm in height for case A and between 4.8 to 7mm for case B. For the torsion angle the maximum error is 5.6°.

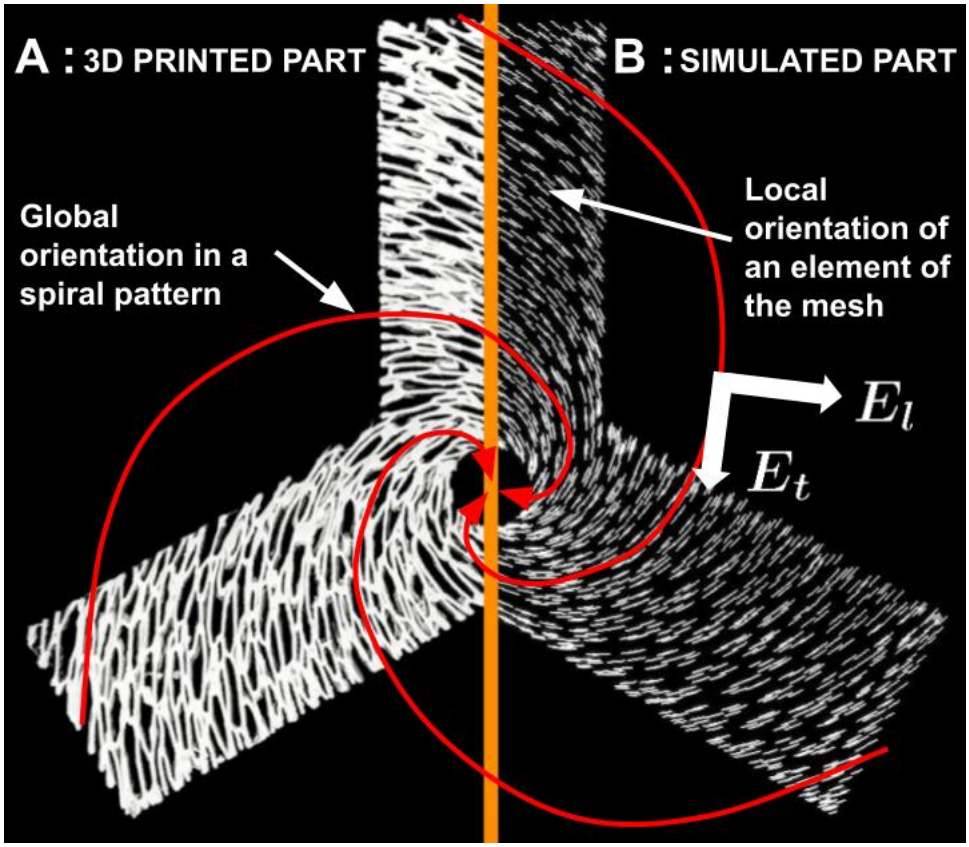

Figure 4.5: View from above of a flattened flexible sheet with a comparison between the simulated part (**B**) where each elements has a specific orientation allowing to have a global spiral pattern and the 3D printed real part (**A**). We keep E_t and E_l constant for the whole structure, only the orientation differ.

		Angle *in* °		Height *in mm*	
		simulated	real	simulated	real
CASE A	Rest	-3.36	0	67.57	71.7
	Middle	4.47	3.96	81.95	84.5
	Top	14.85	20.49	89.88	92.9
CASE B	Rest	-9.31	0	68.67	73.5
	Middle	8.15	5.53	80.73	85.8
	Top	27.21	22.1	87	94

Table 4.1: Comparison between simulated tripod and real one for 3 positions. We measure only the *Height* and *Angle* of the tip of the tripod.

It can be explained by the successive approximations made in the method. The homogenization is inherently a simplification of the behavior of the stochastic foam. In particular self-collisions inside the structure due to large displacement are not taken into account. These particular issue with the approximated models will be addressed in the following chapter.

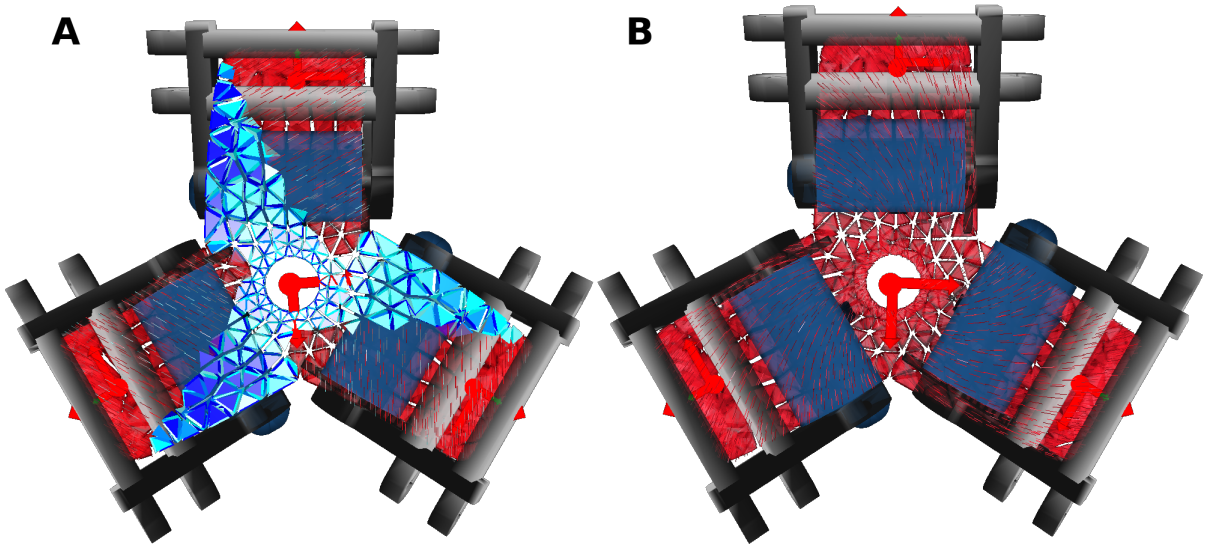

Figure 4.6: Simulation of the 2 presented cases **A** and **B**. There is a visual representation of each elements direction with a little line. On case (**A**) the lines directions are all the same depending on the tripod branch and for case (**B**) each elements has a different direction reproducing the spiral pattern.

Given these results, we could envision to use this modeling process – that do not require any fabrication – to have a good idea of the kinematics of the robot but not to have a fully predictive model. We could use the robot during the design phase, so that the designer has a better understanding of the behavior or to apply optimization algorithms but we must remain aware of the gaps between simulation and reality.

4.2 Inverse modeling presentation

In the previously presented example the user was giving as input to the simulation a motor shaft angle and the simulation was computing how it impact the deformation of the flexible sheet which create in the end the torsional movement.

But to be able to use the design workflow in an iterative manner, predict any setup capabilities and latter on, control more intuitively our robot, it is interesting to be able to control directly what we call an end-effector. For example with the tripod example our end-effector is the tip. By defining it as an end-effector, we now want to be able as a user to control its position and orientation directly. The simulation has to be able to determine how to actuate the motors in order to minimize the distance/orientation between the real tip position and a user controlled tip position.

In this section we will present inverse modeling and how with it and a QP minimization we can actually control the end-effector.

4.2.1 Robot kinematic control via external target

In the case of inverse problem, the two unknowns of the system presented in section 3 with Eq.(3.14) are the same: $d\mathbf{x}$ which provides the motion of the DoFs, and $\boldsymbol{\lambda}_a$, which is the intensity of the actuators loads. Previously $\boldsymbol{\lambda}_a$ was given by the user but now the simulation will compute it and in addition, a new set of equations is defined to control the shape of the robot through specific points on the FEM mesh called effectors.

We will call effector, each particular point on the robot that we wish to control. The task space is the positions and/or orientations accessible by the effectors. This space depends on the design of the robot (i.e. geometry, actuation), its boundaries are entirely defined by the actuation limits (stops).

4.2.2 Constraint solving

Free motion

The resolution of the system will be executed in a two steps fashion. The first step consists in obtaining a free configuration $\mathbf{x}_{free}$ of the robot that is found by solving equation Eq.(3.14) while considering that there is no actuation applied to the structure, that is with $\lambda_a = 0$:

$$\mathbf{A}d\mathbf{x}_{free} = \mathbf{b} \tag{4.1}$$

After solving this linear equations, given this new free position $\mathbf{x}_{free} = \mathbf{x} + d\mathbf{x}_{free}$ for all the nodes of the mesh, we can evaluate the values of $\boldsymbol{\delta}_i^{free} = \boldsymbol{\delta}_i(x) + \mathbf{H}_i d\mathbf{x}_{free}$ with $i \in a, e$, respectively for actuators and effectors.

Problem projection

The distance of the effector points to their goal positions are measured by $\boldsymbol{\delta}_e$. Over a time step, this distance can be defined by a linear application of the nodes displacement, using FEM interpolation:

$$\boldsymbol{\delta}_e = \mathbf{H}_e d\mathbf{x} + \boldsymbol{\delta}_e^0 \tag{4.2}$$

with $\mathbf{H}_e$ being a (highly sparse) rectangular matrix, and $\boldsymbol{\delta}_e^0$ the distance vector, evaluated at the beginning of the step. Combining Eq.(3.14) and (4.2), we can derived the

relationship between $\boldsymbol{\delta}_e$ and $\boldsymbol{\lambda}_a$ by:

$$\boldsymbol{\delta}_e = \underbrace{[\mathbf{H}_e\mathbf{K}^{-1}\mathbf{H}_a^T]}_{\mathbf{W}_{ea}}\boldsymbol{\lambda}_a + \underbrace{\mathbf{H}_e\mathbf{K}^{-1}(\mathbf{f}_{\text{ext}} - \mathbf{f}(\mathbf{x}_{i-1})) + \boldsymbol{\delta}_e^0}_{\boldsymbol{\delta}_e^{\text{free}}} \tag{4.3}$$

We now have a projection of the mechanics into the constraint space. As the constraints are the inputs (registered points) and outputs (parameters and forces on boundary) of the inverse problem, we obtain the smallest possible projection space for the inverse problem.

Optimization

We now use this relation in a quadratic programming (QP) problem [154] in order to find the $\boldsymbol{\lambda}_a$ which allows to minimize $\boldsymbol{\delta}_e$, ie: to find how to actuate the robot so that selected points reach the goal positions:

$$\begin{cases} \min \|\mathbf{W}_{ea}\boldsymbol{\lambda}_a + \boldsymbol{\delta}_e^{\text{free}}\|^2 \\ \text{with } \boldsymbol{\delta}_{min} \leq \boldsymbol{\delta}_a = \mathbf{W}_{aa}\boldsymbol{\lambda}_a + \boldsymbol{\delta}_a^{\text{free}} \leq \boldsymbol{\delta}_{max} \\ (\text{and } \boldsymbol{\lambda}_a \geq 0) \end{cases} \tag{4.4}$$

with $\boldsymbol{\delta}_{min}$ and $\boldsymbol{\delta}_{max}$ being the stops of the actuators and $\boldsymbol{\lambda}_a \geq 0$ is used in case of unilateral actuation (for instance cable actuators). To have a well posed convex problem and converge to a unique solution and avoid instabilities, the QP matrix $\mathbf{W}_{ea}^T\mathbf{W}_{ea}$ has to be positive-definite. To have this property, it is necessary (but not sufficient) that the size of the actuator space is equal or less than the size of the effector space.

4.3 6 DOF controllable parallel soft robot

In a the previous example we have used one tripod robot to show that we were able to create new kinematics by changing the soft sheet composition and organisation from isotropic silicone to a transverse isotropic soft foam. We were able to create a torsion as a new movement, but this torsion was coupled with a translation along the same axis.

Intuitively, by putting two of them face to face and connecting them by a rigid body, we can constrain the translation allowing the system to have an additional independent DoF. This last example has for objective to control, via the simulation the central rod displacement in x, y and z axis and their associated rotations in an independent manner. This show the benefit of the metamaterial in the control/programming of the compliance creating new controllable behavior without adding new actuation sources. Fig. 4.7 show the final real setup that will be presented later. All the following experimentation will follow this configuration.

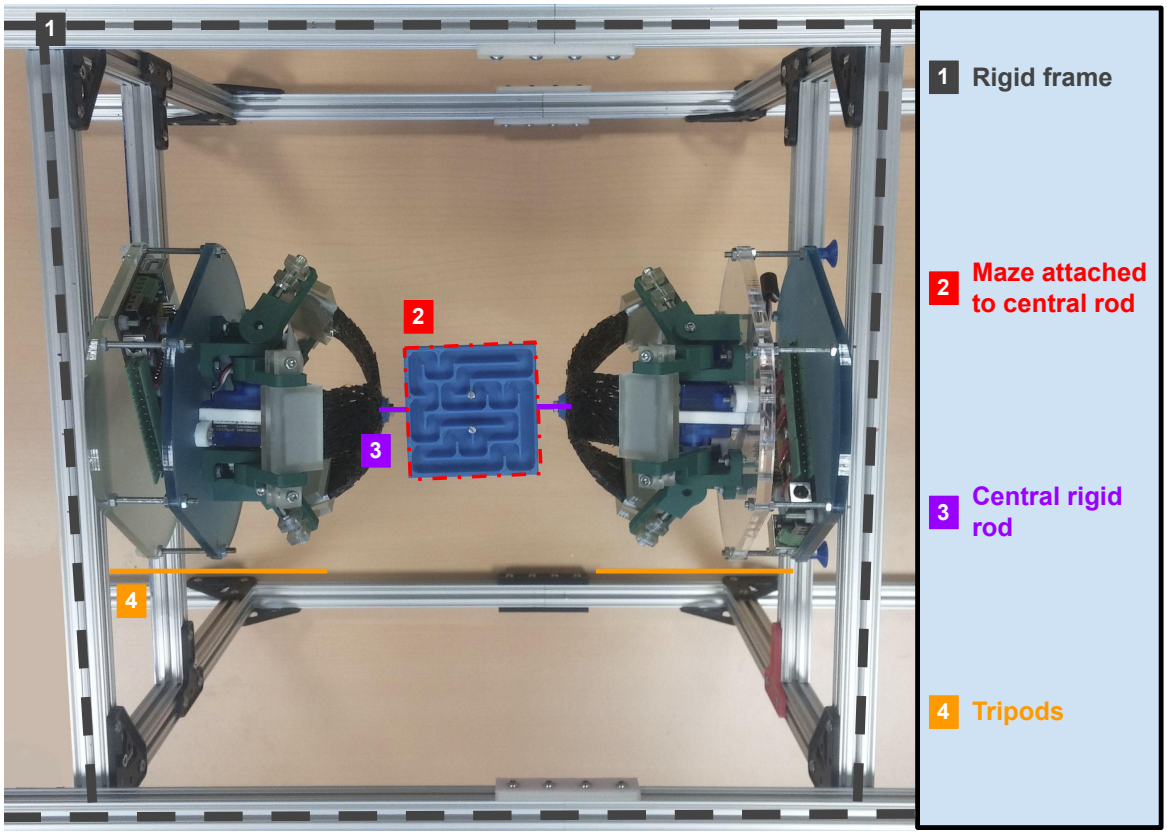

Figure 4.7: View from above of the real validation setup: the 2 tripods are facing each other and linked with a rigid rod. Additionally we attached on the middle of this link a maze that will be used to visualize more efficiently the controlled movement of the end effector of this system.

4.3.1 Simulation design

We now have a 6 DOF parallel soft robot by combining two existing 3 DOF parallel soft robots. Each tripod is controlled by 3 servomotors. It is particularly cumbersome and difficult to command each of them independently in order to move the central rod.

To avoid that we do an inverse simulation and build it in order to have as input the middle of the central axis (end-effector) and as output the different angles of the motors' shaft.

The central rod is represented by a beam modeled via Kirchhoff rod theory which allows to simulate any 1D flexible structure. In this case we program the beam elements with a really high Young modulus give us a behavior akin to a rigid rod.

For the mesostructure configuration, we will only use the configuration B (Fig. 4.3) with the spiral pattern because we have noticed with the previous experimentation (Tab. 4.1) that we achieved the best rotation with it.

By putting two of them face to face the global system is therefore symmetric. This enable a pure rotation along the axis of the rigid link when all motors have the same actuation, i.e. all motors push or pull. With Fig. 4.8 we have the simulation results of this two scenarios (all pull : A ; all push: B) and the visualization of the rotation created compared to the neutral rest state of the system in the middle.

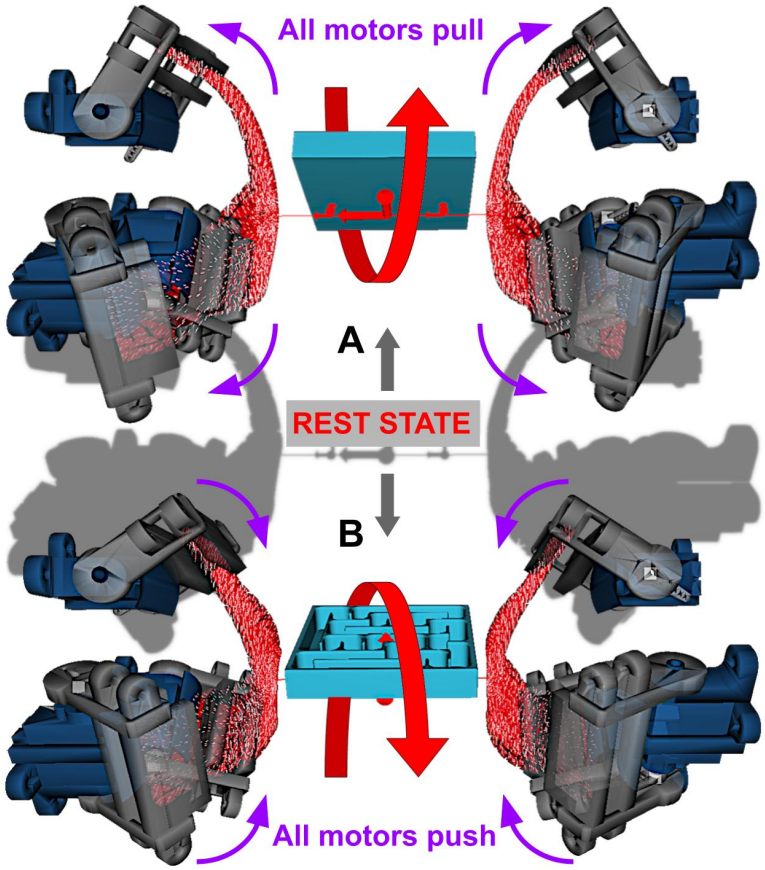

Figure 4.8: Side view of the simulation of the global setup. In the middle, in grey, the system is presented at rest state. The figure show the sixth DOF created around the rod. When both tripod "pull" (**A**), a rotation appears around the rod in one direction and when they "push" (**B**) it rotate on the same axis but in an opposite direction. Due to the fact that motors are either all "pulling" or all "pushing", the maze stay centered during all the actuation enabling a decoupled sixth DOF

The pattern of the flexible sheets are mirrored in order to have the same behavior but if they were inverted, to have the rotations presented in Fig. 4.8, one tripod would need to "push" while the other would "pull" and vice versa to have the rotation in the other direction. We choose the first option because it allows a more independent control of the DOF which we lose with the second option due to side translations.

4.3.2 Workspace capabilities assessment

The simulation is now able to control the sixth independent DOF of our end-effector setup. We can now use the inverse simulation, during a design phase (disconnected from any real setup) to assess the capacity of our system and explore its workspace boundaries.

We will present here how we perform this using the model presented above and provide a discussion about the results. We also present an evaluation of the anisotropy influence on the 6th DOF.

Method of evaluation

The workspace exploration is done in a discrete way using the inverse problem optimization presented in optimization with Eq.(4.4). We constrain the motors with maximum and minimum possible values of their shaft in order to have a range of actuation of 90 degrees in total for each motor, with 0° having the motor totally "horizontal" and 90° "vertical".

We generate a grid of point along the directions of actuation, this produce a kind of 3D star workspace to explore. In total, we have around 1800 points to explore. We choose to remove most of the points around the center in order to gain time during the workspace exploration.

We begin the evaluation by moving the goal from point to point verifying with a error margin of 1 mm if the inverse model succeeds to reach it. We then do the same process again but adding an evaluation of the rotations capability on each point of the workspace. We apply successively 3 rotations (along x, y and z) with minus or plus 10° and with an error margin of 2°. In function of the rotation results we create 3 categories in which the point will be classified : points on which we can do the 3 rotations, points on which we can only do 2 out of the 3 rotations and finally points which are only reachable but on which we can not do any rotation.

The angular boundaries of the motors highly influence the workspace of the robot. We show this influence by doing multiple explorations, each time with different boundaries for our actuators in order to see its repercussion on the final workspace.

Results and interpretation

The workspace exploration is shown on Fig. 4.9. We observe that at the initial position (center of workspace) and in a whole area around it, we have a 6 DOF fully controlled end-effector. Then, as we translate the effector further to the side, we gradually lose the control of the different rotations up to the point where on the boundary of the workspace we are only able to perform translations.

Perpendicular to the rigid link we observe in the front view (**A**) that the workspace is symmetrical which is expected due to the physical symmetry of the system. Another remark is that the final workspace has a star shape which can be explained by the fact that there is an asymmetry between the points lying directly in the direction of the motors axis and other points lying in the directions passing between two motors.

In Fig. 4.9 left, we can see the superposition of different workspace produced by changing successively the possible range of actuation of the motors. As could be expected, as the range decreases, the workspace shrink towards its center.

We noted that the exploration of the workspace is sometimes not realistic. For instance, when increasing the rotation applied on each tested points from 10 to 20 degrees and conducting the same exploration as shown in Fig 4.9 left, we would expect a reduction of the workspace. But, in such case, the working space is only slightly reduced. This is probably due to an idealization of the constitutive law in the FEM model (this will be further discussed in the conclusion).

Anisotropy influence

A new experiment was conducted to demonstrate more clearly the influence of the anisotropy on the kinematics. To this end, we have two extreme cases: on one hand, the isotropic case and on the other hand the anisotropy case used for the final design of the system. To create intermediate cases, we interpolate between this two extreme cases. The Fig. 4.11 demonstrates that the rotation of the end-effector appears progressively for the same input motion on the motors.

4.3.3 Setup presentation and results

In this section we present how the real robot was made and then compare its behavior with its intended design previously simulated and show its maneuverability by using it to solve a maze.

Real Model Construction

We mount the flexible structure produced on the tripods and then link them together with a metal rod on which we attach on the middle a 3D printed (with FDM technique using PLA) maze. This system is afterwards mounted into a rigid box allowing the whole system to stay stable when the two tripods actuate against each other. During the mounting process we put particular attention in keeping the same distance as in the simulation. We can see in Fig. 4.7 the whole final setup at rest state.

Validation

Here, we are looking for the three following properties :

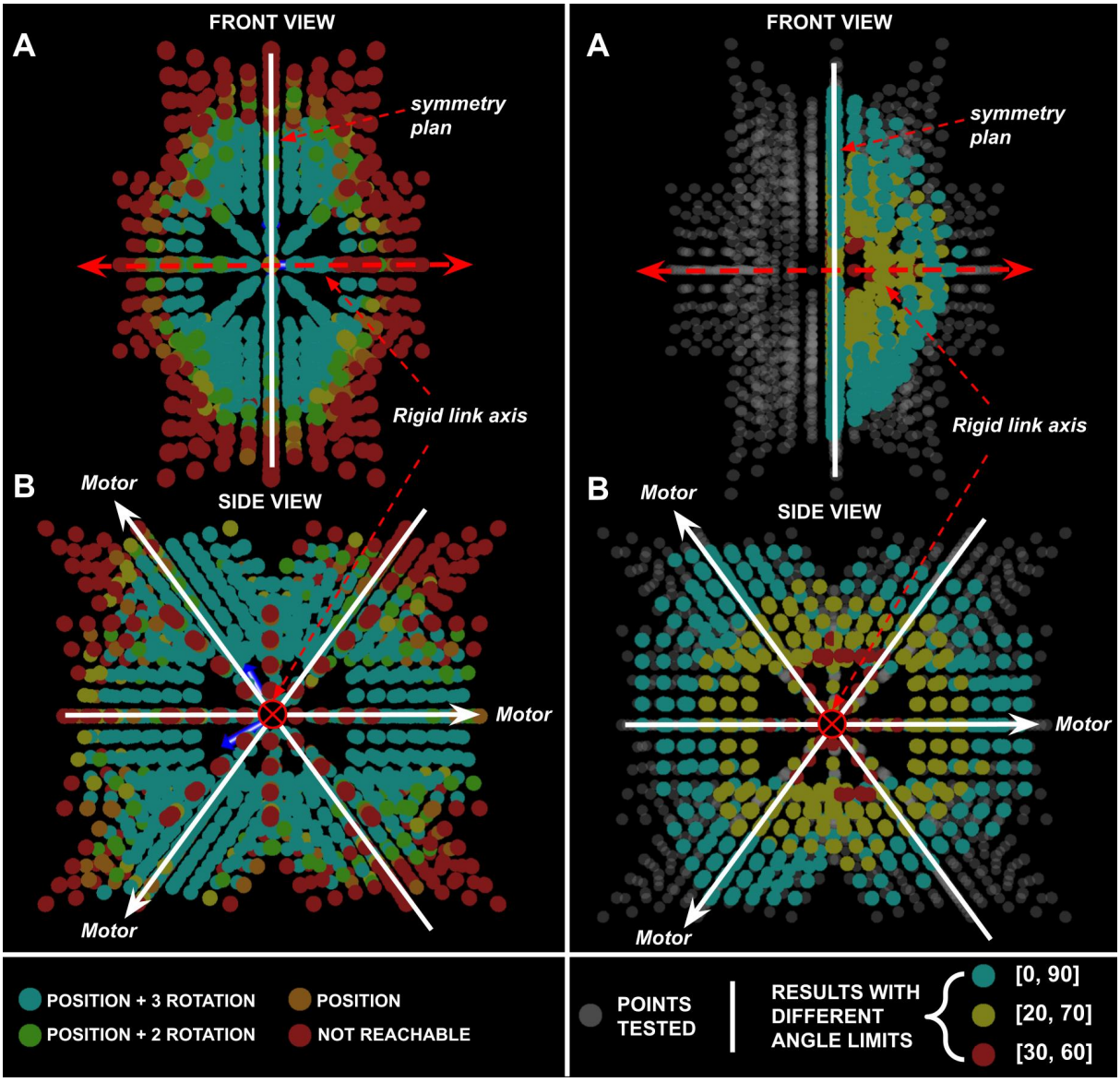

Figure 4.9: LEFT: Workspace exploration with the effector. Starting from rest position, we try to reach each point and if it is reachable we try to do on it 3 orthogonal rotation of -/+10°. Depending on the results the point is classified in the blue, green, orange or red categories. RIGHT: Workspace exploration with different angle limits imposed on the actuators. In this constrained exploration, reaching a points with an error margin of 1 mm validate it. The exploration is done on the same points as LEFT. We test 3 different angle limits producing 3 different possible workspace each including the other : red is included in yellow which is included in blue.

- A new independent DOF is created and controllable.
- We can still control independently the 5 other DOF.
- The numerical model is sufficiently accurate to control the robot in open loop.

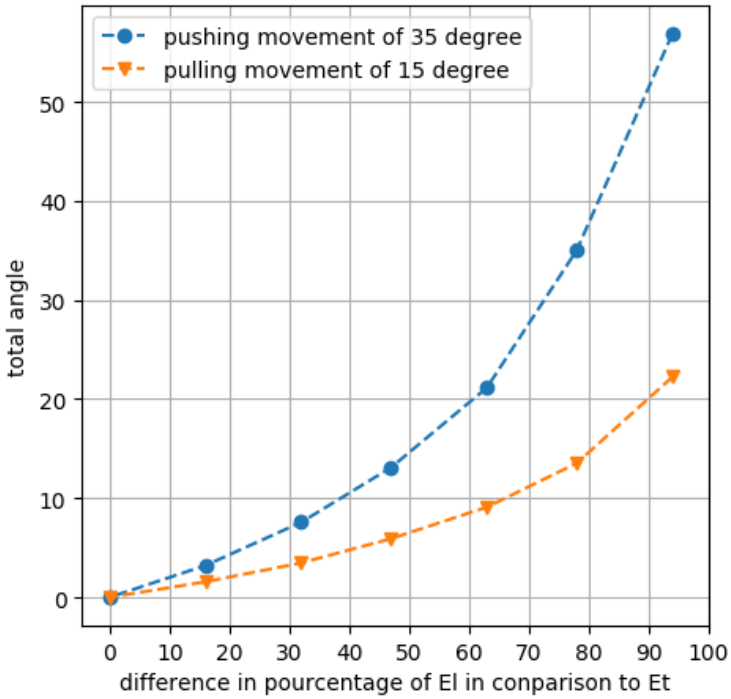

Figure 4.10: Convergence from transverse (right of the figure) to isotropic (origin). Abscissa α represents an anisotropy percentage. $\alpha(\%) = 100 - 100(E_l/E_t)$. The test is done by either pulling all motors of 15° or pushing them of 35° degrees from the rest state as presented in Fig. 4.8.

Additional Independent Controllable DOF

We can see in Fig. 4.11 for the same actuation the different results for a parallel soft robot with sheets made of either silicone or metamaterial. We can confirm that with silicone no central rotation is created but rather that one of the tripod sheet buckle due to the pression of the other resulting in a lateral translation. For the robot made with sheet composed of metamaterial, we have, as expected from the simulation, the creation of a rotation around the rigid axis, while creating no translation. This demonstrates the possibility of controlling a new independent DOF. The rotation the other way around when all the motors are pulling is also verified.

The independent control of the 5 other DOF

Now that we have successfully managed to get control of the rotation of the rod, we make sure all remaining 5 DOF are controllable independently, i.e. we can still translate the effector without parasitic rotations for example. It is the case indeed and can be seen on the video associated to the published work: video.

Maze Solving

We put a marble on the maze and we were able to impose the motion of the effector in the global frame, in order to solve it. What we mean by solving it, is that we were

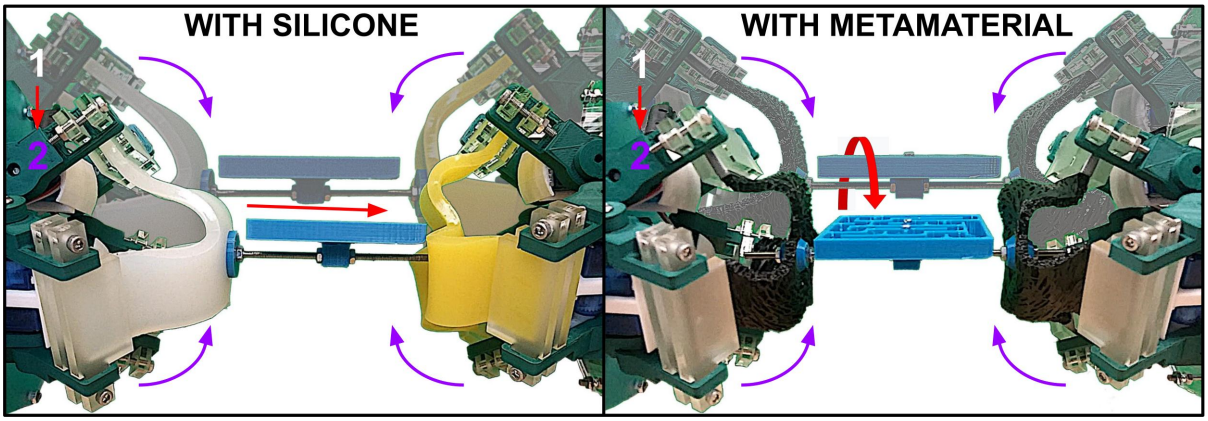

Figure 4.11: Comparison between a parallel soft robot made of silicone (**A**) and one made of our metamaterial (**B**). For both we actuate all servomotors from 1 to 2; action : purple arrow / reaction : red arrow. With traditional homogeneous material (**A**), we can see that the maze translate to the right, but with a mesostructured flexible sheet (**B**) a rotation around the metal rod axes is created.

able, in one go, to make the marble follow the whole path of the maze and come back at the initial position by actuating both tripod and controlling the different inclinations of the maze demonstrating in doing so its maneuverability and controllability. In particular, to solve the maze, we need to use the newly created additional DOF created with the anisotropic material and cannot solve it using a setup built with silicone. As for the previous validation we ask the reader to refer to the video to have a visualization of the resolution of the maze.

4.4 Conclusion and results discussion

In the previous chapter (chatper 3). We presented a workflow approach to design soft robot with mesostructure presenting an anisotropic behavior. In this present chapter we have shown the validation of this workflow with different example having increasing complexity. The anisotropic constitutive law and its implementation in our simulation framework reproduce the general behavior of the real setups.

We have shown the interest of the inverse simulation to ease the design iteration in order to put sufficient anisotropy to create here a certain rotation, but also to have a primary assessment of our setup capabilities.

Finally we have shown concretly the interest of the use of metamaterial and more particularly of the mesostructured foam, by showing its influence on the kinematic and how on a same geomatrical structure and with the same setup we can create a new interesting behavior which we can control precisly with a QP optimisation minimising the distance between an end-effector and a desired goal position/orientation.

But this model of anisotropy is again an approximation and the homogenization is also inherently a simplification of the behavior of the stochastic foam. In particular self-collisions inside the structure due to large strain are not taken into account.

This leads to lacks in precision during simple beam validation and overestimation of movement capabilties, notably for the workspace assessment which is much larger than what is possible with the real setup.

We will adress this issue in the next chapter.

Chapter 5

Optimisation and calibration

Contents

5.1 Differentiation and optimisation on multiple configurations **89**
5.1.1 Differentiable models 89
5.1.2 Sim2real using inverse model 90
5.1.3 Multi-Configuration optimisation 90
5.2 Parameterisation of anisotropy **92**
5.2.1 Simulation - mechanical structure 92
5.2.2 Fabrication - slicing configuration 92
5.3 Problem conditioning **93**
5.3.1 Simple problem setup 94
5.3.2 Influence of the configurations on the convergence 94
5.3.3 Conditioning analysis on soft anisotropic beams 95
5.4 Practical use: calibration of a real anisotropic parallel robot **97**
5.4.1 QP problem setup 98
5.4.2 Results 99
5.5 Conclusion **101**

CONTENT

In this chapter we present a new optimisation approach based on differentiable simulation using multiple configurations. We show how we can with it, calibrate the simulation to have significant precision improvement for the control of an anisotropic soft robot.

In section 1 we define what are differentiable simulation and their interest for soft robotics design/control/calibration. We then present our approach, based on defining mechanical parameters as Lagrange multipliers as presented previously for actuators. We finally present a new optimization method: it allows to optimize on numerous mechanical parameters while still having a well defined QP thanks to a multi-configuration approach.

In section 2 we will explain how we parameterise the simulation in order to have complex anisotropic behavior defined with as few as possible parameters using control point (CP) put on a geometry. Between these CPs we perform an interpolation, i.e. we set the mechanical constants of all of the elements of the mesh depending on their respective position to the different CPs. We verify with the geometry slicing if the interpolation is find back in the generated foam.

In section 3 we will discuss the conditioning of the optimization problem. Depending on the problem setup we can be stuck into local minima. We show the difference of convergence between not well defined problem and good ones and verify that for good one we attain each times an optimal solution. We finish by an in-depth matrix conditioning analysis and underline means to determined well defined problems or how to improve its convexity.

Finally, in section 4 we will show a practical example of calibration with the parallel soft robot. We explain the problem settings and present its the calibration results using our new methods. We show that we ameliorate significantly the simulation precision on the calibrated real data but also on newly tested points.

5.1 Differentiation and optimisation on multiple configurations

Sim2real is one of the key challenge in robotics, and perhaps even more in soft robotics. By having an accurate physical model of a robot, robust control methods can be derived. Moreover the robot can be simulated in its operating environment to plan and learn automatically [161, 162]. In soft robotics, the challenge of having an accurate physical model is even more important because it must take into account deformations, which are derived from sometimes complex material properties. In this section we will describe a method allowing to calibrate these models by optimising the material parameters using differentiable simulation. We hope that this contribution could be a step forward for sim2real transitions in soft robotics.

5.1.1 Differentiable models

Before describing our methods we will first present a short state of the art. Here we will place ourself in the domain of differentiable simulation.

The literature named differentiable simulation, simulation tools that provides a principled mathematical framework to:

- **(1)** Solve complex characterization problems to detect and close application-specific sim2real gaps.
- **(2)** Optimally control embedded soft actuators for grasping or locomotion tasks (actuation problem).
- **(3)** Estimate the mechanical state of the soft system from a set of embedded sensors.

While **(1)** improves the prediction accuracy of simulations, **(2,3)** enable optimal open and closed-loop control of manually designed soft robots [163]. This definition particularly suits what we want to achieved : optimise our material properties to properly characterize it and lower the sim2real gap. Moreover the resolution of these problems are done using gradient-based approach which is the same approach we have already presented with the QP optimisation.

In the soft robot community gradient-based optimisation to improve accuracy and have a better fit with real data was especially investigated in machine learning approaches which can be easily differentiated, for example [164, 165]. In [166], a differentiable model based on material point method was proposed. In a finite element modeling (FEM) context, an analytical gradient with respect to design variables is used in [167] to optimise sensors positioning. In the particular context of soft robotics materials, [168] proposes to fit a model with data from several mechanical tensile tests, thanks to an analytical gradient and a quasi-Newton optimisation method. It was successfully applied for hyperelastic models. Similarly in [169], FEM simulations are used to fit data obtained with simple tensile tests. See also [163] for an in depth review on differentiable simulation.

In this study, we focus on differentiable models for soft robots made of anisotropic materials, which implies differentiating with respect to anisotropy direction.

We will fit the mechanical model parameters with sensor measurements of the systems deformation under different constraints. We use these measures as calibration input to find the best mechanical settings of our system allowing to reach each configurations.

5.1.2 Sim2real using inverse model

In the model calibration problem, we aim at estimating the mechanical parameters that best fit the robot that was actually built. To verify that the model fits the data, we will continue to use an optimisation based on a set of effector points placed on the robot. This was presented in chapter 4.2. We were using it to do workspace estimation. However, this time, it is not about optimising the force on the actuators ($\boldsymbol{\lambda}_a$) but the mechanical parameters contribution on the FEM, $\boldsymbol{\lambda}_p$.

The mechanical parameters $\mathbf{p}$ of the constitutive law influence the computation of the internal forces. To use our method, these parameters need to be differentiable, which is the case for the anisotropic case described below.

$$\mathbf{f}(\mathbf{x}+d\mathbf{x},\mathbf{p}+d\mathbf{p}) \approx \mathbf{f}(\mathbf{x},\mathbf{p}) + \underbrace{\frac{\partial \mathbf{f}}{\partial \mathbf{x}}}_{\mathbf{K}(\mathbf{x},\mathbf{p})} d\mathbf{x} + \frac{\partial \mathbf{f}}{\partial \mathbf{p}} d\mathbf{p} \tag{5.1}$$

In practice, we perform a numerical differentiation of the internal forces to obtain the value of $\mathbf{H}_p^T$ which is equal to $\frac{\partial \mathbf{f}}{\partial \mathbf{p}}$. Written like this, the variation of the parameters $d\mathbf{p}$ can be assimilated to a Lagrange multipliers $\boldsymbol{\lambda}_p$. Additionally, to have parameters working in a uniform space (for example between -1 and 1), we can apply scaling factors. For consistency of notations, we introduce $\mathbf{S}\boldsymbol{\lambda}_p = d\mathbf{p}$, where $\mathbf{S}$ is a diagonal scaling matrix allowing to have all parameters in a uniform space and $\mathbf{H}_p^T(\mathbf{x},\mathbf{p}) = \frac{\partial \mathbf{f}}{\partial \mathbf{p}}\mathbf{S}$.

Combining with Eq. (3.14) we now have the quasi-static equilibrium defined by:

$$\mathbf{K}(\mathbf{x}_{i-1},\mathbf{p}_{i-1})d\mathbf{x} = \mathbf{f}_{\text{ext}} - \mathbf{f}(\mathbf{x}_{i-1},\mathbf{p}_{i-1}) + \mathbf{H}_a^T\boldsymbol{\lambda}_a + \mathbf{H}_p^T\boldsymbol{\lambda}_p \tag{5.2}$$

Once the optimisation problem (which will be presented below) is solved, we update the parameter $\mathbf{p}_i$ using $\mathbf{p}_i = \mathbf{p}_{i-1} + \mathbf{S}\boldsymbol{\lambda}_p$ and determine the new $d\mathbf{x}$ then continue to iterate to progressively reach an equilibrium ($d\mathbf{x} = 0$ and $\boldsymbol{\lambda}_p = 0$). Note that in the case of a robot calibration, we will impose references to the actuators (so we know $\boldsymbol{\lambda}_a$ or $\boldsymbol{\delta}_a$).

5.1.3 Multi-Configuration optimisation

Now that we have shown that the parameters where differentiable and how to write their contributions we will present how we integrate them into our optimisation scheme.

The goal of the optimisation is to update the parameters $\mathbf{p}$ so that the positions of the effector points on equilibrium are as close to the data as possible. But, unlike the optimisation presented previously, we seek to optimise the parameters over several different static equilibrium configurations, representative of the robot workspace.

This will allows to have informations about the system under different actuation or strain to have have a better fitting between the simulation and the real setup. Additionally it will permit us to guarantee well defined QP problem with numerous parameters to optimise.

For each of these configurations j, we will launch different simulation each with the same material parameters initial value but they will distinguish themselves from each other by having different value of actuation $\boldsymbol{\lambda}_a^j$ (or $\boldsymbol{\delta}_a^j$). Each simulation compute the FEM separately (each of them solves a different version of Eq. (3.14)). When the equilibrium is reached for each configuration, we start the optimisation of the parameters which will link them all together. Indeed the modification of the parameters has repercussions on the static equilibrium for all the configurations. To conduct the optimisation, we will look at the errors on the effectors at the level of each j configuration, and we will do the same type of condensation as the one done in Eq. (4.3):

$$\boldsymbol{\delta}_e^j = \mathbf{W}_{ep}^j \boldsymbol{\lambda}_p + \mathbf{W}_{ea}^j \boldsymbol{\lambda}_a^j + \boldsymbol{\delta}_e^{\text{free},j} \tag{5.3}$$

Note that $\boldsymbol{\lambda}_p$ is the only term that do not depends on the configuration since we look for one set of material parameters that is identical across all configurations, and again that $\boldsymbol{\lambda}_a^j$ is known (or we can define equality equations to impose $\boldsymbol{\delta}_a^j$ by computing $\boldsymbol{\lambda}_a^j$).

Let's suppose that we perform the optimisation on n configurations, we can aggregate these equations as follow:

$$\underbrace{\begin{bmatrix} \boldsymbol{\delta}_e^1 \\ \vdots \\ \boldsymbol{\delta}_e^n \end{bmatrix}}_{\boldsymbol{\Delta}_e} = \underbrace{\begin{bmatrix} \mathbf{W}_{ep}^1 \\ \vdots \\ \mathbf{W}_{ep}^n \end{bmatrix}}_{\mathbb{W}_{ep}} \boldsymbol{\lambda}_p + \underbrace{\begin{bmatrix} \mathbf{W}_{ea}^1 \boldsymbol{\lambda}_a^1 + \boldsymbol{\delta}_e^{\text{free},1} \\ \vdots \\ \mathbf{W}_{ea}^n \boldsymbol{\lambda}_a^n + \boldsymbol{\delta}_e^{\text{free},n} \end{bmatrix}}_{\boldsymbol{\Delta}_e^0} \tag{5.4}$$

The vector $\boldsymbol{\Delta}_e$ gathers the effectors distances to the objectives on all configurations. The goal of the minimisation is to find the set of parameters $\boldsymbol{\lambda}_p$ which minimise the square norm of this vector:

$$\min \|\mathbb{W}_{ep} \boldsymbol{\lambda}_p + \boldsymbol{\Delta}_e^0\|^2 \tag{5.5}$$

When a new value of $\boldsymbol{\lambda}_p$ is found, the parameters $\mathbf{p}$ are updated and each configuration can update its quasi-static equilibrium. This ends a simulation step. It is repeated a number of steps until $\boldsymbol{\lambda}_p \to \mathbf{0}$, we reach a minima and stop the optimisation.

5.2 Parameterisation of anisotropy

In this section we present how we define varying mechanical properties of a mesh to create transverse behavior with as little parameters as possible in order to simplify later on the optimisation presented previously (chapter 4.2.2). Then we explain how we transfer these parametric mechanical description of our mesh into a real 3D printed part.

5.2.1 Simulation - mechanical structure

We optimise the mechanical parameters over a FEM. In this work we focus on a special case of anisotropy which is transversely isotropic material.

As presented in chapter 3.2.1 we have 5 mechanical parameters to define the elasticity tensor of any element of the mesh and using the approach of [160] presented in chapter 3.3.4, we can reduce the parameters needed to only E_t, E_l and ν_t while insuring a stable anisotropy. To simplify further, we focus on optimising only the Young modulus by setting ν_t to a chosen value.

In addition to these mechanical parameters we have the "fiber" direction that we define with the angle θ (chapter 3.2.1). In the end, we can define a transversely isotropic tetrahedron with only 3 parameters: $\{E_t, E_l, \theta\}$.

Even with these simplifications, we cannot optimise these 3 parameters for each tetrahedron of the mesh: the number of unknowns would be too high and dependent on the mesh resolution. Moreover there is a necessary continuity of parameters between neighboring elements. This is why we place what we call control points (CP) upon the mesh, we can see on Fig. 5.1 a visual representation of them (red dots).

Each CP will be independent from each other and will have the triplet of parameters presented above characterising them. Then the parameters of each CP are diffused on the mesh: for each tetrahedron of the mesh the triplet of mechanical parameters are obtained by interpolation, depending on their relative proximity to the different CP. For that we use a simple spacial interpolation called Inverse Distance Weighting (IDW) [170] that allows to have a smooth transition between the different values while never going above the values it interpolate on. Using the CP and doing an IDW between them we only have to optimise 3 parameters times the number of CP used.

5.2.2 Fabrication - slicing configuration

We have already presented the material used and the different slicing parameters in chapter 3.4.1. We have shown that we can specify in 3D the coefficient of anisotropy as well as a direction and a density.

We check here if we are able to reproduce the interpolated direction and with the different structure generated we make a choice concerning the power parameters of the IDW (refer to [170] for its details).

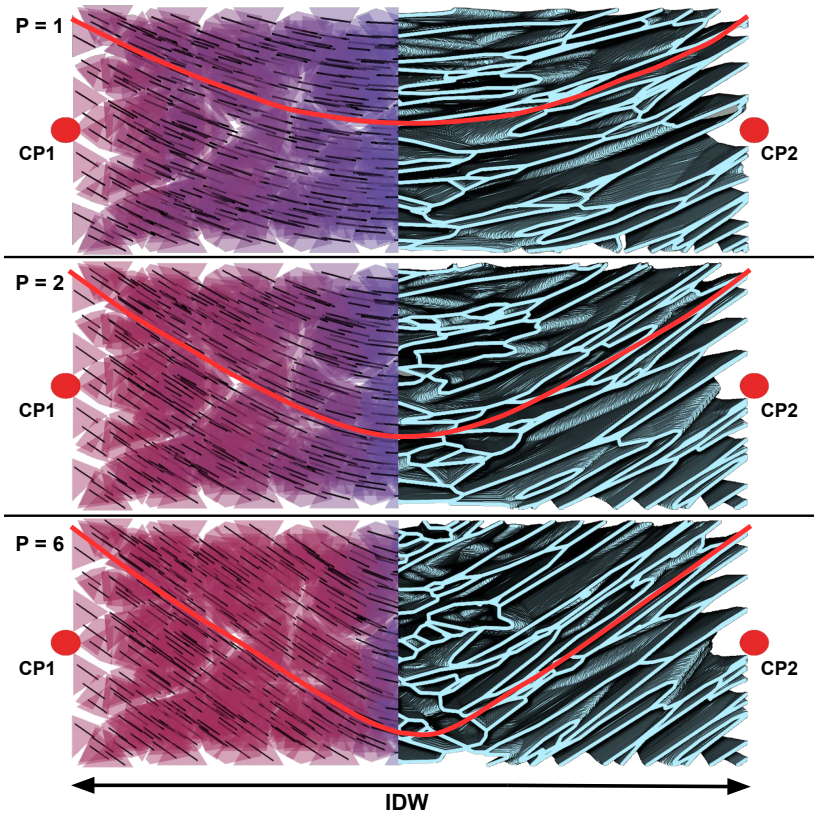

Figure 5.1: Interpolation between 2 CP (red dot) with, on the left each little black lines corresponding to a tetrahedron's direction and on the right we have the corresponding 3D shape generated. The right/left CP have respectively a set direction of $-35°/35°$. There is also a comparison with different values of p for the IDW interpolation [170].

We can see on Fig. 5.1 different interpolation results between two CP for different values of the power parameter p used in the IDW. It shows that with $p = 1$ the transition is too smooth and with $p = 6$ too sharp. As a middle ground we choose to use for all the presented examples in this paper a value of 2. This figure also demonstrate that we have a close match between the different interpolated directions of the simulation and reality.

5.3 Problem conditioning

The approach proposed in 5.1.3 is based on a convex optimisation. This type of optimisation is sensitive to conditioning, which can be seen as a drawback. On the contrary, we show in this section that an in-depth analysis of the matrices conditioning allow to get practical and intuitive information, useful for the calibration. Given the number and the type of parameters, are there enough effector points on the structure? Are there enough configurations tested in the workspace? Were all parameters excited in the configurations so they can be identified?

As presented in 5.3.1, the number of parameters is directly proportional to the number

of CP. If the number of CP is high, the number of unknown parameters is high and the data collected during the calibration has to be rich enough to insure convergence during the optimisation. On the other hand, having few CP is not enough to have a well posed problem: indeed if we place two CP too close to each other, especially on a area which has only small deformation, then the set of parameters of these two CP will be redundant and the problem ill-defined.

The input data can vary in two ways: we can place several effector points on the robot and we can choose several configurations on which we do the calibration. All these choices will have a direct impact on the convergence of the parameters, we will study this in the following sections.

5.3.1 Simple problem setup

To illustrate the mathematical analysis, we will use the relatively simple example of optimising the anisotropy parameters on a cantilever soft anisotropic beam. This beam has a rectangular section and we place on its 2 extremities a CP. We suppose that the mass is known and we optimise only the two elasticity parameters and the anisotropy direction so $\mathbf{p}$ to be optimised is a vector of dimension 6 ($dim(\mathbf{p}) = 2 \times 3 = 6$).

We artificially generate objectives for a set of input data of $\mathbf{p}_{target}$ with a direct simulation and we will try to find back with the optimization $\mathbf{p}_{target}$ by starting with random values of $\mathbf{p}_{init}$.

We can see in Fig. 5.2 the simulation setup with the different configurations having all the same common parameters $\mathbf{p}_{init}$. The configurations 2 and 3 are rotated along their longitudinal axis to have information about the fiber direction influence. We also add configuration 4 where we attached the beam from the other end to equalize the importance of the mechanical parameters on either side of the beam.

5.3.2 Influence of the configurations on the convergence

As explained above the number of parameters, the variety of configurations and the placement of effectors are key. They have a direct link with the optimisation convergence. To illustrate this, we can see on Fig. 5.3 different optimisation convergence each with a different number of configurations of the simple beam presented previously (Fig. 5.2) with only one effector at its tip. When we only have one configuration (red) the QP problem get stuck on a local minima which does not allow to reduce further $\mathbf{\Delta}_e$. With 2 and 3 configurations we get to a $\mathbf{\Delta}_e \approx 0$ but around simulation step 65. The third configuration probably does not provide enough relevant information. In comparison, the fourth configuration (the beam is now attached by its other end) brings useful information by making "visible" the effect of some parameters. The problem converges more quickly ($\approx$ step 50). Through this example, we can see that it is useful to have mathematical tools to understand if the optimisation problem we are creating is well posed.

Then in order to insure that well posed problems converge effectively to the same values

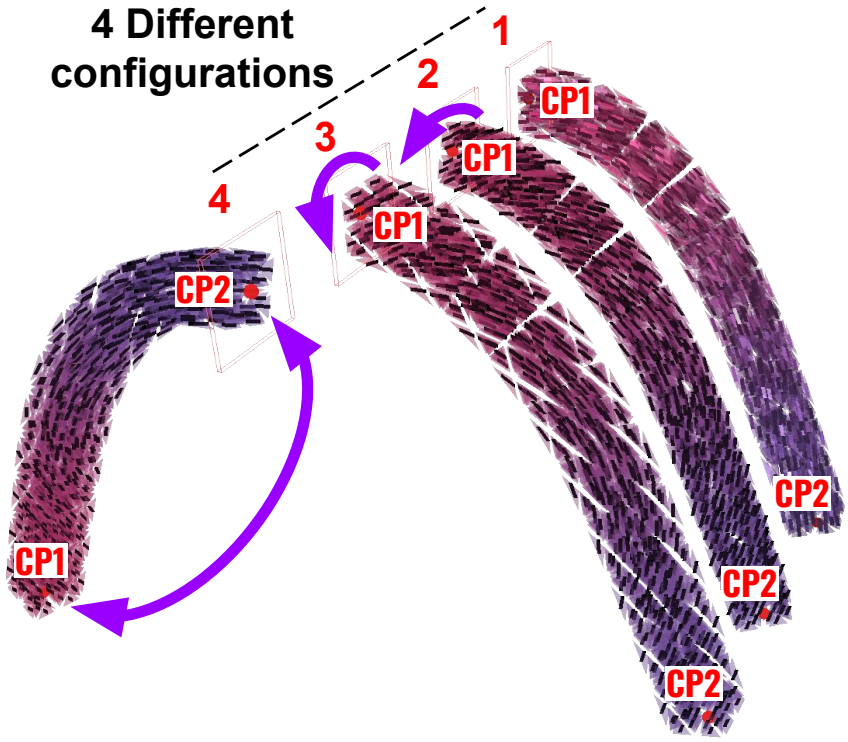

Figure 5.2: QP simulation with 4 configurations of a simple beam subject to only gravity. The purple arrows represent the new modification of the configuration compared to the first one (**1**): configuration **2** & **3** have two different rotation around there longitudinal axis and for **4** the tip and attached part were switched.

every time we test the optimisation when starting with random initial $\mathbf{p}_{init}$. By minimising the beam tip position difference between the input data and the position obtained in the optimisation, we test the convergence and observe if we reach the same $\mathbf{p}_{target}$.

We have launched the optimisation 30 times with, each time, a new randomized $\mathbf{p}_{init}$ and as we can see on Fig. 5.4 for the parameters E_t and E_l of the 2 CP, the QP problem converge each time to the same values which are the right $\mathbf{p}_{target}$. Note that we have chosen a certain range on the parameter space : $[E_{min}, E_{max}]$. Also, for stability issues, we have forced the following inequality between longitudinal and transverse Young modulus: $E_l < E_t$.

5.3.3 Conditioning analysis on soft anisotropic beams

Through this optimisation example of anisotropic beams, we illustrate in this section how it is possible to study the compliance matrix conditioning, to have a better understanding about the convergence/divergence of the QP problem.

In Eq. (5.5), the matrix $\mathbb{W}_{ep}$ represents the influence of the mechanical parameters variations on the effectors positions since we have, for each configuration j, $\boldsymbol{\delta}_e^j = \mathbf{W}_{ep}^j \boldsymbol{\lambda}_p^j + \boldsymbol{\delta}_e^{j,0}$. To study conditioning, one can do a singular value decomposition (SVD) of the

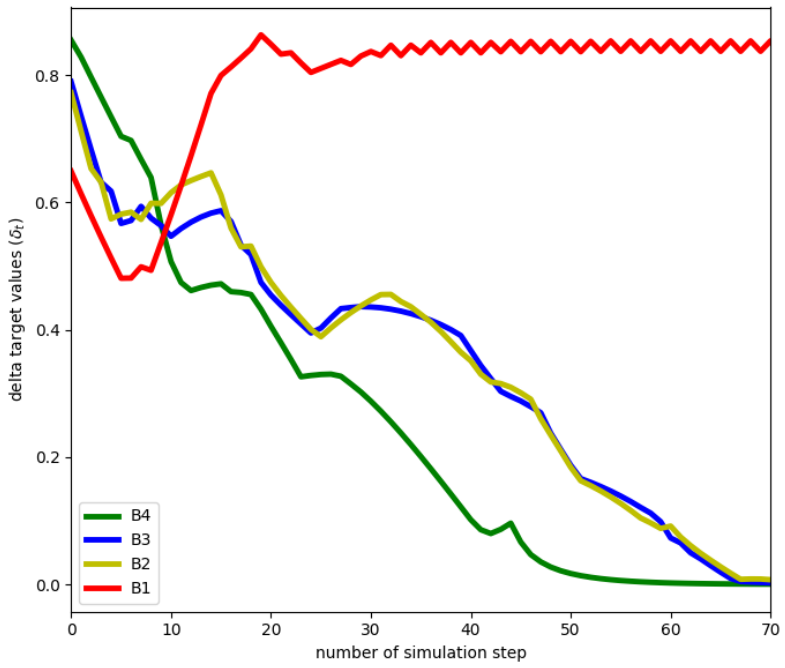

Figure 5.3: Minimisation of $\mathbf{\Delta}_e$ with QP problem having different number of configuration: from 1 up to 4. B1 corresponds to a QP problem with configuration 1, B2 optimizes on configuration 1 and 2, B3 optimizes on configurations 1,2 and 3 and finally, B4 optimizes on the 4 configurations.

compliance $\mathbb{W}_{ep} = \mathbf{USV}^T$. The range of values in the matrix $\mathbf{S}$ (between the largest and the smallest) is related to the conditioning value of the problem. If this matrix is poorly conditioned, i.e. with a high condition number, there will be modifications of parameters that will have no effect on the movements of effectors. In practice this will be likely to make the QP optimisation fail.

In this situation, we can extract the corresponding kernel vectors (the vectors of $\mathbf{U}$ corresponding to the small singular values, say $\mathbf{U}_s$) that will provide the directions in which modifying the mechanical parameters has almost no influence on the movement of the effector points. In practice, it means the effector points do not change positions using 2 different sets of mechanical parameters $\mathbf{p}$ and a variation of $\mathbf{p}$ along the direction $\mathbf{U}_s$: $\mathbf{p} + \alpha\mathbf{U}_s$.

This information is very rich as it provides parameter directions that have not been sufficiently excited in the input data set of the calibration. This allows to point out which parameter or combination of parameters needs to be particularly exposed in additional configurations, allowing to improve the conditioning.

However, analysing the concrete conditioning values obtained for the matrix $\mathbb{W}_{ep}$ could be difficult as they are also dependent of nominal parameters, such as the global compliance. So a large conditioning value could still sometimes be acceptable. We can reduce this effect by using the square matrix $\mathbb{W}_{pp}$ (similar to $\mathbb{W}_{aa}$ definition) obtained by summing

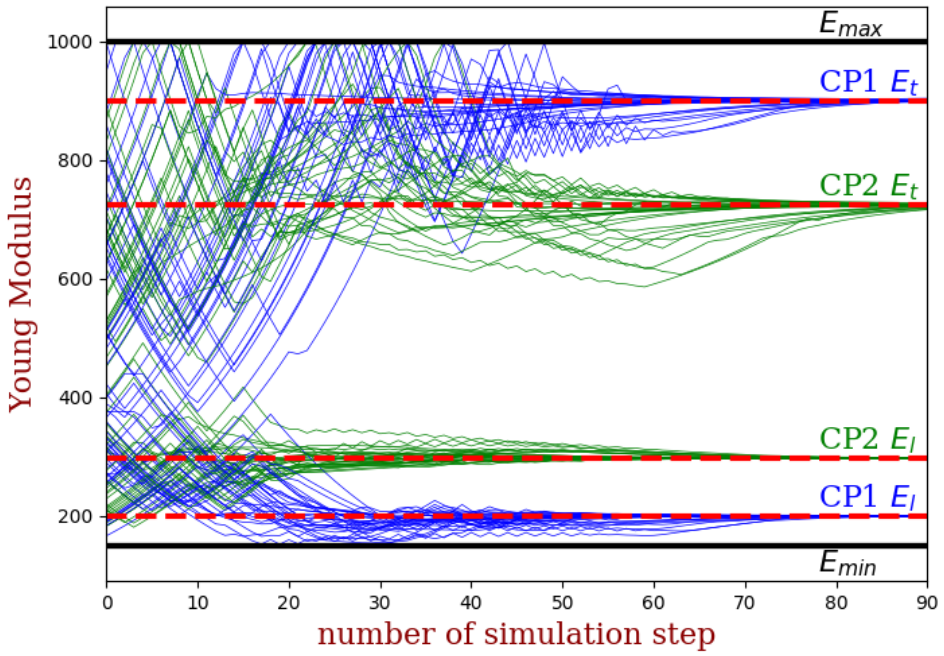

Figure 5.4: E_t and E_l convergence from the simulation of Fig. 5.2 for 30 different starting of $\mathbf{p}_{init}$. Blue/green lines are respectively for CP_1/CP_2 parameters and the red dotted lines correspond to the different parameters objectives. The 2 black lines represent the upper/lower bound (E_{max}/E_{min}) we have put for E.

up $\sum^j \mathbf{H}_p\mathbf{K}^{-1}\mathbf{H}_p^T$ on each of the j configurations. If we compute $\mathbb{W}_{ep}\left(\mathbb{W}_{pp}\right)^{-1}$ we obtain a dimensional link between the parameters and the effectors for which the conditioning number is easier to interpret.

We can see in Tab. 5.1 different results of conditioning for $\mathbb{W}_{ep}\left(\mathbb{W}_{pp}\right)^{-1}$ depending on combinations of number of parameters/effectors/configurations. We can see that when we optimise with less parameters and with more configurations, the conditioning values tends to decrease which improve the convergence. On the contrary, we rapidly tend to diverging cases when we have less configurations with less effectors.

These conditioning values are therefore good indicators of the variety of data used for calibration (with respect to the tested parameters) but unfortunately, we cannot yet presume what is the bound from which the problem will diverge/converge.

5.4 Practical use: calibration of a real anisotropic parallel robot

In chapter 4 we have shown that we were able to create a new DOF on a 6-DOF parallel soft robot using metamaterial and simulate this new behavior. We had also done an initial workspace assessment on the simulation. The mechanical parameters were fed to the model in a fairly accurate way through theoretical mechanical parameters of the soft

Number of		configurations		
parameter	effector	3	4	6
4	1	112	8	4
	4	27	5	4
6	1	1413	221	143
	4	84	72	53

Table 5.1: Comparison of different conditioning values of $\mathbb{W}_{ep}\left(\mathbb{W}_{pp}\right)^{-1}$ with different number of parameters $\{4, 6\}$ per beam and effector on them $\{1, 4\}$ and finally with 3, 4 or 6 configurations. **Green** correspond to converging cases, **orange** to oscillating and **red** to diverging.

plastic used in the 3D-printer as well as numerical homogenisation to take into account the particular foam structure of the meta-material. Nevertheless, we were controlling the robot on open loop and we witnessed large differences between the simulated workspace capability and the reality. This can come from multiple factors/errors :

- Printing technique adding defects into the structure and also adding some anisotropy along the printing direction (see in chapter 3.4.1).
- Homogenisation of the generated mesostructure mechanical properties (see section chapter 3.2.2).
- Setup little errors (placement, motors position, mechanical fatigue...).

A calibration of the model based on real data, taken from the robot, should allow to significantly improve the results of the model, in particular by reducing the first two error factors.

5.4.1 QP problem setup

As effector, we have chosen the frame placed at the middle of the rod linking the 2 tripods. We have placed on it a Polhemus[1] sensor that allows us to get accurate position as well as orientation of the effector during the calibration. To characterize our soft sheet mechanical properties we choose to put CP as shown on Fig. 5.5: two for each branch (without any at their end, because they are rigidified to represent the part attached to the motors and therefore do not deform) and then 6 around the center where most of the precision is needed. The $\mathbf{p}_{init}$ are given in order to be as close as possible with the previous simulated model (see A of Fig. 5.5), which means a uniform value of the Young modulus E_t and E_l along the structure and the same spiral pattern parameterized with θ.

Assuming that 3D printing is sufficiently reproducible, we consider that the robotic

[1] https://polhemus.com/

setup is symmetrical. The same parameters will be used in the two soft sheets. Consequently, we have 12 CP with 3 parameters each, so a problem of $dim(\mathbf{p}) = 36$. For the calibration, we choose 7 configurations (which is the minimum to guarantee the positiveness of the QP matrix) giving 7 effector positions well distributed inside the workspace. Each effector position is described with 6 parameters (3 for translations, 3 for orientations) so we have $dim(\mathbf{\Delta}_e) = 42$.

5.4.2 Results

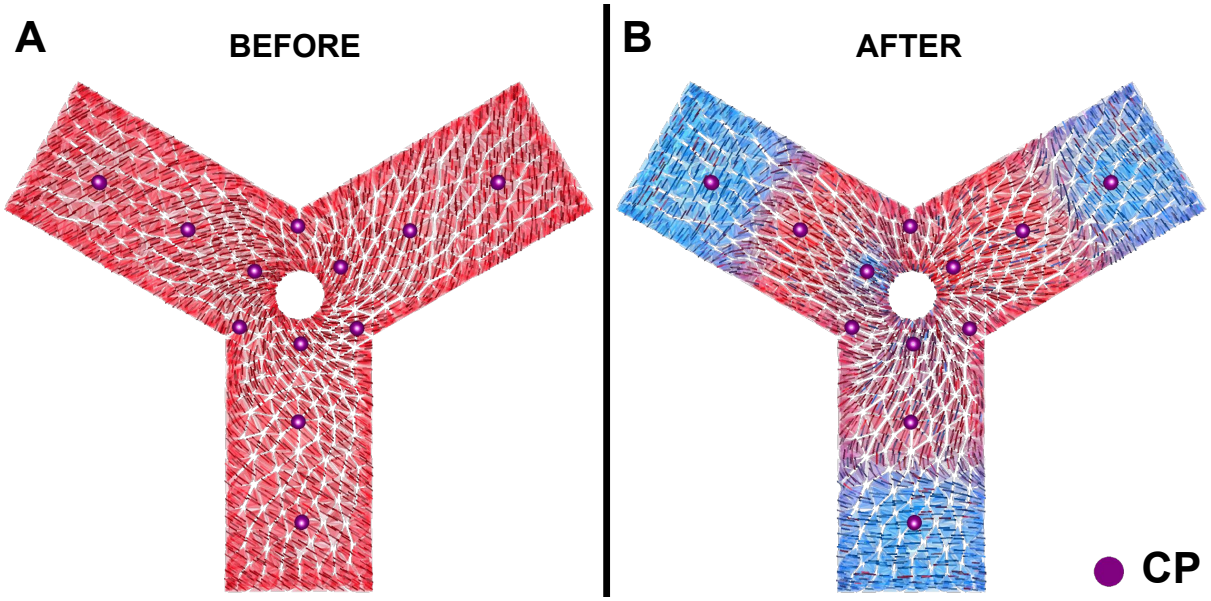

Figure 5.5: Flexible sheet before (A) and after (B) optimisation with the CP repartition (purple dot).

The optimisation converged to 36 new values giving to a new visual representation of the results with the interpolation shown on Fig. 5.5.B. It clearly show the shortcomings of 3D printing with respect to anisotropy and expected mechanical properties: compared to Fig. 5.5.A, $\mathbf{p}_{init}$, E_t and E_l are no more homogeneous over the sheet with blue pockets being less stiff than the red. Moreover, the spiral pattern is much less pronounced.

In contrast, with this new set of mechanical parameters the general error reduction between the goal and effector was reduced by 46% as can be seen on Tab. 5.2. It correspond to a mean error distance of 1.2mm with the previous value and 0.49mm with the new set of parameters found by the optimisation. Concerning the error in angle we pass from 6.35°to 3.21°.

To show the validity of the calibration, we also consider new positions in the workspace (that were not used for calibration), and we compare the evolution of the error between the model using the initial (not calibrated) parameters and the new results. We can see that it was also reduced in average by 43% which shows the FEM ability to interpolate the behaviour beyond the positions on which it was calibrated.

	configurations (effector position)							mean
	1	2	3	4	5	6	7	
error reduction (%)	60	70	55	47	46	68	-23	46
	new configurations (taken in workspace)							
error reduction (%)	65	65	27	5	17	48	76	43

Table 5.2: Errors reduction of the effector position in percent between the real setup and the simulation before and after optimisation. The first line correspond to the error reduction on configuration on which the optimisation was done and the second on newly tested configurations.

A part of the remaining error (which is noticeably smaller than before) comes from the fact that the model is not perfect (mechanical parameters comes from homogenisation, internal contact are not taken into account, model for small displacement for linear elastic material...) and another part comes from the real setup noises that are not taken into account in the calibration (positioning error of the motors, dimension and attachment of the sheet with the motors, placement of the rigid marker...). To further decrease the error, more CPs could be added to refine the parameters evolution over the robots shape but it will require to calibrate on more configurations.

Nevertheless, the QP optimization was able to find better parameters given the input data. The improved model parameters can be used for more accurate control of the robot, including when looking into closed-loop control.

5.5 Conclusion

We have presented a new method allowing to optimise mechanical parameters of a FEM as well as to formulate and solve multi-configuration QP problems. The method allows to calibrate a complex anisotropic FEM with a relatively high number of parameters (here up to 36) while using a relatively low number of different configurations (only 7), with a single 6D-measurement per configuration, and succeeds to achieve an average error reduction, before/after calibration, of more than 40%. The number of input data remains reasonable. The method is frugal compared to model-less methods.

The method is based on convex optimisation and we have shown that the combination of the number of configurations, the number of parameters, and the number of effectors have to be carefully chosen to guarantee the well-posedness of the QP problem. In section 3, we give an indicator to evaluate the conditioning of the QP problem. However that is not a strict criteria that will predict whether the optimisation will converge or not.

Furthermore another aspect of the problem must be mentioned: convex optimisation can lead to getting stuck on local minima. In particular when the choice of parameters or the stresses in terms of deformations lead to important non-linearities where it is difficult to reach the global optimum. Moreover, we rely on numerical differentiation that assumes a good continuity of the influence of the parameters on the expression of the internal forces.

We have discussed ways to set the optimisation problem properly but it still needs some investigation in order to have a better knowledge about the problem conditioning and as much as possible, we would like to provide an automatic calibration workflow. We could test the method on various soft robots, with other actuator types and also other sensors to make the calibration.

Also we have to keep in mind that the optimisation process over real life data will try to correct the total error of our real setup (motors actuation / mounting errors...) and not only the mechanical parameters of the soft structure. It would need more effort to have a more reliant setup in order to decouple the mechanical errors specifically. Note that we are doing open loop simulation for the motors control, closing the loop and sending back more sensors information (like real motor positions and/or torques) can help achieve this mechanical decoupling.

Conclusion

Summary and assessment

In this work, we have shown how the kinematics of soft robots can be dramatically modified by changing their material composition - but not their geometry - using metamaterials. We presented a first generic simulation framework to include anisotropy in the soft robot finite element model, allowing open loop control. It brings exciting new research paths, notably as a way to program compliance in soft systems. Indeed, by fully harnessing the structure potential of a soft system with metamaterials, we can program its heterogeneities and bring further the fields of morphological computation. This allows soft systems to incorporate control and sensing into their structures and reduce the number of actuation sources needed.

We have shown in chapter 2 that the literature of soft robots using metamaterials is not yet really consequent due to the recent interest on the matter. The metamaterial community, however, is really important, particularly thanks to the computer graphics fields which proposes numerous different approaches and designs. The current lack of bridges between these two communities (metamaterials and soft robotics) comes from two main factors:

- **Difficult to simulate**: metamaterials are generally based on a lattice of repeated patterns ranging from micro to meso scale. These lattices can sometimes be assimilated as linear materials but a larger number of metamaterials harness instabilities as a mean to create new behaviours. They also have applications on different fields: electromagnetic, optical, acoustic and mechanical which add a multi-physics aspect. As a consequence, it is complicated to have an accurate representation of metamaterials without having heavy computation involved, which hampers any interactive simulation of their behaviors.
- **Difficult to design**: the available metamaterial solutions are diverse in properties, compositions and geometries. This has led to diverse design methods around some types of metamaterials and in general to a case-by-case approach for each new design.

The work of this thesis contributes to resolving some of these difficulties.

Concerning metamaterial simulation in chapter 3, we have presented a modeling of a foam mesostructure with graded anisotropic properties. By using homogenisation and some continuum assumptions, we were able to formulate a FEM implementation allowing to reproduce transverse behavior and parameterise it. With this implementation we can program a given compliance on any geometry with the simulation software SOFA.

We have evaluated in chapter 4 the correspondence of our model with its real counterpart and showed that we were able to control new complex behaviors. We demonstrated that with a metamaterial structure we were able to design with the simulation a setup allowing to control a new DoF without adding new actuation sources. We verified that we had a good match in the kinematics between the designed and the real setup results.

Finally, in chapter 5, we have presented a method to reduce the simulation errors coming from the simplification of the mesostructure model. This method is generic for any differentiable mechanical parameter. We have used it in the case of anisotropic parameters and calibrated them with real setup data. We can optimise many parameters at the same time (we have tested up to 36) and still have a well posed convex problem thanks to the multi-configuration approach we use. We show on a real example that we were able to improve the overall simulation precision of around 44%.

Future work and perspectives

Modeling and design

We can envision in the short term to use the multi-configuration optimisation for helping the design process of a soft robot. Instead of using real robot data and optimise the model mechanical parameters on it, we can set artificial data that will represent a theoretical system behavior. The simulation will then produce the best possible set of parameters that matches the behavior. Moreover, the presented method could be used for the definition of trajectories that are discretised into multiple configurations. We could thus optimise both the structure parameters and the actuators inputs in the inverse problem, which would bring us closer to the methods used in optimal control. We will then be able to create soft robot designs optimised for certain tasks thanks to the simulation.

It can also be interesting to grade not only the transverse direction but also the anisotropic behavior in all directions by implementing an orthotropic material model inside our software. We will have a wider range of possible designs and be able to do a smooth transition between isotropy and orthotropy. However if we want to still be able to do optimisation for design and/or calibration, we will have to represent orthotroptic behavior with less parameters. We can also search for ways to determine how to have better conditioning, maybe with some hyperparameters, taking inspiration from machine learning.

In a longer term perspective, we can work on more accurate simulations for systems showing large deformations. In this direction, implementation of a hyperelastic model for anisotropic materials can be really interesting. In addition, concerning self contact influence, it may be valuable to quantify their contribution on the whole compliance and find ways to take them into account while keeping an interactive simulation. Doing offline learning of the self contacts contribution, for example by taking them into account in the

manner of model reduction approach, can be a path to explore.

Soft robot fabrication

For the fabrication of soft systems with metamaterials in general and in particular with the foam, there are many implementations which can be tested. Indeed, in this thesis we were designing real setups with simulation validation in mind. The first intention was not to create new efficient soft systems using mesostructures.

Thus, there are many possibilities offered by the foam that we have not explored. Notably, design systems using full orthotropy gradation. We can also experiment on the integration of sensors and actuators in the foam and assess the influence of these rigid devices on the global compliance. Taking inspiration from electromagnetic metamaterials we can even explore the actuator/sensors mechanical cloaking in the case haptic interface.

Finally, for the foam but also for the use of metamaterials in soft robotics in general, exploring their use in combination with multimaterial or smart material (SMA,SP) can offer interesting new behaviors to experiment upon. We can also envision the use of metamaterials of other fields (electrodynamic, acoustic) in combination with mechanical metamaterials to create multi-physics devices.

To conclude, this work shows the growing interest of metamaterial incorporation into soft robotics systems. It offers interesting perspectives to create completely untethered soft robots with monolithic structures. These structures could have integrated actuation and sensors capabilities while having optimised mechanical properties to achieve specific tasks. With the development of additive manufacturing, we can even consider creating these complex structures in a single integrated manufacturing process.

List of Figures

1.1 Total number of publications in soft robotics research for each year from 2010 to 2020. Figure from [17]. 5
1.2 Approximate tensile modulus (Young modulus in pascal (Pa)) of selected engineering and biological materials. Figure from [19]. 5
1.3 Soft systems classified according to their dependence on rigid structures. Octobot (A) is an untethered robot comprising only soft components [21]. Marchese and Rus's soft spatial manipulator (B), the multigait soft robot (C) (a precursor to (G)), and the spherical jamming mobile robot (D) comprise only soft materials but require external supplies [22, 15, 23]. The lightweight soft robotic arm (E) moves using pneumatic actuators that also provide a compliant covering [24]. OctArm (F) uses pneumatic actuators to create a continuum manipulator but requires rigid plates to separate each section of the manipulator [25]. The resilient untethered soft robot (G) moves using pneumatically powered actuators but relies on hard batteries, compressors, and micro-controllers [26]. DLR Robotics' LWR-III (H) [27] achieves softness through lightweight materials, sensor redundancy, and active compliance control. Variable impedance actuators (I) incorporate compliance into a rigid robot, creating a 'soft' robot, by exploiting passive or actively controlled elastic elements [28]. Figure from [20]. 6
1.4 Differentiation of the soft robot components (Actuator/Sensor/Controller/Power) of the top 10% soft robotics paper in number of citation per year. They are classified based on their tether composition (Physical/Non-Physical and totally Untethered). a) Tethering category examples and legend. b) Device tethering shown relative to the number of component types a given device contained. Figure from [17]. 7
1.5 Visual representation and description of the different available technologies of additive manufacturing. Figure from [34]. 8
1.6 The Five categories of 3D printing materials for soft robotics with commercially available examples. Figure from [36]. 10
1.7 Comparison of hardness, or softness, of materials suitable for use in soft robots. Some common materials have known hardness values and are shown in the figure. Figure from [14]. 11
1.8 (**1**) 3D printed silicone from [37]. (**2**) graded properties of silicone with bubbles of liquids from [38]. 11

1.9 Overview of soft systems material composition of top 10% of publications by average citations per year (aCPY). a) Material category examples and legend. b) Number of robotic components using a given material in each year. c) aCPY based on the material used for a given robotic component. Figure from [17]. 12
1.10 In this example a tendon is pulled to create the motion of an elastic soft robot. Starting with the same geometry, the material stiffness has an influence on the kinematics (output vs input displacements). Figure from [39] 14
1.11 SOFA logo with two example of medical application. (**1**) Representation of organs in order to assist or train surgeon [50] for example with cochlea operation (**2**) [51]. 16
1.12 From left to right and top to bottom : control of a deformable manipulator robot based on a compliant spine [59], control from inverse simulation of pneumatic manipulator [60], Stiffness rendering [61], Optimization-based inverse model of soft robots with contact handling [62], Coupling numerical deformable models in global and reduced coordinates [63], Visual servoing control of soft robots [64]. 17

2.1 Multifunctional metamaterial composites considered under acoustic, electrodynamic and mechanical realms with a artist representation of a typical structure for each. Figure from [69]. 23
2.2 (**1**) a) When a wave strikes a positive refraction index material from a vacuum. b) When a wave strikes a negative-refraction-index material from a vacuum. c) When an object is placed in front of an object with n=−1, light from it is refracted so it focuses once inside the lens and once outside. This allows subwavelength imaging. (**2**) A split-ring resonator array arranged to produce a negative index of refraction, constructed of copper split-ring resonators and wires mounted on interlocking sheets of fiberglass circuit board [77]. (**3**) Three-dimensional optical metamaterial with a negative refractive index [78]. 25
2.3 3D labyrinthine channel system that leads to slowing down of sound propagation. Figure from [81]. 26

2.4 Example of one flexible metamaterial of each categories. (**1**) **Instability-based** : A rubber slab patterned with circular holes undergoes a reversible pattern transformation when compressed as a result of a collective buckling-like instability [95]. (**2**) **Mechanism-based** : Jansen walker build with metamaterial (a) leg of the Jansen walker has 6 hinges (b) As the center is actuated by a crank, the legs deform in a walking motion. (c) two hinges are constrained to rotate, but not translate, using a layer of hinges. (d) The complete walker [96]. (**3**) **Topological** metamaterials : sculpted localized buckling regions in the interior of periodic cellular metamaterials. They are robust against structural perturbations [90]. (**4**) **Linear mechanical** metamaterials : Tilings geometry with complex mechanical behavior characterized by anisotropy, nonlinearity, and large variations in stiffness among different patterns [97]. 27
2.5 Categories of cellular solids from [98] 29
2.6 Example of different lattice structures. (**1**) Given a virtual object with specified elasticity material parameters (blue=soft, red=stiff), the method computes an assemblage of small-scale structures that approximates the desired elastic behavior [99]. (**2**) 3D Periodic Cellular Materials with Tailored Symmetry and Implicit Grading [100]. (**3**) 2D functionally graded materials optimized for maximum bulk modulus under linearly-varying volume [101]. (**4**) Two-scale topology optimization framework allowing to optimize continuous material properties mapping to printable microstructures [102]. 29
2.7 Example of different stochastic structures. (**1**) Additive manufacturing and characterisation of brittle foams [103]. (**2**) Adaptive anisotropic porous structure design and modeling for 2.5D mechanical parts [104]. (**3**) Microstructures well suited for FDM fabrication which afford a wide range of elastic behaviors, from isotropic to orthotropic [105]. 30
2.8 Example of different soft robotics systems using auxetic behavior has main principle. (**1**) Application of 6×6 soft capacitive auxetic sensor array to soft universal jamming gripper [116]. (**2**) Soft Robotic Grippers with 3D Printed handed shearing auxetics material [115]. (**3**) Poisson Induced Bending Actuator for Soft Robotic Systems [114]. (**4**) Locomotion of a soft metamaterial robot based on complementary auxetic materials acting as passive clutches [111]. 33
2.9 Distribution of the Poisson ratio depending on the structure geometry. Figure from [114]. 33
2.10 Example of different soft robotics systems using lattice structure. (**1**) Multidirectional locomotion of starfish robot with legs composed of cylindrical tensegrity beam [119]. (**2**) Hybrid lattice structure configurations allowing stiffness modulation for soft robot joint [121]. (**3**) Textile actuators (textuators) used as an artificial muscles and (**4**) schematic of its concept [122]. 34

2.11 Example of different soft robotics systems using instability-based metamaterials. (**1**) Bio-inspired soft robot (Metarpillar) based on buckling actuator metamaterial units [127]. (**2**) 3D sketch of two soft pneumatic robots using buckling for (A) a soft gripper and (B) locomotion [126]. (**3**) A VAMP (vacuum-actuated muscle- inspired pneumatic structures) lifting 500g [125]. (**4**) Schematic of a robot actuated with two bistable element–muscle pairs [128]. 35
2.12 Schematics of a buckling actuator with two actuation units inducing a rotary actuation mechanism. Figure from [124]. 35
2.13 Example of different soft robotics systems using mechanism-based metamaterials. (**1**) Sensorized, soft robotic arm segment using kirigami conductive sensors [135]. (**2**) Jansen walker build with metamaterial using hinges [96]. (**3**) Kirigami-skinned soft crawlers using controllable buckling anchors [133]. (**4**) Morphing and deployable underwater machine using a multimaterial kirigami composite allowing shape and rigidity morphing [139]. (**5**) OrigamiBot-II: Three-finger origami manipulator using the origami twisted tower concept [130]. 36
2.14 Generic architecture for design optimization of soft robots. Figure from [144]. 38

3.1 Foam elastic behaviors variation from isotropic to orthotropic by a continuous variation of its density and its material orientation. From [149] 44
3.2 Generation of the eight types of linear elastic symmetry by the successive introduction of planes of symmetry. Figure from [150] 48
3.3 Example of a foam representative volume (RVE) used to find the homogenised properties. Here the foam shows a strong transverse isotropy. . 51
3.4 Data from homogenization of 4 samples with a relative density varying between 9 to 34%. A and B are for the transverse isotropic case and C correspond to the isotropic case. The Young's modulus shown here are normalized to a base isotropic material having a Young's modulus E = 1 and Poisson's ratio v = 0.3 53
3.5 Co-rotational FEM : a local frame is computed on each element to handle large rotations. Figure from [44]. 55
3.6 Image of a Prusa 3D printer with an additionnal schematic showing the different parts composing the "hot end" and their emplacements. 60
3.7 3D visualisation of a slicing of a 3D bunny made in the Cura slicer. 60
3.8 3D visualisation of a slicing of a 3D bunny made in the IceSL slicer. 61
3.9 Visualisation in IceSL of a the gradation of the density applied with a "brush" (less to more density: blue to red) on a bear geometry (left). Results of the 3D printing geometry (middle) with its different compliance (right). 62

3.10 Different faces of a same beam showing the differences added due to the printing technique. The beam was printed vertically from A being the first layer to B the last. —A We can see that the filament deposit is broader. —B We clearly see the difference with the first layer —C Due to oozing the sides are rigidified. 63
3.11 Workflow proposed: from the homogenization of the mechanical properties of the meso-structure, through the design of a robot on simulation, to the fabrication of the robot with a 3D-printer. 65

4.1 Comparison between simulated beams ($\approx 20k$ tetrahedra) and their real counter part in bending under gravity. —A. Simulation regrouping the isotropic case with the transverse isotropic in Z and Y direction with the colors blue, red and green respectively —B. correspond to the blue beam ; real bending: -48mm, simu: -47.2mm —C. correspond to the red beam; real: -24mm, simu : -22.2mm —D. correspond to the green; real: -23mm, simu: -19.1mm 70
4.2 The Tripod Robot is composed of a soft silicone piece actuated by three servomotors, the robot can achieve a nearly infinite number of shape configurations. 71
4.3 3D-printed flexible sheets made with IceSL. 72
4.4 Comparison of 3 tripods : one made of silicone and totally isotropic (left) and 2 others corresponding respectively to the case A (middle) and B (right) already presented. 73
4.5 View from above of a flattened flexible sheet with a comparison between the simulated part (**B**) where each elements has a specific orientation allowing to have a global spiral pattern and the 3D printed real part (**A**). We keep E_t and E_l constant for the whole structure, only the orientation differ. . . . 74
4.6 Simulation of the 2 presented cases **A** and **B**. There is a visual representation of each elements direction with a little line. On case (**A**) the lines directions are all the same depending on the tripod branch and for case (**B**) each elements has a different direction reproducing the spiral pattern. 75
4.7 View from above of the real validation setup: the 2 tripods are facing each other and linked with a rigid rod. Additionally we attached on the middle of this link a maze that will be used to visualize more efficiently the controlled movement of the end effector of this system. 78
4.8 Side view of the simulation of the global setup. In the middle, in grey, the system is presented at rest state. The figure show the sixth DOF created around the rod. When both tripod "pull" (**A**), a rotation appears around the rod in one direction and when they "push" (**B**) it rotate on the same axis but in an opposite direction. Due to the fact that motors are either all "pulling" or all "pushing", the maze stay centered during all the actuation enabling a decoupled sixth DOF 79

4.9 LEFT: Workspace exploration with the effector. Starting from rest position, we try to reach each point and if it is reachable we try to do on it 3 orthogonal rotation of -/+10°. Depending on the results the point is classified in the blue, green, orange or red categories. RIGHT: Workspace exploration with different angle limits imposed on the actuators. In this constrained exploration, reaching a points with an error margin of 1 mm validate it. The exploration is done on the same points as LEFT. We test 3 different angle limits producing 3 different possible workspace each including the other : red is included in yellow which is included in blue. . . 82
4.10 Convergence from transverse (right of the figure) to isotropic (origin). Abscissa α represents an anisotropy percentage. $\alpha(\%) = 100 - 100(E_l/E_t)$. The test is done by either pulling all motors of 15° or pushing them of 35° degrees from the rest state as presented in Fig. 4.8. 83
4.11 Comparison between a parallel soft robot made of silicone (**A**) and one made of our metamaterial (**B**). For both we actuate all servomotors from 1 to 2; action : purple arrow / reaction : red arrow. With traditional homogeneous material (**A**), we can see that the maze translate to the right, but with a mesostructured flexible sheet (**B**) a rotation around the metal rod axes is created. 84

5.1 Interpolation between 2 CP (red dot) with, on the left each little black lines corresponding to a tetrahedron's direction and on the right we have the corresponding 3D shape generated. The right/left CP have respectively a set direction of $-35°/35°$. There is also a comparison with different values of p for the IDW interpolation [170]. 93
5.2 QP simulation with 4 configurations of a simple beam subject to only gravity. The purple arrows represent the new modification of the configuration compared to the first one (**1**): configuration **2** & **3** have two different rotation around there longitudinal axis and for **4** the tip and attached part were switched. 95
5.3 Minimisation of $\mathbf{\Delta}_e$ with QP problem having different number of configuration: from 1 up to 4. B1 corresponds to a QP problem with configuration 1, B2 optimizes on configuration 1 and 2, B3 optimizes on configurations 1,2 and 3 and finally, B4 optimizes on the 4 configurations. 96
5.4 E_t and E_l convergence from the simulation of Fig. 5.2 for 30 different starting of $\mathbf{p}_{init}$. Blue/green lines are respectively for CP_1/CP_2 parameters and the red dotted lines correspond to the different parameters objectives. The 2 black lines represent the upper/lower bound (E_{max}/E_{min}) we have put for E. 97
5.5 Flexible sheet before (A) and after (B) optimisation with the CP repartition (purple dot). 99

List of Tables

2.1 Current literature on integration of metamaterials into soft robots/systems and their classification. 31

4.1 Comparison between simulated tripod and real one for 3 positions. We measure only the *Height* and *Angle* of the tip of the tripod. 74

5.1 Comparison of different conditioning values of $\mathbb{W}_{ep}\left(\mathbb{W}_{pp}\right)^{-1}$ with different number of parameters $\{4, 6\}$ per beam and effector on them $\{1, 4\}$ and finally with 3, 4 or 6 configurations. **Green** correspond to converging cases, **orange** to oscillating and **red** to diverging. 98

5.2 Errors reduction of the effector position in percent between the real setup and the simulation before and after optimisation. The first line correspond to the error reduction on configuration on which the optimisation was done and the second on newly tested configurations. 100

Bibliography

[1] Félix Vanneste et al. “Anisotropic soft robots based on 3D printed meso-structured materials: design, modeling by homogenization and simulation”. In: *IEEE Robotics and Automation Letters* 5.2 (2020), pp. 2380–2386 (1, 18).

[2] Félix Vanneste, Olivier Goury, and Christian Duriez. “Calibration method for soft robots modeled with FEM: application to anisotropy”. In: *IEEE Robotics and Automation Letters* (2020) (1, 18).

[3] Félix Vanneste, Olivier Goury, and Christian Duriez. “Enabling the control of a new degree of freedom by using anisotropic material on a 6-DOF parallel soft robot”. In: *Robosoft 2021*. 2021 (1, 18).

[4] Barbara Mazzolai et al. “Roadmap on soft robotics: multifunctionality, adaptability and growth without borders”. In: *Multifunctional Materials* (2022) (1).

[5] Koichi Suzumori. “Elastic materials producing compliant robots”. In: *Robotics and Autonomous systems* 18.1-2 (1996), pp. 135–140 (4).

[6] Cecilia Laschi et al. “Soft robot arm inspired by the octopus”. In: *Advanced robotics* 26.7 (2012), pp. 709–727 (4).

[7] Sangok Seok et al. “Meshworm: a peristaltic soft robot with antagonistic nickel titanium coil actuators”. In: *IEEE/ASME Transactions on mechatronics* 18.5 (2012), pp. 1485–1497 (4).

[8] Andrew D Marchese, Cagdas D Onal, and Daniela Rus. “Autonomous soft robotic fish capable of escape maneuvers using fluidic elastomer actuators”. In: *Soft robotics* 1.1 (2014), pp. 75–87 (4).

[9] Nadia G Cheng et al. “Design and analysis of a robust, low-cost, highly articulated manipulator enabled by jamming of granular media”. In: *2012 IEEE international conference on robotics and automation*. IEEE. 2012, pp. 4328–4333 (4).

[10] Eric Brown et al. “Universal robotic gripper based on the jamming of granular material”. In: *Proceedings of the National Academy of Sciences* 107.44 (2010), pp. 18809–18814 (4).

[11] Filip Ilievski et al. “Soft robotics for chemists”. In: *Angewandte Chemie* 123.8 (2011), pp. 1930–1935 (4).

[12] Panagiotis Polygerinos et al. “Soft robotic glove for combined assistance and at-home rehabilitation”. In: *Robotics and Autonomous Systems* 73 (2015), pp. 135–143 (4).

[13] Pham Huy Nguyen et al. “Soft poly-limbs: Toward a new paradigm of mobile manipulation for daily living tasks”. In: *Soft robotics* 6.1 (2019), pp. 38–53 (4).

[14] Mengjia Zhu et al. “Soft, Wearable Robotics and Haptics: Technologies, Trends, and Emerging Applications”. In: *Proceedings of the IEEE* (2022) (4, 11).

[15] Robert F Shepherd et al. “Multigait soft robot”. In: *Proceedings of the national academy of sciences* 108.51 (2011), pp. 20400–20403 (4, 6).

[16] Elliot W Hawkes et al. “A soft robot that navigates its environment through growth”. In: *Science Robotics* 2.8 (2017), eaan3028 (4).

[17] Barclay Jumet et al. “A Data-Driven Review of Soft Robotics”. In: *Advanced Intelligent Systems* (2021), p. 2100163 (5, 7, 12).

[18] Carmel Majidi. “Soft robotics: a perspective—current trends and prospects for the future”. In: *Soft robotics* 1.1 (2014), pp. 5–11 (4).

[19] Daniela Rus and Michael T Tolley. “Design, fabrication and control of soft robots”. In: *Nature* 521.7553 (2015), pp. 467–475 (4, 5).

[20] Kevin Chubb, Damon Berry, and Ted Burke. “Towards an ontology for soft robots: what is soft?” In: *Bioinspiration & biomimetics* 14.6 (2019), p. 063001 (5, 6).

[21] Michael Wehner et al. “An integrated design and fabrication strategy for entirely soft, autonomous robots”. In: *nature* 536.7617 (2016), pp. 451–455 (6).

[22] Andrew D Marchese and Daniela Rus. “Design, kinematics, and control of a soft spatial fluidic elastomer manipulator”. In: *The International Journal of Robotics Research* 35.7 (2016), pp. 840–869 (6).

[23] Erik Steltz et al. “Jsel: Jamming skin enabled locomotion”. In: *2009 IEEE/RSJ International Conference on Intelligent Robots and Systems*. IEEE. 2009, pp. 5672–5677 (6).

[24] Preston Ohta et al. “Design of a lightweight soft robotic arm using pneumatic artificial muscles and inflatable sleeves”. In: *Soft robotics* 5.2 (2018), pp. 204–215 (6).

[25] William McMahan et al. “Field trials and testing of the OctArm continuum manipulator”. In: *Proceedings 2006 IEEE International Conference on Robotics and Automation, 2006. ICRA 2006.* IEEE. 2006, pp. 2336–2341 (6).

[26] T TolleyMichael et al. “A resilient, untethered soft robot”. In: *Soft robotics* (2014) (6).

[27] Alin Albu-Schaffer et al. “Soft robotics”. In: *IEEE Robotics & Automation Magazine* 15.3 (2008), pp. 20–30 (6).

[28] Ronald van Ham et al. “Compliant actuator designs”. In: *IEEE Robotics & Automation Magazine* 3.16 (2009), pp. 81–94 (6).

[29] Steven I Rich, Robert J Wood, and Carmel Majidi. “Untethered soft robotics”. In: *Nature Electronics* 1.2 (2018), pp. 102–112 (6).

[30] C. Laschi and B. Mazzolai. “Lessons from animals and plants: The symbiosis of morphological computation and soft robotics”. In: *IEEE Robot. Autom. Mag.* 23.3 (2016), pp. 107–114. ISSN: 10709932. DOI: 10.1109/MRA.2016.2582726 (6).

[31] Andre Rosendo, Marco Von Atzigen, and Fumiya Iida. “The trade-off between morphology and control in the co-optimized design of robots”. In: *PLoS One* 12.10 (2017), pp. 1–14. ISSN: 19326203. DOI: 10.1371/journal.pone.0186107. URL: http://dx.doi.org/10.1371/journal.pone.0186107 (6).

[32] Julius E. Bernth, Van Anh Ho, and Hongbin Liu. “Morphological computation in haptic sensation and interaction: from nature to robotics”. In: *Adv. Robot.* 32.7 (2018), pp. 340–362. ISSN: 15685535. DOI: 10.1080/01691864.2018.1447393. URL: https://doi.org/10.1080/01691864.2018.1447393 (6).

[33] Caa J Autom Sinica et al. “So Robotics: Morphology and Morphology-inspired Motion Strategy Cite this paper Soft Robotics: Morphology and Morphology-inspired Motion Strategy”. In: (). URL: http://ieeexplore.ieee.org. (6).

[34] TJ Wallin, J Pikul, and RF Shepherd. “3D printing of soft robotic systems”. In: *Nature Reviews Materials* 3.6 (2018), pp. 84–100 (8, 9).

[35] Dominik Bauer et al. “Design and control of foam hands for dexterous manipulation”. In: *International Journal of Humanoid Robotics* 17.01 (2020), p. 1950033 (10, 15).

[36] Yee Ling Yap, Swee Leong Sing, and Wai Yee Yeong. “A review of 3D printing processes and materials for soft robotics”. In: *Rapid Prototyping Journal* (2020) (10).

[37] Bjorn Sparrman et al. “Printed silicone pneumatic actuators for soft robotics”. In: *Additive Manufacturing* 40 (2021), p. 101860 (11, 12).

[38] Jonas Zehnder et al. “Metasilicone: design and fabrication of composite silicone with desired mechanical properties”. In: *ACM Transactions on Graphics (TOG)* 36.6 (2017), pp. 1–13 (11, 12).

[39] Thor Morales Bieze. “Contribution to the kinematic modeling and control of soft manipulators using computational mechanics”. PhD thesis. Lille 1, 2017 (14).

[40] Costanza Armanini et al. “Soft Robots Modeling: a Literature Unwinding”. In: *arXiv preprint arXiv:2112.03645* (2021) (14).

[41] Pierre Schegg and Christian Duriez. “Review on generic methods for mechanical modeling, simulation and control of soft robots”. In: *Plos one* 17.1 (2022), e0251059 (14).

[42] Michael DM Kutzer et al. “Design of a new cable-driven manipulator with a large open lumen: Preliminary applications in the minimally-invasive removal of osteolysis”. In: *2011 IEEE International Conference on Robotics and Automation*. IEEE. 2011, pp. 2913–2920 (15).

[43] Hossein Habibi et al. “Modelling an Actuated Large Deformation Soft Continuum Robot Surface Undergoing External Forces Using a Lumped-Mass Approacb* Research supported by UK Engineering and Physical Sciences Research Council (EPSRC).” In: *2018 IEEE/RSJ International Conference on Intelligent Robots and Systems (IROS)*. IEEE. 2018, pp. 5958–5963 (15).

[44] Hadrien Courtecuisse. “Nouvelles architectures parallèles pour simulations interactives médicales”. PhD thesis. Lille 1, 2011 (15, 16, 55).

[45] Olivier Goury and Christian Duriez. “Fast, generic, and reliable control and simulation of soft robots using model order reduction”. In: *IEEE Transactions on Robotics* 34.6 (2018), pp. 1565–1576 (15, 17, 56).

[46] Matheus S Xavier, Andrew J Fleming, and Yuen K Yong. “Finite element modeling of soft fluidic actuators: Overview and recent developments”. In: *Advanced Intelligent Systems* 3.2 (2021), p. 2000187 (15).

[47] Philip Moseley et al. “Modeling, design, and development of soft pneumatic actuators with finite element method”. In: *Advanced engineering materials* 18.6 (2016), pp. 978–988 (15).

[48] Charbel Tawk and Gursel Alici. “Finite element modeling in the design process of 3D printed pneumatic soft actuators and sensors”. In: *Robotics* 9.3 (2020), p. 52 (15).

[49] Martin Alnæs et al. “The FEniCS project version 1.5”. In: *Archive of Numerical Software* 3.100 (2015) (15).

[50] Nazim Haouchine. “Image-guided simulation for augmented reality during hepatic surgery”. PhD thesis. Lille 1, 2015 (16).

[51] Olivier Goury et al. “Numerical simulation of cochlear-implant surgery: towards patient-specific planning”. In: *International Conference on Medical Image Computing and Computer-Assisted Intervention*. Springer. 2016, pp. 500–507 (16).

[52] Jérémie Allard et al. “Sofa-an open source framework for medical simulation”. In: *MMVR 15-Medicine Meets Virtual Reality*. Vol. 125. IOP Press. 2007, pp. 13–18 (16).

[53] François Faure et al. “Sofa: A multi-model framework for interactive physical simulation”. In: *Soft tissue biomechanical modeling for computer assisted surgery*. Springer, 2012, pp. 283–321 (16).

[54] Everton Hermann. “Interactive Physical Simulation on Multi-core and Multi-GPU Architectures”. Theses. Institut National Polytechnique de Grenoble - INPG, June 2010. URL: https://tel.archives-ouvertes.fr/tel-00537947 (16).

[55] Hadrien Courtecuisse et al. “Real-time simulation of contact and cutting of heterogeneous soft-tissues”. In: *Medical Image Analysis* 18.2 (Feb. 2014), pp. 394–410. DOI: 10.1016/j.media.2013.11.001. URL: https://hal.inria.fr/hal-01097108 (16).

[56] Hugo Talbot et al. “Towards an interactive electromechanical model of the heart”. In: *Interface focus* 3.2 (2013), p. 20120091 (16).

[57] Hugo Talbot, Frederick Roy, and Stéphane Cotin. “Augmented reality for cryoablation procedures”. In: *ACM SIGGRAPH 2015 Posters*. 2015, pp. 1–1 (16).

[58] Igor Peterlik et al. “Constraint-based haptic rendering of multirate compliant mechanisms”. In: *IEEE Transactions on Haptics* 4.3 (2011), pp. 175–187 (16).

[59] Thor Morales Bieze et al. “Design, implementation, and control of a deformable manipulator robot based on a compliant spine”. In: *The International Journal of Robotics Research* 39.14 (2020), pp. 1604–1619 (17).

[60] Christian Duriez et al. “Framework for online simulation of soft robots with optimization-based inverse model”. In: *2016 IEEE International Conference on Simulation, Modeling, and Programming for Autonomous Robots (SIMPAR)*. IEEE. 2016, pp. 111–118 (17).

[61] Frédérick Largillière et al. “Stiffness rendering on soft tangible devices controlled through inverse FEM simulation”. In: *2016 IEEE/RSJ International Conference on Intelligent Robots and Systems (IROS)*. IEEE. 2016, pp. 5224–5229 (17).

[62] Eulalie Coevoet, Adrien Escande, and Christian Duriez. “Optimization-based inverse model of soft robots with contact handling”. In: *IEEE Robotics and Automation Letters* 2.3 (2017), pp. 1413–1419 (17).

[63] Yinoussa Adagolodjo, Federico Renda, and Christian Duriez. “Coupling numerical deformable models in global and reduced coordinates for the simulation of the di-

rect and the inverse kinematics of Soft Robots". In: *IEEE Robotics and Automation Letters* 6.2 (2021), pp. 3910–3917 (17).

[64] Zhongkai Zhang et al. "Visual servoing control of soft robots based on finite element model". In: *2017 IEEE/RSJ International Conference on Intelligent Robots and Systems (IROS)*. IEEE. 2017, pp. 2895–2901 (17).

[65] Gang Zheng et al. "Controllability pre-verification of silicone soft robots based on finite-element method". In: *2019 International Conference on Robotics and Automation (ICRA)*. IEEE. 2019, pp. 7395–7400 (17).

[66] Christian Duriez. "Control of elastic soft robots based on real-time finite element method". In: *2013 IEEE international conference on robotics and automation*. IEEE. 2013, pp. 3982–3987 (17).

[67] Olivier Goury, Bruno Carrez, and Christian Duriez. "Real-time simulation for control of soft robots with self-collisions using model order reduction for contact forces". In: *IEEE Robotics and Automation Letters* 6.2 (2021), pp. 3752–3759 (17).

[68] Robert K Katzschmann et al. "Dynamically closed-loop controlled soft robotic arm using a reduced order finite element model with state observer". In: *2019 2nd IEEE international conference on soft robotics (RoboSoft)*. IEEE. 2019, pp. 717–724 (17).

[69] Reece L Lincoln et al. "Multifunctional composites: A metamaterial perspective". In: *Multifunctional Materials* 2.4 (2019), p. 043001 (23).

[70] Rodger M Walser. "Electromagnetic metamaterials". In: *Complex Mediums II: beyond linear isotropic dielectrics*. Vol. 4467. International Society for Optics and Photonics. 2001, pp. 1–15 (24).

[71] Karl F Lindman. "Über eine durch ein isotropes System von spiralförmigen Resonatoren erzeugte Rotationspolarisation der elektromagnetischen Wellen". In: *Annalen der Physik* 368.23 (1920), pp. 621–644 (24).

[72] Suyi Li et al. "Architected origami materials: How folding creates sophisticated mechanical properties". In: *Advanced materials* 31.5 (2019), p. 1805282 (24).

[73] Daniela Rus and Michael T. Tolley. "Design, fabrication and control of origami robots". In: *Nat. Rev. Mater.* 3.6 (2018), pp. 101–112. ISSN: 20588437. DOI: 10.1038/s41578-018-0009-8. URL: http://dx.doi.org/10.1038/s41578-018-0009-8 (24, 31).

[74] Muamer Kadic et al. "Metamaterials beyond electromagnetism". In: *Reports on Progress in physics* 76.12 (2013), p. 126501 (24).

[75] Muamer Kadic et al. "3D metamaterials". In: *Nature Reviews Physics* 1.3 (2019), pp. 198–210 (24).

[76] Roderic Lakes. "Foam structures with a negative Poisson's ratio". In: *Science* 235.4792 (1987), pp. 1038–1040 (24).

[77] Richard A Shelby et al. "Microwave transmission through a two-dimensional, isotropic, left-handed metamaterial". In: *Applied Physics Letters* 78.4 (2001), pp. 489–491 (24, 25).

[78] David Schurig et al. "Metamaterial electromagnetic cloak at microwave frequencies". In: *Science* 314.5801 (2006), pp. 977–980 (25).

[79] Jason Valentine et al. “Three-dimensional optical metamaterial with a negative refractive index”. In: *nature* 455.7211 (2008), pp. 376–379 (24).

[80] N I[U+A3AC] Landy et al. “Perfect metamaterial absorber”. In: *Physical review letters* 100.20 (2008), p. 207402 (25).

[81] Tobias Frenzel et al. “Three-dimensional labyrinthine acoustic metamaterials”. In: *Applied Physics Letters* 103.6 (2013), p. 061907 (25, 26).

[82] Yun Lai et al. “Hybrid elastic solids”. In: *Nature materials* 10.8 (2011), pp. 620–624 (26).

[83] Pai Peng et al. “Controlling elastic waves with small phononic crystals containing rigid inclusions”. In: *EPL (Europhysics Letters)* 106.4 (2014), p. 46003 (26).

[84] Jordan R Raney et al. “Stable propagation of mechanical signals in soft media using stored elastic energy”. In: *Proceedings of the National Academy of Sciences* 113.35 (2016), pp. 9722–9727 (26).

[85] Tiemo Bückmann et al. “An elasto-mechanical unfeelability cloak made of pentamode metamaterials”. In: *Nature communications* 5.1 (2014), pp. 1–6 (26).

[86] Midori Isobe and Ko Okumura. “Initial rigid response and softening transition of highly stretchable kirigami sheet materials”. In: *Scientific reports* 6.1 (2016), pp. 1–6 (26).

[87] Babak Haghpanah et al. “Multistable shape-reconfigurable architected materials”. In: *Advanced Materials* 28.36 (2016), pp. 7915–7920 (26).

[88] CL Kane and TC Lubensky. “Topological boundary modes in isostatic lattices”. In: *Nature Physics* 10.1 (2014), pp. 39–45 (26).

[89] Bryan Gin-ge Chen et al. “Topological mechanics of origami and kirigami”. In: *Physical review letters* 116.13 (2016), p. 135501 (26).

[90] Jayson Paulose, Anne S Meeussen, and Vincenzo Vitelli. “Selective buckling via states of self-stress in topological metamaterials”. In: *Proceedings of the National Academy of Sciences* 112.25 (2015), pp. 7639–7644 (26, 27).

[91] Tom Mullin et al. “Pattern transformation triggered by deformation”. In: *Physical review letters* 99.8 (2007), p. 084301 (26).

[92] Sung Hoon Kang et al. “Complex ordered patterns in mechanical instability induced geometrically frustrated triangular cellular structures”. In: *Physical review letters* 112.9 (2014), p. 098701 (26).

[93] Graeme W Milton and Andrej V Cherkaev. “Which elasticity tensors are realizable?” In: (1995) (26).

[94] Katia Bertoldi et al. “Flexible mechanical metamaterials”. In: *Nature Reviews Materials* 2.11 (2017), pp. 1–11 (26, 31).

[95] Katia Bertoldi et al. “Negative Poisson’s ratio behavior induced by an elastic instability”. In: *Advanced materials* 22.3 (2010), pp. 361–366 (27, 34).

[96] Alexandra Ion et al. “Metamaterial mechanisms”. In: *Proceedings of the 29th annual symposium on user interface software and technology*. 2016, pp. 529–539 (27, 28, 31, 36, 37).

[97] Christian Schumacher et al. “Mechanical characterization of structured sheet materials”. In: *ACM Transactions on Graphics (TOG)* 37.4 (2018), pp. 1–15 (27).

[98] Wenjin Tao and Ming C Leu. "Design of lattice structure for additive manufacturing". In: *2016 International Symposium on Flexible Automation (ISFA)*. IEEE. 2016, pp. 325–332 (28, 29).

[99] Christian Schumacher et al. "Microstructures to control elasticity in 3D printing". In: *ACM Transactions on Graphics (TOG)* 34.4 (2015), pp. 1–13 (29, 30).

[100] Semyon Efremov, Jonàs Martı´nez, and Sylvain Lefebvre. "3D periodic cellular materials with tailored symmetry and implicit grading". In: *Computer-Aided Design* 140 (2021), p. 103086 (29).

[101] Eric Garner et al. "Compatibility in microstructural optimization for additive manufacturing". In: *Additive Manufacturing* 26 (2019), pp. 65–75 (29).

[102] Bo Zhu et al. "Two-scale topology optimization with microstructures". In: *ACM Transactions on Graphics (TOG)* 36.4 (2017), p. 1 (29, 30).

[103] Sirui Bi, Enze Chen, and Stavros Gaitanaros. "Additive manufacturing and characterization of brittle foams". In: *Mechanics of Materials* 145 (2020), p. 103368 (30).

[104] Bin Liu et al. "Adaptive anisotropic porous structure design and modeling for 2.5 D mechanical parts". In: *Materials & Design* 206 (2021), p. 109786 (30).

[105] Jonàs Martı´nez et al. "Polyhedral Voronoi diagrams for additive manufacturing". In: *ACM Transactions on Graphics (TOG)* 37.4 (2018), pp. 1–15 (30).

[106] Julian Panetta et al. "Elastic textures for additive fabrication". In: *ACM Transactions on Graphics (TOG)* 34.4 (2015), pp. 1–12 (30).

[107] Jonàs Martı´nez et al. "Orthotropic k-nearest foams for additive manufacturing". In: *ACM Transactions on Graphics (TOG)* 36.4 (2017), pp. 1–12 (30).

[108] Bernd Bickel et al. "Design and fabrication of materials with desired deformation behavior". In: *ACM Transactions on Graphics (TOG)* 29.4 (2010), pp. 1–10 (31).

[109] Ahmad Rafsanjani, Katia Bertoldi, and André R Studart. "Programming soft robots with flexible mechanical metamaterials". In: *Science Robotics* 4.29 (2019), eaav7874 (31).

[110] Arnaud Lazarus and Pedro M. Reis. "Soft actuation of structured cylinders through auxetic behavior". In: *Adv. Eng. Mater.* 17.6 (2015), pp. 815–820. ISSN: 15272648. DOI: 10.1002/adem.201400433 (31, 32).

[111] Andrew G. Mark et al. "Auxetic metamaterial simplifies soft robot design". In: *Proc. - IEEE Int. Conf. Robot. Autom.* 2016-June.c (2016), pp. 4951–4956. ISSN: 10504729. DOI: 10.1109/ICRA.2016.7487701 (31–33).

[112] Melanie F. Simons et al. "Tiled auxetic cylinders for soft robots". In: *RoboSoft 2019 - 2019 IEEE Int. Conf. Soft Robot.* (2019), pp. 62–67. DOI: 10.1109/ROBOSOFT.2019.8722742 (31, 32).

[113] Mingcan Liu et al. "An earthworm-like soft robot with integration of single pneumatic actuator and cellular structures for peristaltic motion". In: *IEEE Int. Conf. Intell. Robot. Syst.* (2020), pp. 7840–7845. ISSN: 21530866. DOI: 10.1109/IROS45743.2020.9341166 (31, 32).

[114] Alexander Hasse and Kristian Mauser. "Poisson Induced Bending Actuator for Soft Robotic Systems". In: *Soft Robot.* 7.2 (2020), pp. 155–167. ISSN: 21695180. DOI: 10.1089/soro.2018.0163 (31–33).

[115] Ryan L. Truby, Lillian Chin, and Daniela Rus. "A Recipe for Electrically-Driven Soft Robots via 3D Printed Handed Shearing Auxetics". In: *IEEE Robot. Autom. Lett.* 6.2 (2021), pp. 795–802. ISSN: 23773766. DOI: 10.1109/LRA.2021.3052422 (31–33).

[116] Leon Yeong Wei Loh et al. "3D Printed Metamaterial Capacitive Sensing Array for Universal Jamming Gripper and Human Joint Wearables". In: *Adv. Eng. Mater.* 23.5 (2021), pp. 1–9. ISSN: 15272648. DOI: 10.1002/adem.202001082. URL: https://doi.org/10.1002/adem.202001082 (31–33).

[117] Huan Jiang et al. "Bending behavior of 3D printed mechanically robust tubular lattice metamaterials". In: *Addit. Manuf.* 50.October 2021 (2022), p. 102565. ISSN: 22148604. DOI: 10.1016/j.addma.2021.102565. URL: https://doi.org/10.1016/j.addma.2021.102565 (31).

[118] Antoine Pfeil et al. "A 3D-printed needle driver based on auxetic structure and inchworm kinematics". In: *International Design Engineering Technical Conferences and Computers and Information in Engineering Conference*. Vol. 51807. American Society of Mechanical Engineers. 2018, V05AT07A057 (31, 32).

[119] Hajun Lee et al. "3D-printed programmable tensegrity for soft robotics". In: *Science Robotics* 5.45 (2020), pp. 1–12. ISSN: 24709476. DOI: 10.1126/SCIROBOTICS.AAY9024 (31, 32, 34).

[120] Liang Wang, Ming Ran An, and Hai Tao Liu. "Compression spin bio-inspired arm: A conceptual model based on compression–torsion cubic mechanical metamaterials with variable cross-section". In: *Extreme Mechanics Letters* 41 (2020), p. 101069. ISSN: 23524316. DOI: 10.1016/j.eml.2020.101069. URL: https://doi.org/10.1016/j.eml.2020.101069 (31).

[121] Zhiping Wang et al. "Stiffness modulation for soft robot joint via lattice structure configuration design". In: *Procedia CIRP* 100 (2021), pp. 732–737. ISSN: 22128271. DOI: 10.1016/j.procir.2021.05.149. URL: https://doi.org/10.1016/j.procir.2021.05.149 (31, 32, 34).

[122] Ali Maziz et al. "Knitting and weaving artificial muscles". In: *Science Advances* 3.1 (2017), pp. 1–12. ISSN: 23752548. DOI: 10.1126/sciadv.1600327 (31, 32, 34).

[123] Min-Woo Han and Sung-Hoon Ahn. "Blooming knit flowers: Loop-linked soft morphing structures for soft robotics". In: *Advanced materials* 29.13 (2017), p. 1606580 (31).

[124] Dian Yang et al. "Buckling of Elastomeric Beams Enables Actuation of Soft Machines". In: *Advanced Materials* 27.41 (2015), pp. 6323–6327. ISSN: 15214095. DOI: 10.1002/adma.201503188 (31, 34, 35).

[125] Dian Yang et al. "Buckling Pneumatic Linear Actuators Inspired by Muscle". In: *Advanced Materials Technologies* 1.3 (2016), pp. 31–33. ISSN: 2365709X. DOI: 10.1002/admt.201600055 (31, 34, 35).

[126] Di Guo and Zhan Kang. "Chamber layout design optimization of soft pneumatic robots". In: *Smart Materials and Structures* 29.2 (2020). ISSN: 1361665X. DOI: 10.1088/1361-665X/ab607b (31, 34, 35).

[127] B. Grossi et al. "Metarpillar: Soft robotic locomotion based on buckling-driven elastomeric metamaterials". In: *Materials and Design* 212 (2021), p. 110285. ISSN:

18734197. DOI: 10.1016/j.matdes.2021.110285. URL: https://doi.org/10.1016/j.matdes.2021.110285 (31, 34, 35).

[128] Tian Chen et al. "Harnessing bistability for directional propulsion of soft, untethered robots". In: *Proceedings of the National Academy of Sciences* 115.22 (2018), pp. 5698–5702. ISSN: 0027-8424. DOI: 10.1073/pnas.1800386115. URL: http://www.pnas.org/lookup/doi/10.1073/pnas.1800386115 (31, 34, 35).

[129] E. Hawkes et al. "Programmable matter by folding". In: *Proc. Natl. Acad. Sci. U. S. A.* 107.28 (2010), pp. 12441–12445. ISSN: 00278424. DOI: 10.1073/pnas.0914069107 (31).

[130] Donghwa Jeong and Kiju Lee. "Design and analysis of an origami-based three-finger manipulator". In: *Robotica* 36.2 (2018), pp. 261–274 (31, 36).

[131] Soroush Kamrava et al. "Programmable Origami Strings". In: *Adv. Mater. Technol.* 3.3 (2018), pp. 1–8. ISSN: 2365709X. DOI: 10.1002/admt.201700276 (31).

[132] Jakob A. Faber, Andres F. Arrieta, and André R. Studart. "Bioinspired spring origami". In: *Science (80-.).* 359.6382 (2018), pp. 1386–1391. ISSN: 10959203. DOI: 10.1126/science.aap7753 (31).

[133] Ahmad Rafsanjani et al. "Supplementary Material for Kirigami skins make a simple soft actuator crawl". In: *Sci. Robot.* 3.15 (2018), pp. 1–29. ISSN: 2470-9476. DOI: 10.1126/scirobotics.aar7555. URL: http://robotics.sciencemag.org/lookup/doi/10.1126/scirobotics.aar7555 (31, 36).

[134] Donghwa Jeong and Kiju Lee. "Design and analysis of an origami-based three-finger manipulator". In: *Robotica* 36.2 (2018), pp. 261–274. ISSN: 14698668. DOI: 10.1017/S0263574717000340 (31).

[135] Ryan L. Truby, Cosimo Della Santina, and Daniela Rus. "Distributed proprioception of 3d configuration in soft, sensorized robots via deep learning". In: *IEEE Robot. Autom. Lett.* 5.2 (2020), pp. 3299–3306. ISSN: 23773766. DOI: 10.1109/LRA.2020.2976320 (31, 36).

[136] Fuwen Hu et al. "Origami spring–inspired metamaterials and robots: An attempt at fully programmable robotics". In: *Sci. Prog.* 103.3 (2020), pp. 1–19. ISSN: 20477163. DOI: 10.1177/0036850420946162 (31).

[137] Meng Yu et al. "A crawling soft robot driven by pneumatic foldable actuators based on Miura-ori". In: *Actuators* 9.2 (2020), pp. 1–13. ISSN: 20760825. DOI: 10.3390/ACT9020026 (31).

[138] Fuwen Hu and Tian Li. "An origami flexiball-inspired metamaterial actuator and its in-pipe robot prototype". In: *Actuators* 10.4 (2021). ISSN: 20760825. DOI: 10.3390/act10040067 (31).

[139] Dohgyu Hwang et al. "Shape and Rigidity Morphing Mechanical Metamaterials through Reversible Plasticity". In: *Submiss.* 2171.February (2021) (31, 36).

[140] Catherine Jiayi Cai et al. "Diversified and Untethered Motion Generation Via Crease Patterning from Magnetically Actuated Caterpillar-Inspired Origami Robot". In: *IEEE/ASME Trans. Mechatronics* 26.3 (2021), pp. 1678–1688. ISSN: 1941014X. DOI: 10.1109/TMECH.2020.3028746 (31).

[141] Robert J Lang. "A computational algorithm for origami design". In: *Proceedings of the twelfth annual symposium on Computational geometry*. 1996, pp. 98–105 (36).

[142] Ke Liu and Glaucio H Paulino. "MERLIN: A MATLAB implementation to capture highly nonlinear behavior of non-rigid origami". In: *Proceedings of IASS Annual Symposia*. Vol. 2016. 13. International Association for Shell and Spatial Structures (IASS). 2016, pp. 1–10 (36).

[143] K Liu and GH Paulino. "Nonlinear mechanics of non-rigid origami: an efficient computational approach". In: *Proceedings of the Royal Society A: Mathematical, Physical and Engineering Sciences* 473.2206 (2017), p. 20170348 (36).

[144] Feifei Chen and Michael Yu Wang. "Design optimization of soft robots: A review of the state of the art". In: *IEEE Robotics & Automation Magazine* 27.4 (2020), pp. 27–43 (37, 38).

[145] Cecilia Laschi and Barbara Mazzolai. "Lessons from animals and plants: The symbiosis of morphological computation and soft robotics". In: *IEEE Robotics & Automation Magazine* 23.3 (2016), pp. 107–114 (37).

[146] David Howard et al. "Evolving embodied intelligence from materials to machines". In: *Nature Machine Intelligence* 1.1 (2019), pp. 12–19 (37).

[147] Jonàs Martı´nez, Jérémie Dumas, and Sylvain Lefebvre. "Procedural voronoi foams for additive manufacturing". In: *ACM Transactions on Graphics (TOG)* 35.4 (2016), pp. 1–12 (43).

[148] Ares Lagae et al. "Procedural noise using sparse Gabor convolution". In: *ACM Transactions on Graphics (TOG)* 28.3 (2009), pp. 1–10 (43).

[149] Jonàs Martı´nez et al. "Polyhedral Voronoi diagrams for additive manufacturing". In: *ACM Transactions on Graphics (TOG)* 37.4 (2018), p. 129 (43, 44, 51, 61).

[150] Peter Chadwick, Maurizio Vianello, and Stephen C Cowin. "A new proof that the number of linear elastic symmetries is eight". In: *Journal of the Mechanics and Physics of Solids* 49.11 (2001), pp. 2471–2492 (48).

[151] Tanaka Mori and Kohichi Tanaka. "Average stress in matrix and average elastic energy of materials with misfitting inclusions". In: *Acta metallurgica* 21.5 (1973), pp. 571–574 (50).

[152] Siavouche Nemat-Nasser and Muneo Hori. *Micromechanics: overall properties of heterogeneous materials*. Elsevier, 2013 (50).

[153] JC Michel, H Moulinec, and P Suquet. "A computational scheme for linear and non-linear composites with arbitrary phase contrast". In: *International Journal for Numerical Methods in Engineering* 52.1-2 (2001), pp. 139–160 (50).

[154] Eulalie Coevoet et al. "Software toolkit for modeling, simulation, and control of soft robots". In: *Advanced Robotics* 31.22 (2017), pp. 1208–1224 (52, 77).

[155] Carlos A Felippa. "A systematic approach to the element-independent corotational dynamics of finite elements". In: (2000) (56).

[156] Matthias Müller and Markus H Gross. "Interactive Virtual Materials." In: *Graphics interface*. Vol. 2004. 2004, pp. 239–246 (56).

[157] Fun Shing Sin, Daniel Schroeder, and Jernej Barbič. "Vega: non-linear FEM deformable object simulator". In: *Computer Graphics Forum*. Vol. 32. 1. Wiley Online Library. 2013, pp. 36–48 (56).

[158] Joe Dellinger, Dan Vasicek, and Carl Sondergeld. "Kelvin notation for stabilizing elastic-constant inversion". In: *Revue de l'Institut Français du Pétrole* 53.5 (1998), pp. 709–719 (56).

[159] Sandrine Germain. *On inverse form finding for anisotropic materials in the logarithmic strain space*. Friedrich-Alexander-Universitaet Erlangen-Nuernberg (Germany), 2013 (56).

[160] Yijing Li and Jernej Barbič. "Stable anisotropic materials". In: *IEEE TVCG* 21.10 (2015), pp. 1129–1137 (58, 92).

[161] Scott Kuindersma, Frank Permenter, and Russ Tedrake. "An efficiently solvable quadratic program for stabilizing dynamic locomotion". In: *ICRA 2014*. IEEE. 2014, pp. 2589–2594 (89).

[162] HeeSun Choi et al. "On the use of simulation in robotics: Opportunities, challenges, and suggestions for moving forward". In: *Proceedings of the National Academy of Sciences* 118.1 (2021) (89).

[163] Moritz Bächer, Espen Knoop, and Christian Schumacher. "Design and Control of Soft Robots Using Differentiable Simulation". In: *Current Robotics Reports* (2021), pp. 1–11 (89).

[164] James M Bern et al. "Soft robot control with a learned differentiable model". In: *RoboSoft 2020*. IEEE. 2020, pp. 417–423 (89).

[165] Sam Kriegman et al. "Scalable sim-to-real transfer of soft robot designs". In: *RoboSoft 2020*. IEEE. 2020, pp. 359–366 (89).

[166] Yuanming Hu et al. "Chainqueen: A real-time differentiable physical simulator for soft robotics". In: *ICRA 2019*. IEEE. 2019, pp. 6265–6271 (89).

[167] Javier Tapia et al. "Makesense: Automated sensor design for proprioceptive soft robots". In: *Soft robotics* 7.3 (2020), pp. 332–345 (89).

[168] Christian Schumacher, Espen Knoop, and Moritz Bächer. "Simulation-ready characterization of soft robotic materials". In: *IEEE Robotics and Automation Letters* 5.3 (2020), pp. 3775–3782 (89).

[169] S Connolly, Donald MacKenzie, and Tugrul Comlekci. "Multi-objective optimization of hyperelastic material constants: A feasibility study". In: *Constitutive Models for Rubber X*. CRC Press, 2017, pp. 273–278 (89).

[170] Donald Shepard. "A two-dimensional interpolation function for irregularly-spaced data". In: *Proceedings of the 1968 23rd ACM*. 1968, pp. 517–524 (92, 93).